The Effect of Milling Time on the Structure and Properties of Mechanically Alloyed High Carbon Iron-Carbon Alloys

by

Ibrahim Youniss A. Khalfallah

Dissertation submitted to the faculty of the
Virginia Polytechnic Institute and State University
in partial fulfillment of the requirements for the degree of

Doctor of Philosophy

in

Materials Science and Engineering

Alexander O. Aning, Chair

William T. Reynolds

Guo-Quan Lu

Christopher Winkler

October 23, 2017

Blacksburg, VA

Keywords: Mechanical alloying, Milling time, high-carbon Fe-C alloys, fully pearllitic structure

The Effect of Milling Time on the Structure and Properties of Mechanically Alloyed High Carbon Iron-Carbon Alloys

Ibrahim Youniss A. Khalfallah

ABSTRACT

The effects of mechanical alloying milling time and carbon concentration on microstructural evolution and hardness of high-carbon Fe-C alloys were investigated. Mechanical alloying and powder metallurgy methods were used to prepare the samples. Mixtures of elemental powders of iron and 1.4, 3, and 6.67 wt.% pre-milled graphite were milled in a SPEX mill with tungsten milling media for up to 100h. The milled powders were then cold-compacted and pressure-less sintered between 900°C and 1200°C for 1h and 5h followed by furnace cooling. Milled powders and sintered samples were characterized using X-ray diffraction, differential scanning calorimetry, Mossbauer spectroscopy, scanning and transmission electron microscopes. Density and micro-hardness were measured. The milled powders and sintered samples were studied as follows:

In the milled powders, the formation of Fe_3C was observed through Mossbauer spectroscopy after 5h of milling and its presence increased with milling time and carbon concentration. The particle size of the milled powders decreased and tended to become more equi-axed after 100h of milling. Micro-hardness of the milled powders drastically increased with milling time as well as carbon concentration. A DSC endothermic peak around 600°C was detected in all milled powders, and its transformation temperature decreased with milling time. In the literature, no explanation was found. In this work, this peak was found to be due to the

formation of Fe_3C phase. A DSC exothermic peak around 300°C was observed in powders milled for 5h and longer; its transformation temperature decreased with milling time. This peak was due to the recrystallization and/or recovery α-Fe and growth of Fe_3C .

In the sintered samples, almost 100% of pearlitic structure was observed in sintered samples prepared from powders milled for 0.5h. The amount of the pearlite decreased with milling time, contrary to what was found in the literature. The decrease in pearlite occurred at the same time as an increase in graphite-rich areas. With milling, carbon tended to form graphite instead of Fe_3C. Longer milling time facilitated the nucleation of graphite during sintering. High mount of graphite-rich areas were observed in sintered samples prepared from powders milled for 40h and 100h. Nanoparticles of Fe_3C were observed in a ferrite matrix and the graphite-rich areas in samples prepared from powders milled for 40h and 100h. Micro-hardness of the sintered samples decreased with milling time as Fe_3C decreased. The green density of compacted milled powders decreased with milling time and the carbon concentration that affected the density of sintered samples.

The Effect of Milling Time on the Structure and Properties of Mechanically Alloyed High Carbon Iron-Carbon Alloys

Ibrahim Youniss A. Khalfallah

General Audience Abstract

The effects of milling time and carbon composition of the alloy on microstructural evolution and hardness of high-carbon Fe-C alloys were investigated. Mixtures of elemental powders of iron and 1.4, 3, and 6.67 wt.% nano graphite were milled, pressed and the sintered between 900°C and 1200°C for 1h and 5h. Milled powders and sintered samples were characterized. Density and hardness were measured. The milled powders and sintered samples were studied as follows:

In the milled powders, the formation of iron carbide was observed through Mossbauer spectroscopy after 5h of milling and its amount increased with milling time and carbon composition of the alloy. The particle size of the milled powders decreased with milling time. Hardness of milled powders increased with milling time as well as carbon composition of the alloy.

In the bulk samples, almost 100% of pearlitic structure was observed in samples prepared from powders milled for 0.5h. The amount of the pearlite decreased with milling time. The decrease in pearlite occurred at the same time as an increase in graphite with milling time. High mount of graphite areas were observed in samples prepared from powders milled for 40h and

100h. Hardness of the sintered samples decreased with milling time as iron carbide (hard phase) decreased. The density of bulk samples decreased with milling time and the carbon composition.

Acknowledgements

First and foremost, I would like to thank **ALLAH** who has given me the will to achieve this work and pursue my dream. Firstly, I would like to express my sincere gratitude to my academic advisor **Dr. Alex O. Aning**. Without his patience, teaching, guidance, and motivation, this dissertation could have not been accomplished. Beside my advisor, I would like to thank my dissertation committee members (i) **Dr. William Reynolds**, for his patience, helpful discussions, and guidance, (ii) **Dr. Guo-Quan Lu**, for his insightful comments and motivation, (iii) **Dr. Christopher Winkler**, for his helpful discussions and the help with transmission electron microscopy. Without their help and guidance, it would be difficult for me to accomplish this work. I would like also to thank **Dr. Carlos Suchicital** and **Ms. Christine Burgoyne** for their insightful comments and help in writing. My sincere thanks also go to **Dr. Karen P. DePauw, Vice President and Dean for Graduate Education of Virginia Tech** and **Dr. David Clark, Department Head of The Virginia Tech's Materials Science and Engineering Department** for providing financial support. Without their help, I would not have achieved my dream. I would like also to acknowledge **Ms. Kim Grandstaff, Graduate Program Coordinator,** for her help and guidance with all the paper work for the graduate school.

I would also like to thank **Dr. Aning's research group**: Hesham Elmkharram and Jonathan Angle for helpful discussions and great company. Last but not least, I would like to thank my family, wife, children, and friends for helping and supporting me throughout my study journey.

Table of Contents

List of Figures

List of Tables

1 Introduction

Mechanical alloying (MA) has been found to be one the most effective techniques to produce materials with unique microstructures and excellent properties. The goal of using such a technique is to enhance materials performance and broaden their applications. However, a variety of equilibrium and non-equilibrium phases have been successfully produced using MA [1]. MA parameters such as milling time, charge ratio, mill type, and milling temperature broadly affect the microstructure of the final product [2]. MA technique has been widely used to process metal alloys, ceramics, and polymers. Among the metal alloys, the iron-carbon system has been extensively studied via MA and other processing techniques because of its importance in the steel industry and its wide range of applications.

Processing iron-carbon alloys with high carbon content are treated on a limited scale only. In the steel industry, slabs are brought to a uniform temperature and then continue to be hot-rolled to reach the final shape [3]. It is difficult to process the slabs which contain high-carbon concentrations, because of their limited ductility leads to cracking even during the hot working. MA makes it possible to process iron-carbon alloys with ultra-high carbon concentrations with very fine microstructure and excellent properties [4-6]. Literature shows that the final Fe-C alloys structures and properties are controlled by the starting composition and MA parameters [7]. Among the MA parameters, milling time is one of the most effective in accomplishing the desired structure and properties [8]. Carbon content is also another parameter that influences the microstructure and the properties of Fe-C alloys [9]. The effects of MA milling time and carbon content on the microstructural evolution and properties of Fe-C alloys have been studied by a number of research groups [5-7, 9-13].

In preliminary work for this dissertation, iron and graphite (1.4, 3, and 6.67 wt.% C) were mechanically alloyed for up 100h. The milled powders were cold-compacted and sintered between 900°C and 1200°C followed by furnace cooling. Preliminary results showed that the amount of Fe_3C in the sintered samples decreased with milling time, contrary to what was found in the literature. Moreover, an exothermic peak around 300°C was detected in a powder mix milled for 5h and longer. This peak was shifted to the lower temperatures with milling time. The energy released from this exothermic reaction decreased with milling time and carbon concentration. Literature shows that this exothermic was due to crystallization of amorphous Fe_3C [14], this conclusion was supported by T. Tanaka et al. [15] and N. Rochman et al. [16, 17]. The author, who does this work, did not agree with their explanation. Using x-ray diffraction and differential scanning calorimetry were not sufficient to confirm the formation of the amorphous phases. In this work, more experiments were designed to find a better explanation for the origin of this exothermic peak. Additionally, an endothermic peak around 600°C was observed in powders milled for 0.5h and longer and it transformation temperatures decreased with milling time. Previous researchers who have observed this peak gave no explanation for its underlying.

1.1 Project Goal

The current research seeks to investigate the effects of milling time and carbon concentration on the microstructural evolution and the properties of sintered high-carbon Fe-C alloys. This work also seeks to better understand the suppression of Fe_3C evolution with MA milling time found in the preliminary results. Therefore, this work attempts to explain the origin of the exothermic peak around 300°C and the endothermic peak around 600°C, which were detected in mechanically alloyed high-carbon Fe-C alloy powders. There is a gap in knowledge concerning the effects of milling time on the exothermic and endothermic peaks.

1.2 Objectives

The purpose of this work is to investigate the effects of MA milling time and carbon concentration on the microstructural evolution and the properties of high-carbon Fe-C alloys. The specific objectives of this work are addressed as follows:

- Explain why the amount of Fe_3C decreased with milling time. The following experiments were performed to find an explanation for this objective:
    i. The chemical composition of sintered samples was checked to find out if there was a match in the carbon composition.
    ii. Transmission electron microscopy was used to observe the presence phases in the sintered samples.

- Determine what caused both the exothermic peak around 300°C and the endothermic peak around 600°C in Fe-C mechanically alloyed powders. This objective was tested using the following experiments:
    i. Milled powders were annealed enclose the peak observation in the DSC.
    ii. The annealed milled powders were then analyzed using XRD and TEM to determine if there was any phase transformation or crystalline phase change.

1.3 Dissertation Organization

Chapter two includes background information on mechanical alloying, energy transfer in MA, powder compaction and sintering methods, and the effects of milling time and carbon concentrations on microstructural evolution and properties of Fe-C alloys. Chapter three describes the experimental procedures as well as the characterization techniques employed. Chapters four through six are written as journal articles. Chapter four discusses powder processing and characterization of mechanically alloyed high-carbon Fe-C alloys. Chapter five discusses the effects of milling time on the microstructural evolution of high-carbon Fe-C alloys. Chapter six discusses the effects of milling time on the densification and the hardness of sintered high-carbon Fe-C alloys. Chapter seven summarizes the dissertation’s conclusions. Chapter eight includes summary of accomplishments of this work followed by a list of references.

2 Background

2.1 Mechanical Alloying

Since the 1960s, mechanical alloying (MA) has been known as a useful technique in powder processing, due to the successful use of ball milling in producing an oxide dispersed strengthing superalloy. During MA, powder particles are repeatedly deformed, fractured, and cold welded by the high impact energy of ball to the powder particles [8]. As a result of the high impact energy, MA has now been intensively used to synthesize a wide variety of equilibrium and non-equilibrium structures. The non-equilibrium structures include supersaturated solid solution, nanostructured, intermetallic, and amorphous alloys [18, 19]. Employing mechanical alloying in powder metallurgy is consider a promising powder fabrication technique, which may be used to fabricate novel alloys [20]. MA is usually carried out under an inert atmosphere in either high-energy or low-energy ball mills. High-energy ball mills include Attritor, planetary, and vibratory-types [8]. In this work a SPEX shaker/mill, which is considered as a high-energy ball mill, was used.

The mechanical alloying process begins with loading a vial with a mixture of powders and milling medium. Loading the vial usually carried out in an inert gas environment to minimized oxidation. After loading the vial into the mill, the mixture is then milled for the desired length of time. The milled powders are then compacted and sintered into a bulk shape. Heat treatment sometimes is needed to obtain the desired microstructure and properties [8]. During high-energy milling, the powder particles are trapped between two rapidly colliding balls (Fig. 2.1) or a colliding ball with the vial walls. The trapped powder particles are repeatedly welded, fractured, and rewelded.

Further, the powder particles are plastically deformed via the compressive impact forces during milling that leads to work hardening, fracturing, and particle size reduction [8, 21]. The repeated fracturing and welding during MA creates new surfaces and increases the particle temperature, and both enhance the diffusion kinetics [22, 23].

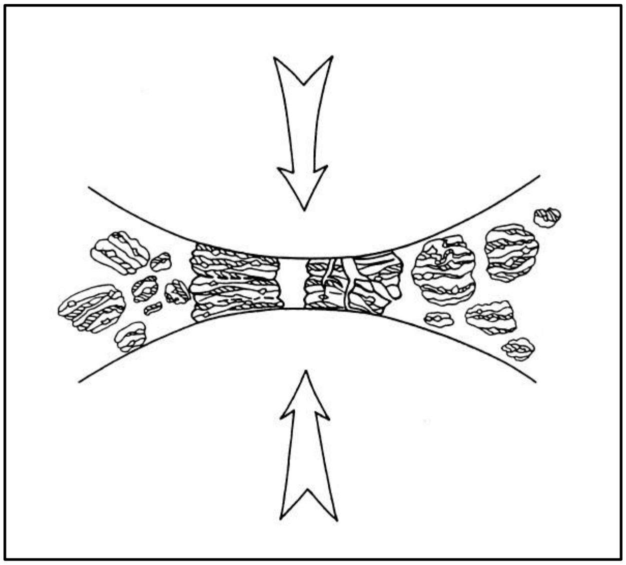

Fig. 2.1 Schematic diagram of ball-powder-ball collision of powder mixture during MA [1].

Like any other fabrication technique, mechanical alloying processing parameters are affected by several factors. These factors need to be optimized to achieve the desired phase or microstructure of the final product [8]. The properties of the milled powders, such as morphology, the degree of disorder, and particle size, depend on the milling conditions. For example, particle size distribution of the milled powder depends on milling time and the ball-to-powder weight ratio (BPR) [8, 24]. The following are some of the MA processing parameters that have a direct impact on the microstructure and properties of the final product.

- Milling time
- Milling speed
- Ball-to-powder weight ratio

- Temperature of milling
- The materials of the milling tool
- Types of mills (e.g., high-energy mills and low-energy mills)

These MA processing parameters are not completely independent; for example, selecting the milling time is based on the BPR, type of mills, and temperature of milling, etc.[8]. The main mechanical alloying parameters which relate to this work will be discussed in the following sections.

2.1.1 Milling Time

Milling time is one of the most important MA processing variables to be considered. Choosing the milling time depends on the desired phase or microstructure of the final products [8]. Milling for different times allows the researchers to monitoring of the progress of the reactions that have taken place during ball milling and is one advantage of the mechanical alloying technique over any other fabrication techniques [24].

It should be considered that some undesired phases may form and the level of contamination from the milling medium increases when milling parameters are not optimized. The milling time that is required to achieve the desired phase depends on some other variables [8]. For example, the type of mill, using high-energy ball mill leads to a decrease of the milling time. S.R. Chauruka et al. [25] studied the effect of mill type on the size reduction of gamma alumina. They used three different mill types: air jet mill, single ball mill, and planetary ball mill. Based on the particles size reduction, they found that the air jet mill is the most effective one. Gamma alumina powder particles size was reduced from 37µm to 2.9µm using air jet, to 10.5 µm using single ball mill, and to 30.2µm using planetary ball mill. G. M. Wang et al.[26] found that a Fe_3C phase was formed after 140h of milling in Fe-25 at.% C alloy powder using the planetary mill, while the Fe_3C was observed after 10h of milling using SPEX mill [6].

BPR is an important variable in the MA process and has a significant effect on the milling time selection. Milling for short time sometimes is sufficient to accomplish the desired microstructure using high BPR. It was reported that an amorphous phase in a Ti-33 at.% Al alloy was observed in milled powder in SPEX mill for 7h at a BPR of 10:1, for 2h at a BPR of 50:1, and for 1h at a BPR of 100:1 [27]. On the other hand, high BPR may lead to increase the level of contamination, which comes from the wear of the mill chamber and milling balls. Contamination sometimes influences the transformation path and forms undesired phases [28]. S. J. Campbell et al. [29] reported that high contamination level of Fe has been found in pure W and a mixture of W-C from the milling medium during milling using SPEX and BPR about 30:1. About 33 at.% Fe was found in the pure milled W after 45h and around 20 at.% Fe in the W-C milled mixture after 310h. Another type of contamination comes from the process control agent (PCA). Ethanol, oleic acid, methanol, and stearic acid are some of the PCAs used in the mechanical alloying process. B.V. Neamtu et al. [30] reported that adding PCA into the mill charge decreased the milling time required for powder amorphization. They reported that the presence of carbon in the PCA helped to form an amorphous $Fe_{75}Si_{20}B_5$ powder after 40h of wet milling, while no amorphization was detected after dry milling for 140h.

Milling temperature is another important parameter that influences the milling processing and the microstructure of the final product, and has a significant effect on the diffusion processes that take place during milling [28]. The effect of milling temperature on the phase transformations of mechanically alloyed powders has been intensively studied. For instance, liquid nitrogen is used to lower the milling temperature, by flowing liquid nitrogen on the milling container (cryomilling). Another way of controlling the milling temperature is by electrically heating up the milling container, to increase the milling temperature intentionally [8]. Lee et al. [31] studied the effect of milling temperature on the mechanical alloying processes using Ni_{50}-Zr_{50} powders ($\Delta H_{mix} < 0$). Ni_{50}-Zr_{50} powder was milled for 5h at temperatures ranging between -123°C to 200°C. They found that the amorphization kinetics increased with increasing temperature. Similar results were also observed by other researchers in the Zr-Al [32] and Cu-Ag [33]. In contrast to these observations, others have reported that the amorphization kinetics increased with decreasing temperatures. C. C. Koch et al.[34] reported that lowering the milling temperature decreased the milling time to form an amorphous phase in NiTi system. Milling at 220°C, amorphization was observed after 18h, while it took only 2h for amorphization at liquid nitrogen temperature. Shorten milling times for amorphization were also reported for CoZr and $NiZr_2$ intermetallic [34]. Varying the milling temperatures may also shorten the milling time to achieve the desired microstructures.

2.1.2 Types of Mills

A variety of milling equipment has been used to carry out mechanical alloying. The most common milling equipment employed for laboratory investigations includes planetary ball mills, attritor mills, and vibratory mills. They differ in their efficiency of milling, capacity, and transfer energy to the milled powder, etc. [8]. A brief description is provided for SPEX shaker/mill since it was used in this work.

SPEX shaker/mill, which is manufactured by SPEX CertPrep, Metuchen, NJ, has been commonly used for laboratory investigations. There are two types of SPEX shaker/mill, but the most common one has only one vial. The vial containing the milling balls and the sample (capacity: 10-20g), and it is secured by a clamp, which energetically moves back and forth several thousand times a minute. Because of the high speed of the clamp motion (about 1200 rpm) and the high velocities of the balls (on the order of 5 m/sec), SPEX mill is considered as a high-energy ball mill [8]. Figure 2.2 shows a typical SPEX shaker/mill and tungsten carbide vial set.

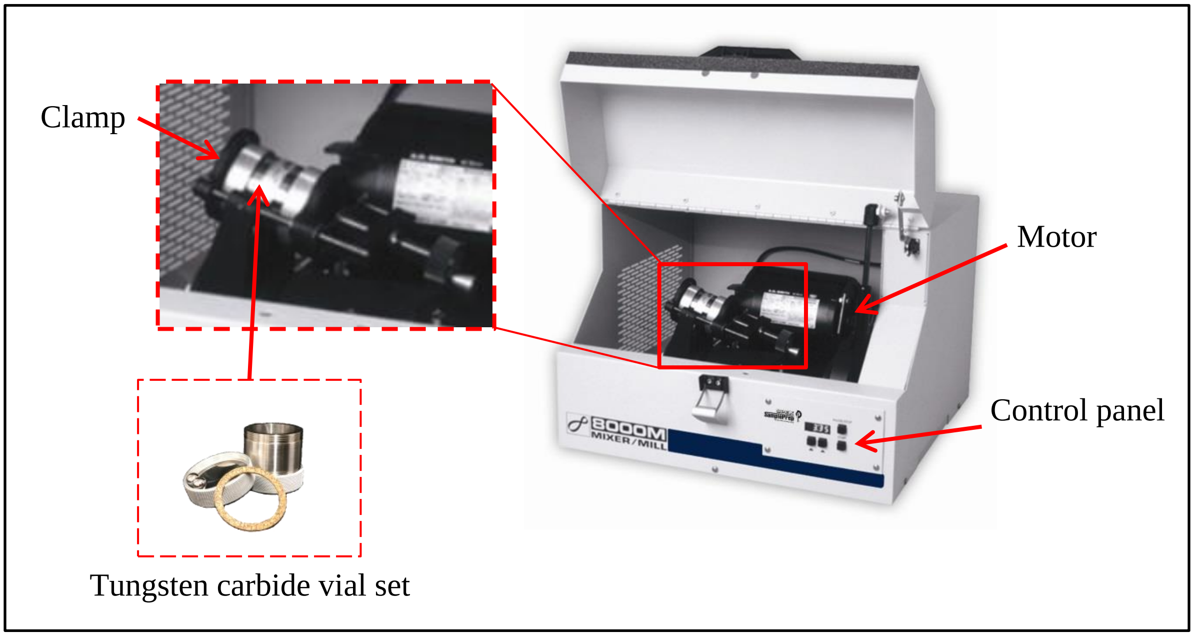

Fig. 2.2 SPEX 8000 shaker/mill with tungsten carbide vial secured in the clamp and tungsten carbide vial set consisting of the vial, lid, gasket, and balls (http://www.spexsampleprep.com).

2.2 Energy Transfer in Mechanical Alloying

The amount of energy transfer from the milling tool to the milled powders depends on the mill design (dynamics of the milling medium), impact times, and areas of colliding surfaces. In a vibratory mill, the energy transfer to the powder mixture is through the collisions of the balls to one another and to the vial walls [28]. The impact forces in a vibratory mill depend on the amplitude and frequency of vibration and the mass of the milling medium. Because of the high impact forces, the vibratory mill is considered as one of the most energetic ball milling devices [8]. A number of attempts have been made to understand the mechanism of energy transfer to the powder during the milling process [35-37]. However, collisions are considered to be the prevailing energy transfer event when the filling charge is low. On the contrary sliding and rolling (attrition) dominate more than collisions when the filling charge is high. Both attrition and collision mechanisms are effective and cannot be separated in a real mill process but for simplicity, only one of the two mechanisms is considered, by controlling the filling charge [37].

M. Magini [38] studied the energy transfer in the mechanical alloying process using both planetary and vibratory mills. The experiment was done on the $\mathrm{Pd_{80}Si_{20}}$ system. The collision was assumed to be the dominant energy transfer mechanism. Both the rotation speed and the ball diameter were varied when using the planetary mill. In the vibratory mill, only the ball diameter was freely varied. In their study, the main parameters evaluated were: (i) the kinetic energy of the ball; (ii) the fraction of the kinetic energy given to the powder; (iii) the amount of the materials being trapped in the collision. These parameters were evaluated in other investigations as well [2, 36, 37, 39]. The energy transferred per collision was given by Eq. (2.1):

$$\Delta E = K_c \, \frac{1}{2} \, m_b \, V_b^2 \tag{2.1}$$

where V_b the relative impact velocity, m_b is the mass of ball, and K_c is equal to one for inelastic collisions. The quantity of powder trapped during a collision between a ball and container wall was considered by calculating the maximum radius of the contact surface (a circular area) as following Eq. (2.2):

$$R_{h,max} = 0.8394 V_b^{0.4} m_b^{0.2} d_b^{0.4} / E^{0.2} \tag{2.2}$$

where V_b the relative impact velocity, m_b is the mass of ball, $d_b$is the ball diameter and E is the Young’s modulus of the ball. The maximum quantity of the material (Eq. (2.3)) can be evaluated by the contact surface and by assuming that the surface density is twice the quantity covering the ball.

$$Q_{max} = 2\sigma\pi R_{h,max}^2 \tag{2.3}$$

where σ is the surface density, which is assumed = 0.2 mg/mm^2. The energy transfer per unit mass can be calculated as (Eq. (2.4)):

$$\Delta E/Q_{max} = (4.33 \times 10^4) d_b \omega_p^{1.2} /\sigma. \tag{2.4}$$

where ω_p is the angular velocity. By varying the ball diameter (d_p)and the angular speed (ω_p), the energy transfer per unit mass was calculated and plotted, as shown in Fig. 2.3.

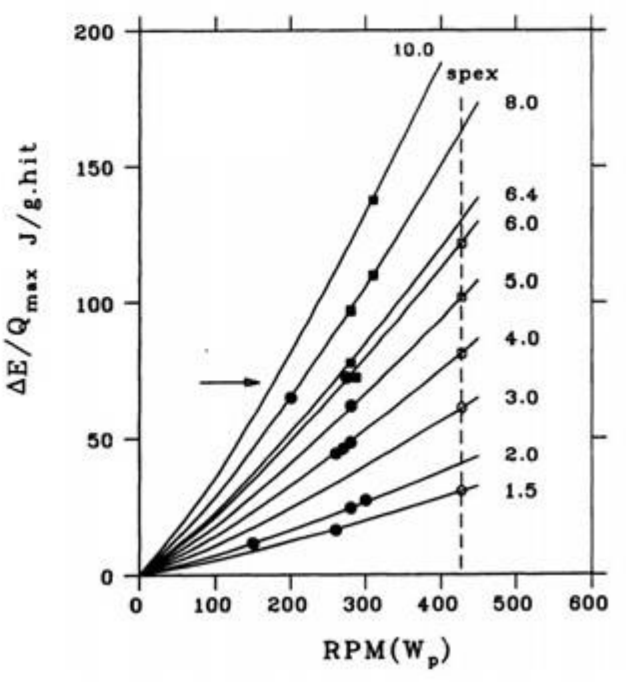

Fig. 2.3 Energy map for the Pd-Si system. The continuous lines represent the energy transferred per unit mass of powder against rotation speed of the planetary mill (rpm) for different ball diameter in millimeters. The solid squares and circles identify the intermetallic and amorphous regions, respectively. The hollow circles represent the energy transfer per mass using SPEX mill [38].

E. Dastanpoor et al. [2] investigated the effect of milling intensity on mechanical alloying of the Cu-Zr-Al system using SPEX and low and high-energy planetary mills. Using the already existing collision models, they calculated the ball velocity, the kinetic energy, and the total energy per unit mass as a function of milling time. The kinetic energy for the ball in SPEX mill, the energy of each ball (E_b') and the total energy transferred per hit (E_t) were determined by S. H. Singh et al. [40].(Eqs. 2.5 – 2.7).

$$E_b = \frac{1}{2}(\, m_b\, V_b^2) \tag{2.5}$$

$$E_b' = \varphi_b E_b \tag{2.6}$$

$$E_t = t\, n_b E_b^{'} \tag{2.7}$$

where m_b is the ball mass, V_b is the ball impact velocity, and φ_b is the correlation factor for different degree of filling of the vial. $\varphi_b = 1$ for only one or few balls [41, 42]. t is the milling time, n_b is the balls number

B. Diego et al. [43] measured the relative impact velocity of milling balls to vial walls from indent size. They determined the impact velocities of the balls for SPEX mill and a new high capacity high-energy mill using tungsten carbide milling media, and the results are presented in Fig. 2.4. They found that the ball impact velocity decreased with ball size. Based on the ball diameter, the ball impact velocity can be obtained from Fig. 2.4, and then the total energy transfer per hit can be calculated using Equation (2.7). D. Basset et al. [44] reported that the impact speeds in a high-energy ball mill are in the range of 2.6-3.8 m/sec, and they are strongly dependent on the ball diameter. In this work, the total energy transfer per hit, based on the MA milling time, was calculated using Equation (2.7) and the ball impact velocity was the average of 2.6 m/sec and 3.8 m/sec when tungsten carbide milling media was used.

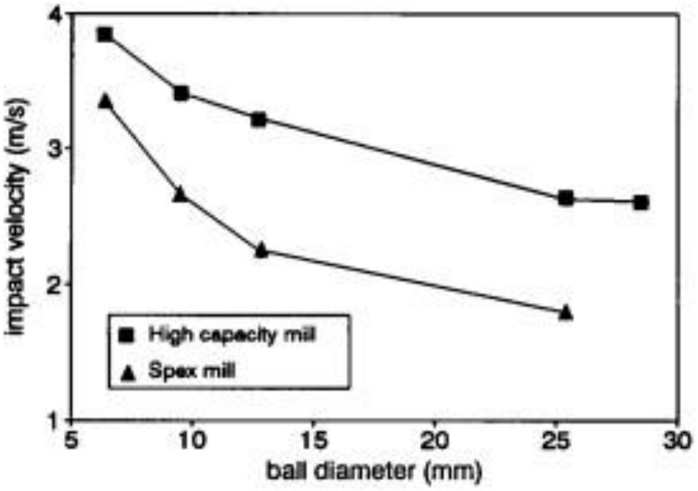

Fig. 2.4 Impact velocity against ball mill diameter for SPEX mill and high capacity high-energy mill using tungsten carbide milling media [43].

2.3 Powder Compaction and Sintering methods

2.3.1 Powder Compaction Methods

After processing, a powder mixture needs to be densified to have a bulk compact, and that can be achieved through one of these following methods: (i) compaction to a high density followed by sintering or (ii) simultaneously compaction and sintering. Powder compaction depends on an external source of pressure for deforming the powders into a high-density component. High pressures increase the green density by contact enlargement through plastic deformation. A compaction process can be divided into three stages. The first stage is a packing process, while the second stage is characterized by surrounding of the particles by connected pores. The relative density range at the second stage is from 0.6 up to 0.8. In the third stage, the pores between the powder particles are filled.

The main problem in a uniaxial compaction is the friction of the powder with die wall, which leads to a decrease of the applied pressure as the thickness of the compacted powder increases. Sometimes the powder mixture is mixed with a binder or lubricant to reduce the friction effects between the powders and the mold parts [45].

Material properties such as hardness, work hardening rate, surface friction, and the chemical bonding between the powder particles have a direct effect on the relationship between the applied pressure and the compact density. Other factors that may affect the density include powder size, shape, lubrication, and the compaction mold. For examples, a small particle size impedes compaction because of the higher particle work hardening rate and higher interparticle friction.

Compaction can be divided into two different methods cold compaction and hot compaction. Cold compaction is accomplished using uniaxial pressing or cold isostatic pressing. Cold compaction is carried out at room temperature. Thus, no sintering is achieved during the cold compaction process. High dense green compacts can be obtained using the isostatic pressing, while the uniaxial pressing can be used to produce large and complex shapes [46]. The second type of the compaction is the hot compaction. Compaction and sintering are done simultaneously via hot compaction. The most common hot compaction methods include spark plasma sintering (SPS) [47], combustion driven compaction (CDC) [48], and hot isostatic pressing (HIP) [49].

2.3.2 Sintering Process

A typical sintering process begins with heating up the compact to a high temperature but below the melting temperature of the material, soaking, and then cooling or quenching. The most important factors involved during the sintering process are sintering temperature, sintering time, and furnace atmosphere. The higher the sintering temperature, the shorter is the sintering time required to achieve the desired density and properties. The main important reason of using a sintering atmosphere is to protect sintered powder metal against oxidation. Hydrogen and argon are the most commonly reducing atmospheres used for sintering metal parts [50]. Both particle size and shape have a direct effect on the sintering process. The small particle size is favorable in sintering because of the large pore/solid interfacial area produced, which increases the driving force for sintering. Also, a small particle size promotes surface and grain boundary diffusion. Increasing the internal surface area by decreasing the sphericity and increasing the roughness of the powder particles promotes sintering process [51]. The categories of sintering are solid solution sintering and liquid phase sintering. The liquid phase sintering involves sintering under conditions where solid grains coexist with a wetting liquid. Here, the focus is only on solid solution sintering. The major processes of sintering are characterized by densification and grain growth. The kinetics of densification are commonly described regarding the density of the bulk as a function of sintering temperature and time.

Without prior compaction, the sintering process is divided into four stages, as presented in Fig. 2.5. With prior compaction, sintering starts with the initial stage, connection of separate particles. A neck is produced at the point of contact between the powder particles. This stage proceeds by plastic deformation and boundary diffusion. In the intermediate stage, the growth of the neck leads to pore volume reduction, and more particle-particle connections. The final stage is characterized by the presence of isolated pores [50]. However, in crystalline materials, sintering occurs through six mechanisms: (i) surface diffusion, (ii) lattice diffusion, (iii) grain boundary diffusion, (iv) vapor transport, (v) plastic flow [51]. Figure 2.6 shows a schematic of the sintering mechanisms for a system of two particles. Surface diffusion, lattice diffusion from the surface, and vapor transport are non-densifying mechanisms. They lead to microstructural changes without causing shrinkage. Whereas, grain boundary diffusion, lattice diffusion from the grain boundary to the neck, and plastic flow are densifying mechanisms, which cause neck growth and densification. Plastic flow (dislocation motion) responses to the sintering stress in the initial stage of sintering. The main important densification mechanisms in metals however, are lattice diffusion and grain boundary diffusion [51].

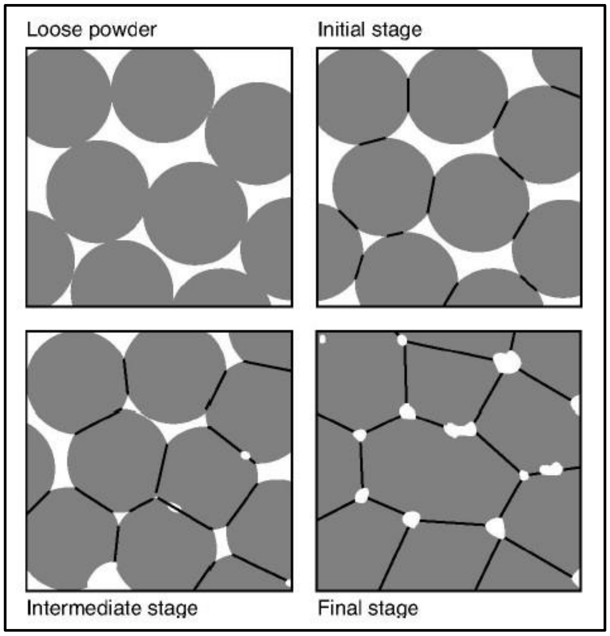

Fig. 2.5 Demonstration of the sintering stages with the focus on the change in the pore structure during sintering [50].

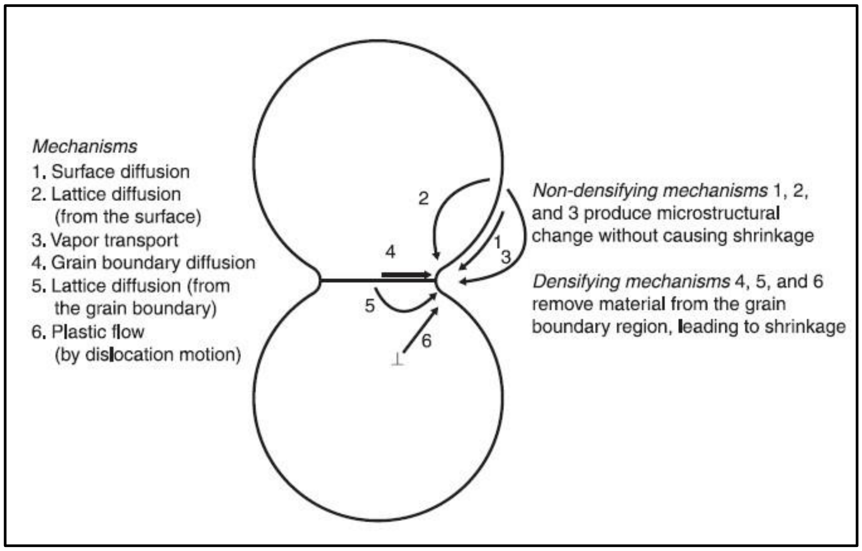

Fig. 2.6 Schematic diagram illustrates the sintering mechanisms for a system of two particles [51].

2.4 The Effect of Milling Time and Carbon Concentration on Microstructural Evolution and Properties of Fe-C Alloys

2.4.1 The Effect of Milling Time

Mechanical alloying (MA) is a powder processing technique that has been intensively used to produce equilibrium and non-equilibrium phases with unique properties [8]. MA is also considered as one of the most effective approaches to produce fully pre-alloyed powders. The effect of mechanical alloying parameters (milling time, ball-to-powder mass ratio, etc.) on the structural evolution and the properties of alloys have been widely investigated over the years. Several studies show that the milling time is one of the most effective mechanical alloying parameters on accomplishing the desired structure and properties. A number of research groups have used different mill type and ball-to-powder mass ratio to study the influence of milling time on the microstructural evolution, density, and hardness of Fe-C alloys [6, 7, 9, 11-15, 52-54] it is summarized here.

Hussain Zuhailawati et al. [7] investigated the effect of milling time and carbon concentration on the microstructure and hardness of Fe-C alloys. Iron and graphite (1, 2, 3, and 4 wt.% C) were milled for up to 8h in a planetary Mono Mill with stainless steel milling media and charge ratio was 4:1. The milled powders were compacted and then sintered at 1150°C for 0.5h. For the case of bulk Fe-1 wt.% C alloy, they reported that the amount of Fe_3C increased with milling time. Similar results were reported elsewhere [4, 12, 13, 15, 52]. Their explanation was that during milling carbon diffused into iron which facilitated the formation of Fe_3C during sintering. This explanation was supported by H. Arik et al. [53]. Ghosh et al. [11] also studied the effect of milling time on the microstructure of Fe-C alloy. Their goal was to investigate the formation of Fe_3C during ball milling. A mixture of pure iron and graphite with 3:1 molar ratio milled for up to 8h in a planetary mill with stainless steel milling media and the charge ratio was

40:1. In the milled powder, they found that after 0.5h of milling, graphite peaks disappeared and they believed that might be due to the formation of amorphous graphite early in mechanical alloying, which is also supported by Arik et al. [53] and Nowosielski et al. [6]. After 2h, Fe_3C phase was observed and its amount increased continuously with milling time, as shown in Fig. 2.7. They concluded that the nanocrystalline Fe_3C phase was formed by the re-welding mechanism of α-Fe and graphite layer. Ghosh et al. [11] also reported that the formation of Fe_3C during milling depends on different parameters: (i) lattice imperfections generated during ball milling, (ii) mass fraction content of C and α-Fe, (iii) ball milling condition such as milling time, charge ratio. This was also supported by several research groups [9, 12, 13, 55].

S. J. Campbell et al. [14] investigated the formation of Fe_3C and Fe_7C_3 compounds in $Fe_{75}C_{25}$ alloy using a Uni ball mill with stainless steel milling media. Iron and graphite were milled for up to 285h. Differential scanning calorimetry (DSC) was used to investigate the thermal stability of the milled powders.

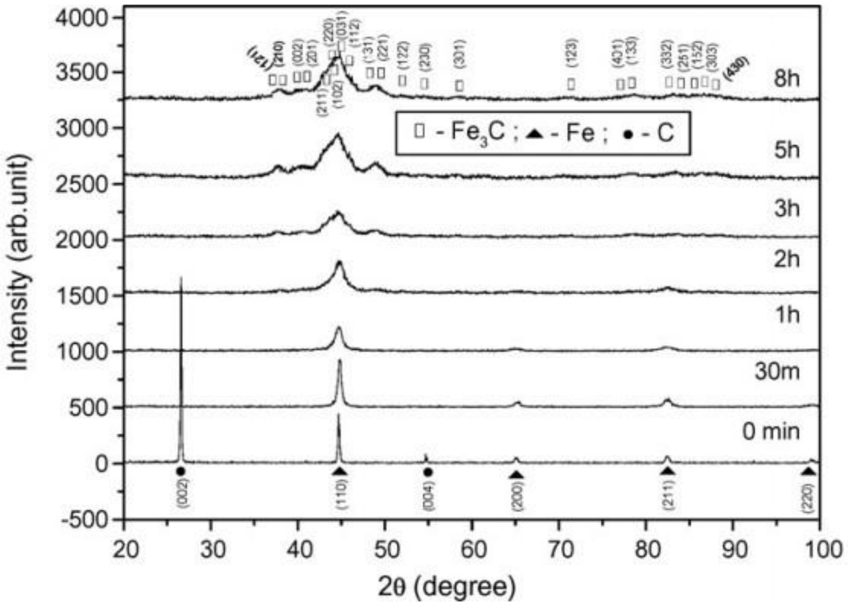

Fig. 2.7 X-ray diffraction profiles of unmilled and ball-milled iron and graphite powders (3:1 molar ratio) for different milling time [11].

In their results, they noticed that an exothermic peak was observed in powders milled for 320°C at 45h and 75h, and the same peak was absent after 140h, as shown in Fig. 2.8. They concluded that an amorphous Fe_3C was formed at 45h, and with continue milling the crystalline Fe_3C was eventually formed as a result of thermally activated crystallization after 140h.

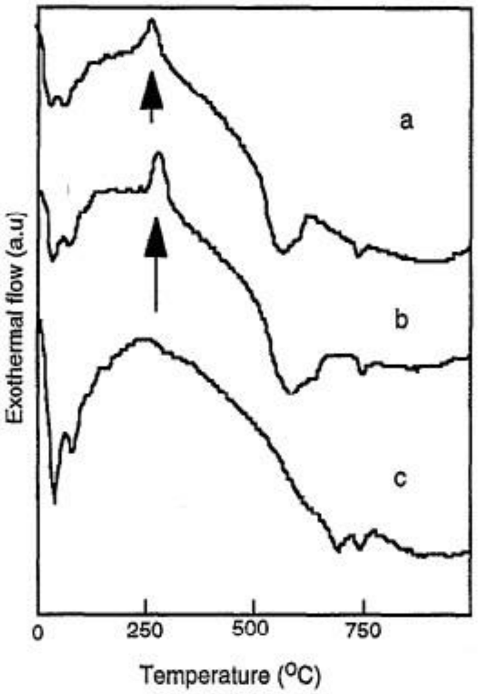

Fig. 2.8 DSC curves of $Fe_{75}C_{25}$ powders milled for (a) 45h, (b) 75h, and (c) 140h [14].

The effect of milling time on Fe-C alloys sintered samples' density has been investigated. Arik et al. [53] studied the effect of milling time on the microstructural evolution of Fe-C alloy. Iron and graphite powders were milled in a SPEX mill with tungsten milling media for up to 5h. They noticed that samples milled for a longer time were more porous than the one milled for a short time. Similar results were reported by H. Zuhailawati et al. [7] and Y. Z. Chen et al. [9]. Figure 2.9 illustrates that the effect of milling time on the green density of unmilled and milled Fe-1 wt.% C alloy at different compacting pressures. It shows that the green density increased with compaction pressure and decreased with milling time. They concluded that the decrease of samples densities with milling time was due to the work hardening and deformation during milling, which negatively affects the compaction process of the milled powder. Particle shape and size distributions could also lead to poor compaction. The effect of work hardening and particle size distribution on milled powder compaction were also in agreement with R. William et al. [56]. It was also reported that the solid-solution strengthening of the ball milled powders led to poor compressibility, which limits the density of the sintered parts [26]. Zuhailawati et al. [7] observed that hardness of Fe-1 wt.% C alloy sintered at 1150°C increased with milling time, as shown in Fig. 2.10. Similar results were reported by Arik et al. [53]. They reported that this increase in hardness was due to the increase in diffusion rate during the repeated welding and fracturing, because it increased the amount of dissolved carbon in α-Fe and increased the amount of iron carbide and pearlite structures.

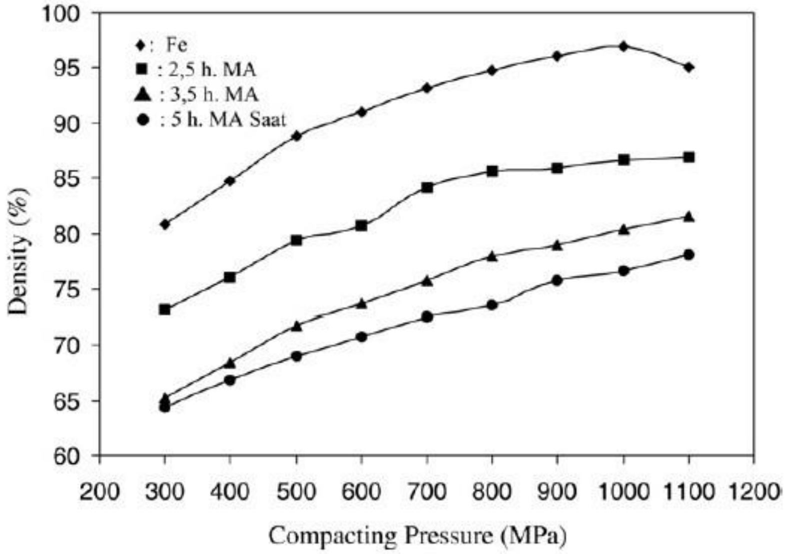

Fig. 2.9 The effects of compacting pressure and milling time on the green density of unmilled and ball-milled Fe-1 wt.% C alloy (density of compacted powders) [53].

2.4.2 The Effect of Carbon Concentration

The carbon concentration of Fe-C alloys can be both a blessing and a curse. The carbon is a blessing when it forms iron carbide compounds, while it is a curse when it exceeds the solubility limit and forms graphite-rich regions instead of iron carbide. The effect of carbon content on structural evolution, density, and hardness of Fe-C alloys has been investigated by several research groups [7, 9, 52, 53, 57-59]. The effects of the carbon concentration on the structure, density, and hardness of mechanically alloyed Fe-C alloys are summarized here. Also, the works are summarized here were conducted using different mill type, charge ratio, and milling time.

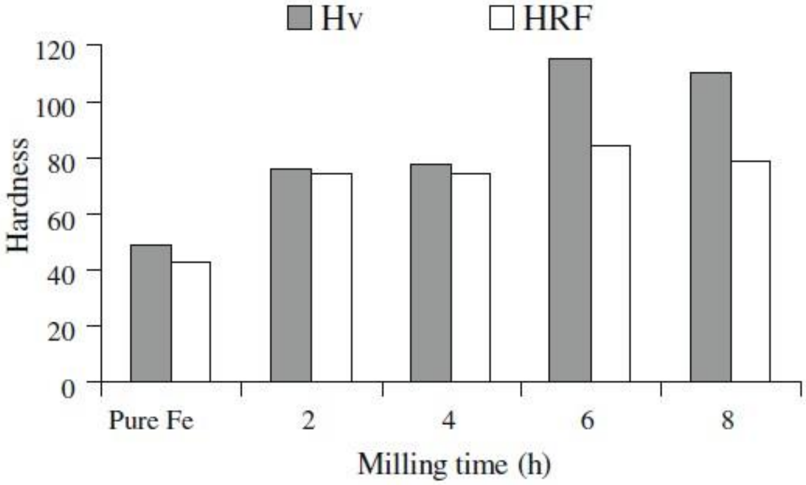

Fig. 2.10 Hardness values of Fe-1 wt.%C alloy sintered at 1150°C against different milling time. Hv: Vickers hardness, HRF: Rockwell F hardness [7].

R. Nowosielski et al.[52] discussed the effect of carbon concentration and milling time on the microstructural evolution of Fe-C alloys. The iron and graphite mixture were prepared with a concentration of 0.4 and 6.67 wt.%. The mixture was milled in a SPEX mill with tungsten carbide milling media for up 150h. The charge ratio was 2:1. In their experiment, they found that the formation of Fe_3C phase increased with carbon concentration. Figure 2.11 shows the XRD profiles of Fe-0.4 and 6.67 wt.% C alloy powders with different milling times. After milling, the graphite peak was not detected, while α-Fe peaks broadened and their intensity decreased due to the refinement of Fe grain size, increasing microstrain, and dissolution of more graphite into α-Fe. The Fe_3C peaks were observed after 75h of milling in Fe-6.67 wt.%C alloy as seen in Fig. 2.11b. That was due to high carbon concentration as compared with Fe-0.4 wt.%C alloy (Fig.

2.11a) [52]. Therefore, in this case, the formation of Fe_3C was controlled by carbon concentration, not milling time. Zuhailawati et al. [7] noticed that the amount of pearlite structure increased with carbon concentration. Also, high amounts of residual carbon were observed in high carbon content samples. Based on the XRD data, the maximum amount of carbon dissolved into ferrite in Fe-C alloy caused by MA has been reported to be 1.3 at.% (0.282 wt.%) [16].

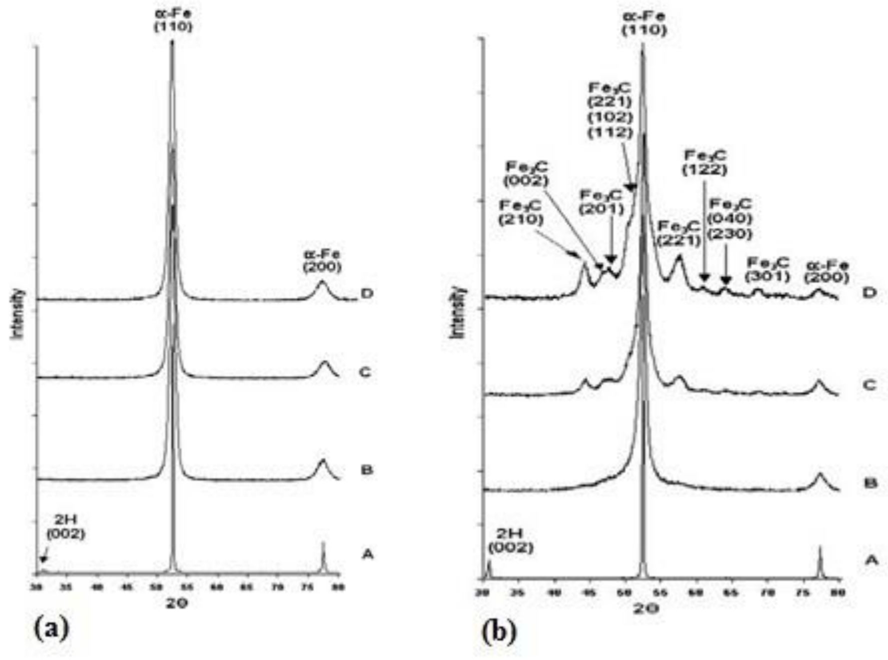

Fig. 2.11 X-ray diffraction of powder of (a) Fe-0.4 wt.%C, (b) Fe-6.67 wt.%C alloys versus milling time, A- 0, B - 25h, C - 75h, and D - 150h [52].

Thus, when the carbon concentration exceeded its limit, the rest of the carbon showed up as amorphous free graphite and amorphous Fe/C phase. Similar results were reported by Arik et al. [53], W. Ángel et al. [57], and Zuhailawati et al. [7]. Figure 2.12 shows the optical micrographs of Fe-1, 2, 3, 4 wt.%C alloys milled for 6h and sintered at 1150°C for 0.5h. It shows that the number and the size of the residual carbon regions are sometimes increased with the carbon concentration in the alloys [7].

The effect of carbon concentration on Fe-C alloys densities is presented in Fig. 2.13, which shows the green and sintered densities of Fe-C alloy samples with different carbon concentration [7]. During sintering, the porosity decreased that helped to improve the sintered samples' density compared to the green samples' density. It was found that both green and sintered samples densities decreased with carbon concentration and MA milling time. A possible explanation of this behavior, firstly, was that the increasing the hardness of the powder with carbon concentration which led to poorly compacted samples. Secondly, the residual carbon somehow hindered the sintering process by covering the surface of Fe particles, which impeded the atomic diffusion during sintering [53]. Theoretically, density is expected to decrease with carbon composition increase, but it is not clear in Fig. 2.13.

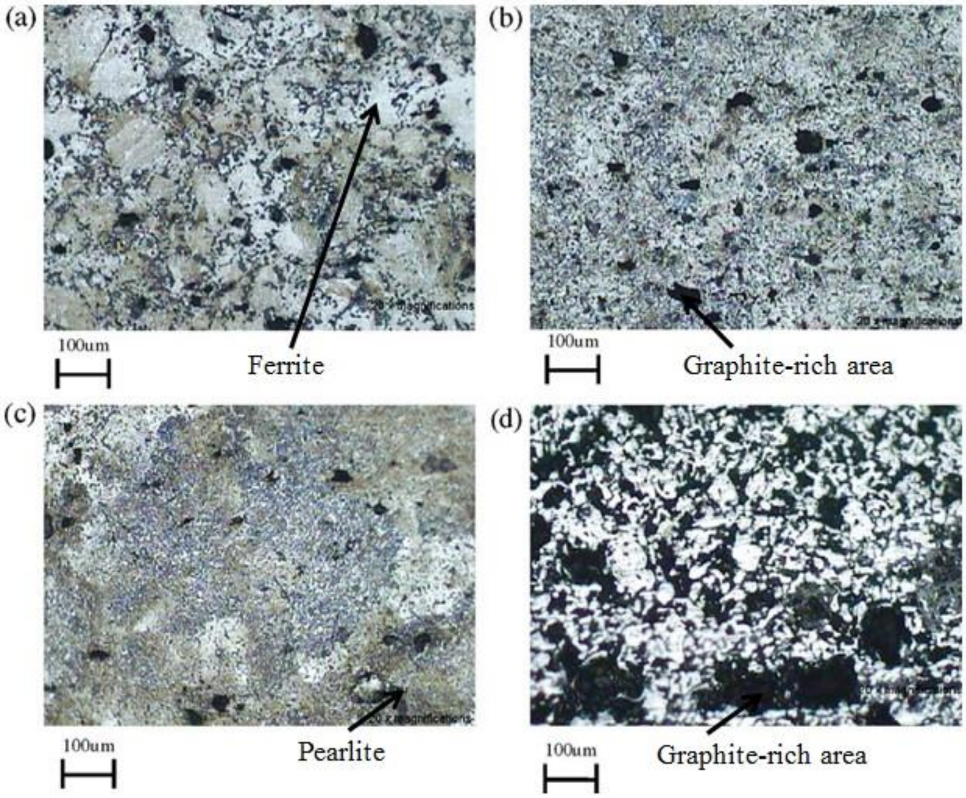

Fig. 2.12 Optical micrographs of Fe-C alloy with different carbon concentration: (a) 1 wt.%, (b) 2 wt.%, (c) 3 wt.% and (d) 4 wt.% . Iron and graphite milled for 6h and sintered at 1150°C for 0.5h. The black areas are residual carbon regions [7].

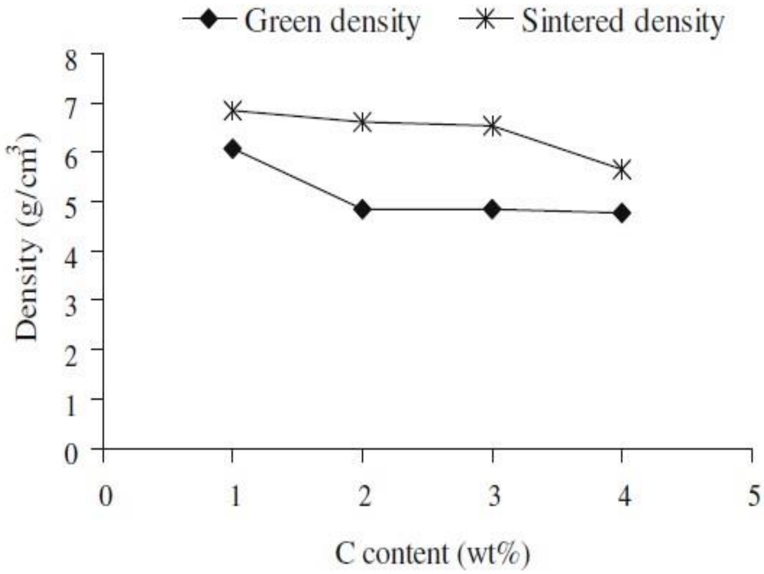

Fig. 2.13 Green and sintered densities of Fe–C alloys with different carbon concentration sintered at 1150°C for 0.5h [7].

It was found that an alloy's hardness depended on its microstructure and density. Ángel et al. [57] reported that hardness of Fe-C alloy increased to a maximum value and then peaked. Regardless of sintering temperature and time, hardness increased with carbon concentration. Alloys properties are affected by processing parameters such as compaction pressure, which correspondingly increased the density of the alloys. Figure 2.14 shows the microhardness of Fe-C alloys with different carbon concentration against compaction pressure. In general, hardness increased with carbon concentration. Also, the hardness increased and peaked with compaction pressure. Figure 2.15 illustrates hardness of Fe-C alloys with different carbon concentration. Contrary to the previous observation, Fig. 2.15 shows that hardness increased and then peaked when the carbon concentration exceeded 2 wt.% and carbon existed as graphite-rich regions. Figure 2.12 shows that the amount of graphite-rich regions increased with carbon concentration.

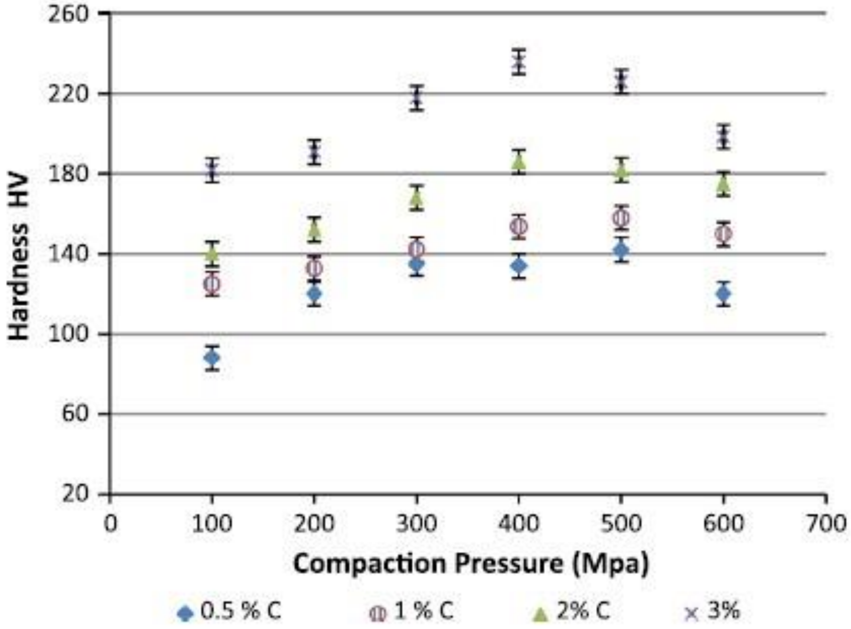

Fig. 2.14 Hardness of Fe-C alloys samples sintered at 1200°C for 0.5h plotted against compaction pressure [57].

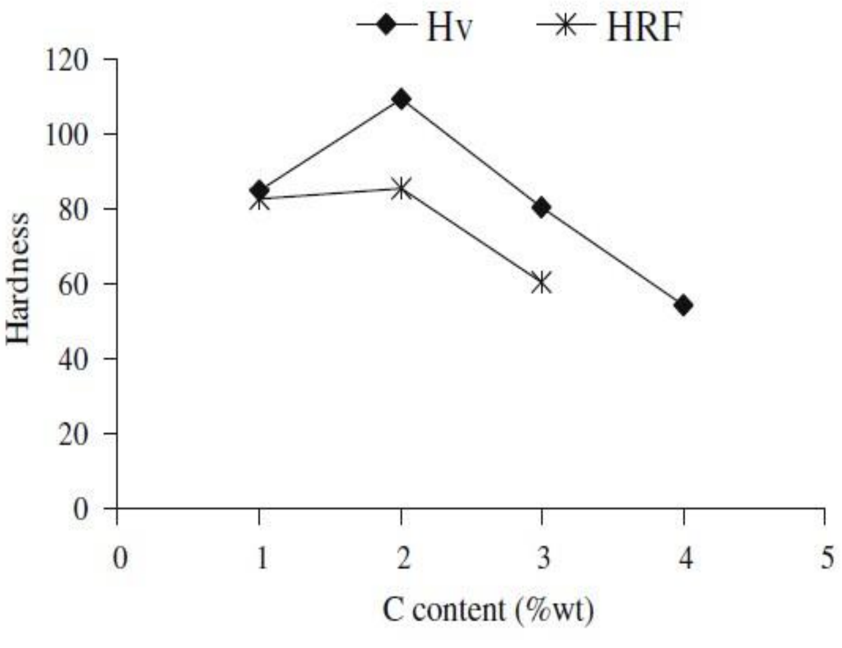

Fig. 2.15 Rockwell F (HRF) and Vickers hardness (Hv) of Fe-C alloy with different carbon concentrations sintered at 1150°C for 0.5h [53].

3 Experimental Procedures

The goal of this work was to further the understanding of the effects of MA milling time and carbon concentration on microstructural evolution, density, and hardness of sintered high-carbon Fe-C alloys. In the preliminary results of this work, the amount of Fe_3C decreased with milling time, contrary to what was found in the literature. Also, an exothermic peak around 300°C was detected in the powders milled for 5h and longer. In addition, an endothermic peak around 600°C was observed in powders milled for 0.5h and longer. The following experiments were designed to further the understanding the suppression of Fe_3C evolution with the milling time. Moreover, the experiments helped to explain what the origin of both the endothermic and exothermic peaks, which were detected in the milled powders of high-carbon Fe-C alloys.

Milling time, type of mill, and charge ratio are the main MA processing parameters on accomplishing the desired structure and properties [8]. In this work, the vibratory mill (SPEX shaker/mill) was used. Reduced elemental iron and graphite powders were mechanically alloyed in a SPEX mill with tungsten carbide milling media, cold-compacted, sintered and followed by furnace cooling. Milled powders and sintered samples were prepared using standard metallographic techniques and then characterized. In this work, the milled powders were characterized using X-ray diffraction (XRD), scanning electron microscopy (SEM) coupled with energy dispersive X-ray spectroscopy (EDS), differential scanning calorimetry (DSC), transmission electron microscopy (TEM), particle size analyzing, and Mossbauer spectroscopy. Sintered samples were also characterized using XRD, SEM, and TEM. Micro-hardness was measured for both milled powders and sintered samples. Density was measured for green compacted and sintered samples.

3.1 Powder and Sintered Samples Processing

3.1.1 Milling of Powders

Graphite powder was mechanically milled (Strem Chemicals, 99.999% purity, 70µm particle size) for 35h, to reduce the particle size and form nanoparticles. Iron powder (Alfa Aesar, 99 % purity, 140µm particle size) was reduced in a tube furnace under hydrogen gas flew at 500°C for 1h and followed by furnace cooling. Then, a mixture of the reduced iron and pre-milled graphite powders were milled for different times. The alloys' compositions are pointed in the phase diagram of $\mathrm{Fe} - \mathrm{Fe_3C}$ system (Fig. 3.1). The mechanical alloying process was carried out in a laboratory SPEX 8000 shaker/mill with tungsten carbide milling media and charge ratio (ball weight to powder weight) was 2:1. MA milling times of 0.5h, 5h, 40h and 100h were used to estimate the effect of milling time (the energy transfer to the powder) on microstructure, densification, and hardness of the alloys. Energy transfer during milling to the powder per hit was calculated as a function of milling time using Eq. (2.7) [40], as shown in Fig. 3.2. Tables 3.1, 3.2 and 3.3 summarized the test matrixes (milling times and sintering temperatures). The handling of the powders and the sealing of the vial were performed under an argon atmosphere in a glove box to minimize oxidation during milling.

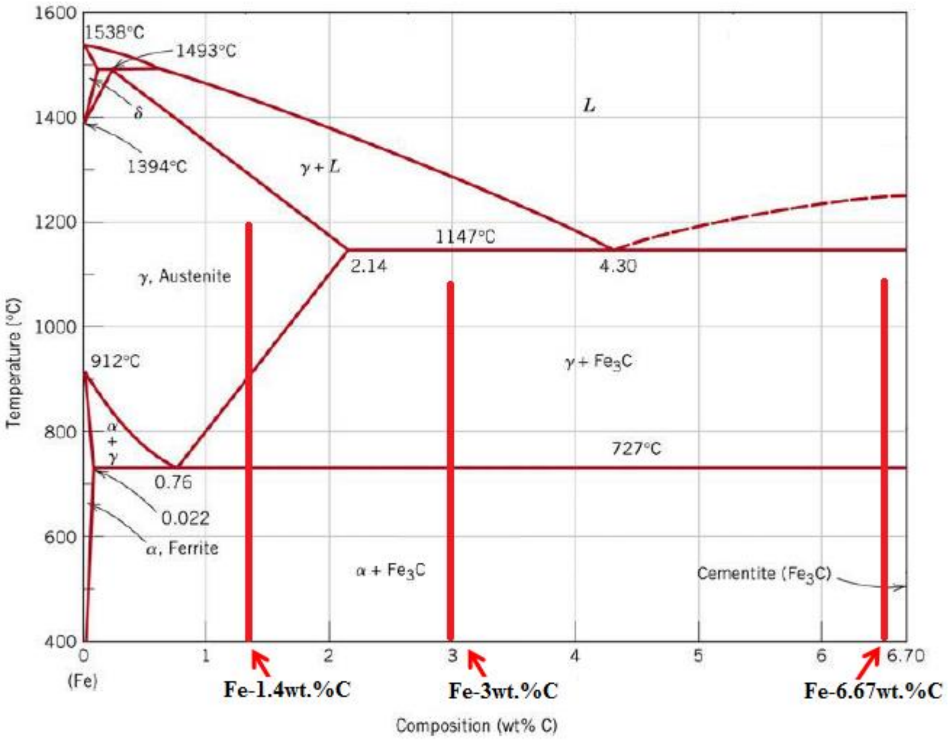

Fig. 3.1 Phase diagram of Fe-Fe_3C system shows the alloys composition [60].

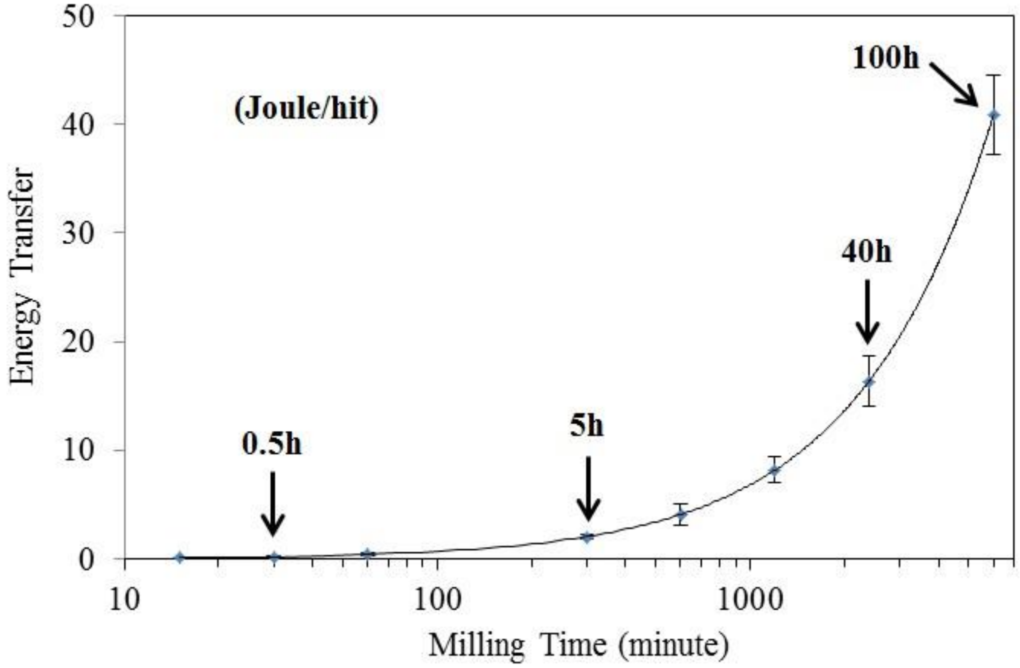

Fig. 3.2 Energy dissipated per hit plotted against milling time when using SPEX mill. The calculation was done using Eq. (2.7).

Table 3.1: Milling times and sintering temperatures test matrix of Fe-1.4 wt.% C alloy

Sintering Temperature (°C)	Milling Time			
	Hour			
	0.5	5	40	100
900	×	×	×	×
1000	×	×	×	×
1100	×	×	×	×
1200	×	×	×	×

Table 3.2: Milling times and sintering temperatures test matrix of Fe-3 wt.% C alloy

Sintering Temperature (°C)	Milling Time			
	Hour			
	0.5	5	40	100
900	×	×	×	×
1000	×	×	×	×
1100	×	×	×	×

Table 3.3: Milling times and sintering temperatures test matrix of Fe-6.67 wt.% C alloy

Sintering Temperature (°C)	Milling Time			
	Hour			
	0.5	5	40	100
900	×	×	×	×
1000	×	×	×	×
1100	×	×	×	×

3.1.2 Cold-Compaction and Sintering

After milling, the powders were cold-compacted into coins of 12.7mm in diameter, and around 3mm thickness in a uniaxial steel mold at 550 MPa stress using a uniaxial press and held for 5 minutes. The cold-compacted samples were then sintered (pressure-less sintering) in a tube furnace under 90% argon and 10% hydrogen atmosphere at ranging temperatures between 900°C and 1200°C for 1h and 5h. Sintering temperatures were selected based on the alloy composition and the nature of the Fe-Fe_3C phase diagram. After sintering, samples were furnace cooling to room temperature under the flow of hydrogen and argon gases to minimize oxidation of the samples during cooling.

3.1.3 Sample Preparation for Characterization

After sintering, the density was measured, and then the XRD was performed. The sintered samples were cut and mounted. Mounted samples were prepared for SEM and hardness testing using standard metallographic techniques.

3.2 Milled Powders and Sintered Samples Characterization

Milled powders and sintered samples were characterized to assess the effect of MA milling time and sintering processes (temperature and time) on microstructural evolution, densification, and hardness of high carbon Fe-C alloys.

3.2.1 X-ray Diffraction (XRD)

XRD was used to examine both milled powders and sintered samples of the high carbon Fe-C alloys. XRD was done using a PANalytical X'Pert Pro powder diffractometer with a Bragg angle (2θ) range from 20° to 90°. X-rays generated by a Cu source by using 45KV and 40mA. The sample stage rotated at one revolution per second. Each sample was run twice in the diffractometer. The XRD data was profile fitted using X'Pert High Score Plus software before calculations. Lattice parameter, crystallite size, and lattice strain were calculated as follows:

a. Lattice Parameter

Lattice parameter was calculated for as-received, milled powders, and sintered samples. The diffraction angle is associated with a d-spacing d_{hkl} and lattice parameters were calculated using the d-spacing data. Lattice parameters were calculated based on the three α-Fe planes, (110), (200), and (211), with two XRD runs per sample using Eq. 3.1 [61]. Thus, α-Fe lattice parameter for each sample was the average of six estimates.

$$a_{\alpha-Fe} = d_{hkl} * \sqrt{h^2 + k^2 + l^2} \tag{3.1}$$

where $a_{\alpha-Fe}$ is lattice parameter, d_{hkl} is d-spacing, *hkl* are planes generating the peak. Table 3.4 shows the three primary α-Fe peaks between 20° and 90° and their respective planes, d-spacing, relative intensity, and full width at half maximum (FWHM).

Table 3.4: Primary α-Fe XRD peaks

Position (°2θ)	Generating Plane (hkl)	d-Spacing (Å)	Relative Intensity	FWHM (°2θ)
44.752	(110)	2.0251	100.00	0.2480
65.109	(200)	1.4326	12.77	0.3306
82.419	(211)	1.1692	21.58	0.5040

According to E. Fasiska et al. [62], the relation between the lattice parameters and the carbon content of solid iron solution can be expressed by the following equation (Eq. 3.2):

$$a_{\alpha-Fe} = 2.8664 + 0.0387761\,X \tag{3.2}$$

where $a_{\alpha-Fe}$ is the lattice parameter (Å) of dilated α-Fe and X is the carbon concentration of iron solid solution (wt.%). Plots of lattice parameter and carbon concentration against milling time were generated for the three high-carbon Fe-C alloys. The plots illustrated the effect of milling time on the amount of dissolved carbon in α-Fe for both milled powders and sintered samples.

b. Williamson-Hall Plots

Williamson-Hall plots were also used to analyze peak broadening as a function of milling time and diffraction angle. The contributions of peak broadening to crystallite size and lattice strain can also be separated using a Williamson-Hall plot as defined in Equation 3.3 [63].

$$\beta_{strain+size} * \cos\theta = \eta \sin\theta + \frac{k\lambda}{d} \qquad (3.3)$$

where $\beta_{strain+size}$ is the peak broadening due to crystallite size and lattice strain, θ is one half of the diffraction angle 2θ, η is the lattice strain, *d* is the crystallite size, *k* is the shape factor assumed to be 0.9, and λ is the wavelength of the X-ray (0.15418nm).

FWHM * cos (θ) vs. sin (θ) was plotted for each sample. A best-fit-line was generated for each set of points. The slope of that fit-line represents η (lattice strain) and y-intercept equals $\frac{k\lambda}{d}$. Thus, *d* (crystallite size) was solved from $\frac{k\lambda}{d}$. Plots of lattice strain and crystallite size were generated as a function of milling time for milled powders. These plots illustrated the effect of milling time on crystallite size of the powder and the amount of the plastic deformation which caused by ball milling.

3.2.2 Particle Size Analysis

The particle size distribution was measured for the milled powders using a Horiba LA-950 Laster Diffraction Particle Size Distribution Analyzer to assess the effect of MA milling time on the particle size distribution. Three runs were tested for each sample to ensure confidence in the results. Plots were generated as a function of MA milling time. SEM was also used to image and determine the shape of the milled powder particles. Particle size distribution plots and particles shape explained the effect of the powder particle size distribution on the powder compaction process which affected the sintered samples' density.

3.2.3 Chemical Composition

The chemical composition of selected sintered samples was determined to estimate the loss of carbon during processing. This test was performed using Bruker Q4 Tasman advanced CCD-based optical emission spectrometer (Fig. 3.3).

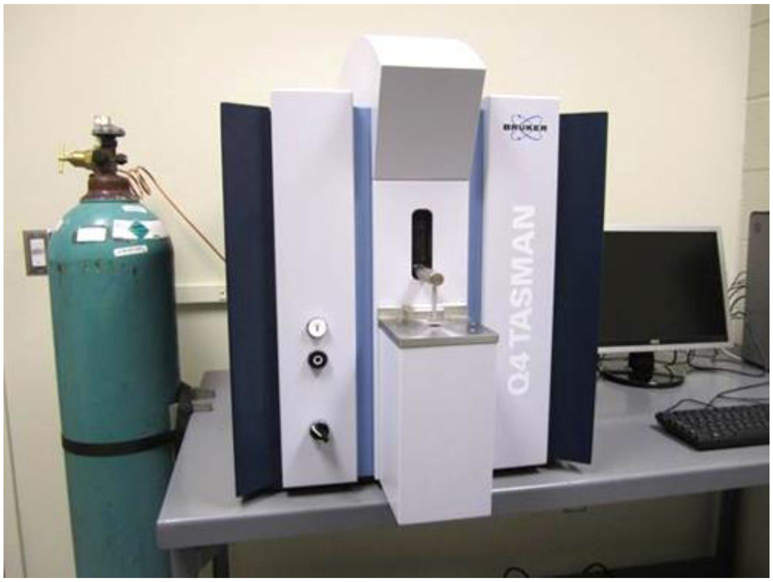

Fig. 3.3 Bruker Q4 Tasman advanced CCD-based optical emission spectrometer.

3.2.4 Differential Scanning Calorimetry (DSC)

Differential scanning calorimetry (DSC) was used to monitor heat effects associated with phase transitions as a function of temperature for the milled powders. The goal of using this technique was to find better explanation for the phase transitions. Three runs for each sample were performed at a heating rate of 10 K/min. The focus was only on the heating cycle. The temperatures ranging was between 200°C and 850°C. After that, DSC curves, which are curves of heat flux versus temperature, were generated for different samples. In the DSC, the focus was on the effect of milling time and carbon concentration on the exothermic peak around 300°C and the endothermic peak around 600°C. To verify the DSC results, selected milled powders samples were annealed enclose reactions observation in the DSC and then furnace cooling.

3.2.5 Density Measurements

First, the density was measured for the green compacts. This step helped to assess the effect of particles size and shape on the green compact's density. Second, the density of the sintered samples was measured to estimate the effects of MA milling time, carbon concentration, and sintering temperature and time. The density measurements were performed using Archimedes' principle. Archimedes' density approach takes the weight of the green compact sample in air (W_{air}) and then in ethanol ($W_{ethanol}$) at room temperature. The densities of air (ρ_{air} = 0.0012 g/cc) and ethanol ($\rho_{ethanol}$ = 0.79 g/cc) were used to determine the density of the green compacts and sintered samples using Equation 3.4 [64].

$$\rho_{measurement} = \frac{W_{air}}{(W_{air}+W_{ethanol})} * (\rho_{ethanol} - \rho_{air}) + \rho_{air} \qquad (3.4)$$

For comparison, the theoretical density was calculated by using Equation 3.5 [65].

$$\rho_{th} = \frac{100}{\frac{C_{Fe}}{\rho_{Fe}} + \frac{C_C}{\rho_C}} \qquad (3.5)$$

where C is the concentration of each alloy element and ρ is the density of each element, ρ_{Fe} (7.87 g/cc) and ρ_C (2.267 g/cc) were used to calculate the theoretical density. Table 3.5 includes theoretical densities the Fe-C alloys.

Table 3.5: Theoretical density of high-carbon Fe-C alloys

Alloy Composition	Theoretical Density (g/cc)
Fe-1.4 wt.% C	7.61
Fe-3 wt.% C	7.33
Fe-6.67 wt.% C	6.76

3.2.6 Scanning Electron Microscopy (SEM)

Selected milled powders and sintered samples were imaged using FEI Quanta 600 FEG environmental scanning electron microscope (ESEM) coupled with energy dispersive X-ray spectroscopy (EDS). The goal of this technique was to estimate the microstructure and the porosity of sintered samples. The samples were mounted, ground, polished, and then etched at room temperature (etchant: 4 ml HNO_3 and 96 ml ethyl, etching time: 20 sec to 1 min). Images with low and high magnification were taken to assess the microstructural evolution, which resulted from varying MA milling time and sintering temperature and time.

3.2.7 Transmission Electron Microscopy (TEM)

Slices of selected sintered samples were ground to a thickness of approximately 100μm. From this thin slice a disc 3mm in diameter was cut using a Gatan ultrasonic cutter. This smaller disc was further thinned a thickness of about 30μm and then ion milled with a Fischione Model 1010 until a hole roughly 100μm in diameter had formed. The sample was then examined by a JEOL 2100 TEM at 120kV. The JEOL 2100 TEM was used to detect the presence cementite (Fe_3C) particles through bright and dark field micrographs and selected area diffraction patterns. As for the milled powders, selected samples were imbedded in epoxy then microtome by a RMC Cryo Ultramicrtome. Once thin sections have been cut from the sample block, the sample was viewed under the TEM by a JEOL 2100 TEM at 120kV.

3.2.8 Hardness Testing

Sintered samples were cut, mounted, ground, and polished for hardness testing. Hardness testing was used to estimate the effects of MA milling time, carbon concentration, and sintering temperature and time on hardness of the high-carbon Fe-C alloys. Hardness testing was performed using a Phase II Micro Vickers Hardness Tester at load 0.98N and dwell time 15 seconds. At least five measurements were taken per sample for statistical reliability. Plots of the average hardness values against MA milling time for different sintering temperature and time were generated. Milled powders were also mounted, ground, and polished. After that, the hardness was measured for the milled powders to determine the effect of milling time. The hardness values led to an explanation of the effect of the hardness of the milled powders on the green compact's density and its effect on the sintered sample density.

3.3 Summary of the Experimental Procedures

Mechanical alloying and powder metallurgy methods were used in this work to prepare sintered samples of high-carbon Fe-C alloys. Mixtures of reduced elemental iron and pre-milled graphite were milled for up to 100h. Tables 3.1 through 3.3 summarized the mechanical alloying milling time and sintering temperature and time. Milled powders were characterized using XRD, SEM, TEM, Mossbauer spectroscopy, and micro-hardness testing. Milled powders were compacted and then sintered at temperatures ranging between 900°C and 1200°C for 1h and 5h followed by furnace cooling. Sintered samples were characterized using XRD, SEM, TEM, micro-hardness testing. Densities of green compaction and sintered samples were measured.

4 Powder Processing and Characterization of Mechanically Alloyed High-Carbon Fe-C Alloys

4.1 Abstract

The effects of milling time and carbon concentration on phase transformation, particle size, thermal behavior, and hardness of the milled powders of high-carbon Fe-C alloys were investigated. Mixtures of elemental powders of iron and 1.4, 3, and 6.67 wt.% pre-milled graphite were milled in a SPEX mill for up to 100h. The milled powders were then characterized using X-ray diffraction, differential scanning calorimetry, Mossbauer spectroscopy, scanning and transmission electron microscopes, and micro-hardness testing. The particles size of the milled powders decreased and tended to become more equi-axed after 100h of milling. Micro-hardness of milled powders drastically increased with milling time as well as carbon concentration. Exothermic and endothermic peaks around 300°C and 600°C were detected in milled powders, respectively. The transformation temperatures of both peaks decreased with milling time. The exothermic peak was due to the recrystallization and/or recovery α-Fe and growth of Fe_3C, while the endothermic peak was due to the formation of Fe_3C phase. Based on Mossbauer spectra, the formation of Fe_3C was observed in milled powders after 5h of milling and its amount increased with milling time and carbon concentration.

4.2 Introduction

Mechanical alloying (MA) has become a popular alloying technique since its development by John Benjamin and his coworkers in 1960s [8]. MA is a solid state powder processing technique involving repeated cold-welding, fracturing, and rewelding of a metal powder mixture. MA is generally performed in a high-energy ball mill in an inert atmosphere.

During milling, the powder particles are trapped between colliding balls or balls with vial walls. The force of the impact plastically deforms the powder particles leading to work hardening and fracture [66]. MA has also been known as one of the best processing techniques to produce materials with homogeneously distributed composite particles in a metal matrix. Alloying by the MA process avoids many problems that are associated with conventional melting and solidification methods [67]. MA has been found to be an effective technique for processing metal alloys such as Fe-C alloys with very high carbon concentration, which are difficult to be produced with conventional methods such as casting [52]. Producing high-carbon Fe-C alloys with fine microstructures and unique properties by MA has attracted the attention of many research groups. A number of research groups have studied the effects of MA processing parameters on the microstructural evolution and the properties of high-carbon Fe-C alloys [6, 7, 9, 11-13, 52, 53, 68].

Most of this work is on the milling of the powders and their characterizations, including the dissolution of the starting elements in each other, the microstructure and hardness of the particles, and mechanochemical reactions. For example, Yong-Goo Yoo et al. [12] studied the effect of alloying time on the structural evolution of mechanically alloyed Fe-C alloys. The MA process was performed in a SPEX mill with stainless steel milling media. In their results, they found that the increase of Fe_3C phase and the decrease of bcc-Fe phase took place in the powder with alloying time. Also, Fe-C amorphous phase was observed in the milled powders after 24 h. S. J. Campbell et al. [14] investigated the formation of Fe_3C and Fe_7C_3 compounds in $Fe_{75}C_{25}$ alloy using ball milling process. Iron and graphite were milled for up to 285h in Uni-ball mill under vacuum. An exothermic peak was observed around 320°C in milled powders for 45h and disappeared after 140h. They believed that an amorphous Fe_3C was formed after 45h and with continued milling the crystalline $\mathrm{Fe_3C}$ was eventually formed as a result of thermally activated crystallization after 140h. In these two examples, different characteristic powders were produced even in the same alloy composition.

This work is the first part of a study dealing with the effect of powder morphology on the microstructure and mechanical properties of parts densified from mechanically alloyed high carbon Fe-C alloys. The effect of temperature on the milled powders is also studied.

4.3 Materials and Methods

High-purity graphite powder (99.999% purity and $<$ 2μm particle size) was mechanically milled for 35h. Reduced elemental iron (99.8% purity and 70μm particle size) powder was mixed with pre-milled graphite powder in weight percentages of 1.4, 3, and 6.67. The mixture was then mechanically alloyed for up to 100h. The mechanical alloying process was performed in a laboratory SPEX mill with tungsten carbide milling media. The ball-to-powder mass ratio was 2:1. The milling was conducted at room temperature and under argon atmosphere to minimize oxidation during milling. Identification of phases was performed by X-ray diffraction (XRD) in a PANalytical X'Pert Pro powder diffractometer using filtered CuKα radiation at 45kV and 40mA and the 2θ range of 20°-90° and by Mossbauer measurements on a Ranger Scientific Mossbauer Spectrometer using the γ ray source of ^{57}Co. In addition, the evolution of the powder morphology and its chemical homogeneity were studied by a scanning electron microscopy (SEM, FEI Quanta 600 FEG) coupled with energy dispersive X-ray spectroscopy (EDS). Transmission electron microscopy (TEM, JEOL 2100) was used to determine the compositional and the crystalline information of milled powders. Selected samples of the milled powders were imbedded in epoxy then microtome by a RMC Cryo Ultramicrtome. Once thin sections have been cut from the sample block, the sample was viewed under the TEM by a JEOL 2100 TEM at

120kV. Particle size distribution of the milled powders was measured using a Horiba LA-950 Laster Diffraction Particle Size Distribution Analyzer. The milled powders were analyzed using a differential scanning calorimeter (DSC, NETZSCH 404) under a flowing purified argon gas atmosphere at heating of 10K/min to 850°C in an alumina container. To verify the DSC results, selected milled powder samples were annealed before and after reactions observation in the DSC. Subsequently, the structure of the samples was evaluated by XRD and TEM. Vickers micro-hardness measurements were made on a Phase II Micro Vickers Hardness Tester using an indentation load of 0.98N for dwell time 15 seconds. Each individual measurement was an average of five different measurements.

4.4 Results and discussion

4.4.1 Structural characterization

Representative XRD profiles of as-received and mechanically alloyed powders as a function of milling time are shown in Fig. 4.1 for Fe-1.4 wt.%C alloy. The primary graphite peak (002) disappeared quickly after only 0.5h of milling. The α-Fe peaks broadened and shifted to lower angles with milling, indicating grain refinement and dissolution of carbon into ferrite, respectively with milling time. Graphite was brittle and hence much easier to refine its particles. Peak broadening would, therefore, be swift in the MA process. Additionally, because the carbon had a smaller atomic scattering factor than iron was not picked up after a short period of milling. Some researchers believed that amorphization of carbon occurred in the milling stage, hence making it harder to detect the graphite peak [7, 9, 52]. The XRD profiles of milled powders of Fe-3 and 6.67 wt.%C alloys were similar to the XRD profiles of Fe-1.4 wt.%C alloy. Other researchers have detected Fe_3C in mechanically alloyed powders of high-carbon Fe-C alloys by XRD [11-13, 15, 52]. No Fe_3C was observed in all the milled powders of the three alloys, studied in this work. It was possible that the detector (PW3015/20 X'Celertator) used in this work was not sensitive enough to pick up Fe_3C phase. Another possible reason was that the amount of Fe_3C was not large enough to be detected and, as stated above, Fe_3C particles could be very fine, and its broad peaks could be hidden in the background noise.

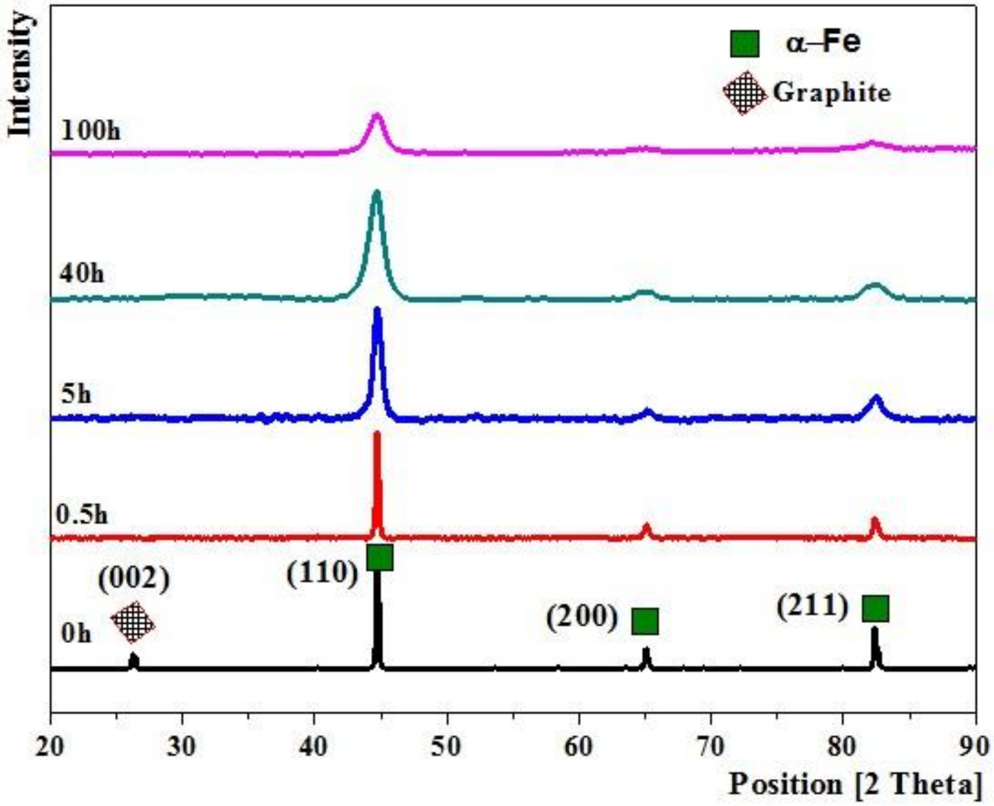

Fig. 4.1 X-ray diffraction profiles of Fe-1.4 wt.%C alloy as-received and milled powders.

The lattice parameter (a) of iron solid solution (α-Fe) was calculated for both as-received and milled powders to estimate the effects of MA milling time and carbon concentration. The lattice parameter of α-Fe phase calculation was based on (110), (200), and (211) planes using Equation (4.1) [61].

$$a_{\alpha-Fe} = d_{hkl} * \sqrt{h^2 + k^2 + l^2} \tag{4.1}$$

where $a_{\alpha-Fe}$ is lattice parameter, d_{hkl} is d-spacing, hkl are planes generating the peaks. The average lattice parameters and carbon concentration of α-Fe of the as-received and milled powders were plotted as a function of milling time as shown in Fig. 4.2. In all milled powders, the lattice parameter of α-Fe increased with milling time and at a faster rate for higher carbon concentrations. The carbon concentration of α-Fe of milled powders was calculated from Equation (4.2) [62].

$$a_{\alpha-Fe} = 2.8664 + 0.0387761\, X \qquad (4.2)$$

where $a_{\alpha-Fe}$ is the lattice parameter (Å) of dilated α-Fe and X is the carbon concentration of the solid iron solution (wt.%). Lattice parameter and carbon concentration both were plotted as a function of milling time in Fig. 4.2. In mechanical alloying, interdiffusion between elemental components occurred, and solid solutions formed. A major result of MA was the extension of the sold solubility in many metal alloys [8]. In all milled powders, the amount of carbon dissolved in α-Fe tended to approach 0.15 wt.% after 100h of milling. This was much higher than 0.02 wt.% maximum amount of carbon dissolved in stable α-Fe phase at 727°C. The amount of carbon dissolved increased by varying the MA processing parameters such as milling temperatures, charge ratio, or mill type. For instance, Literature showed that the amount of carbon dissolved in α-Fe reached about 0.28 wt.% after 100h of milling. The milling was carried out at 50°C [16], while this work was conducted at room temperature.

XRD data was also used to analyze peak broadening by the Williamson-Hall method to observe the degree of strain in the α-Fe lattice as well as the crystallite size. A Williamson-Hall plot allows one to separate out the contributions from peak broadening (crystallite size) and strain by the following relation (Eq.4.3) [69].

$$\beta_{strain+size} * \cos\theta = \eta \sin\theta + \frac{k\lambda}{d} \qquad (4.3)$$

where $\beta_{strain+size}$ is the peak broadening due to crystallite size and lattice strain, θ is one half of the diffraction angle 2θ, η is the lattice strain, *d* is the crystallite size, *k* is the shape factor assumed to be 0.9, and λ is the wavelength of the X-ray. Figure 4.3 shows the variation in the crystallite size and the lattice strain as a function of milling time for high-carbon Fe-C milled alloys powders. There were roughly consistencies between the SEM (Fig. 4.7) and TEM micrographs (Fig. 4.8) and Williamson-Hall calculations.

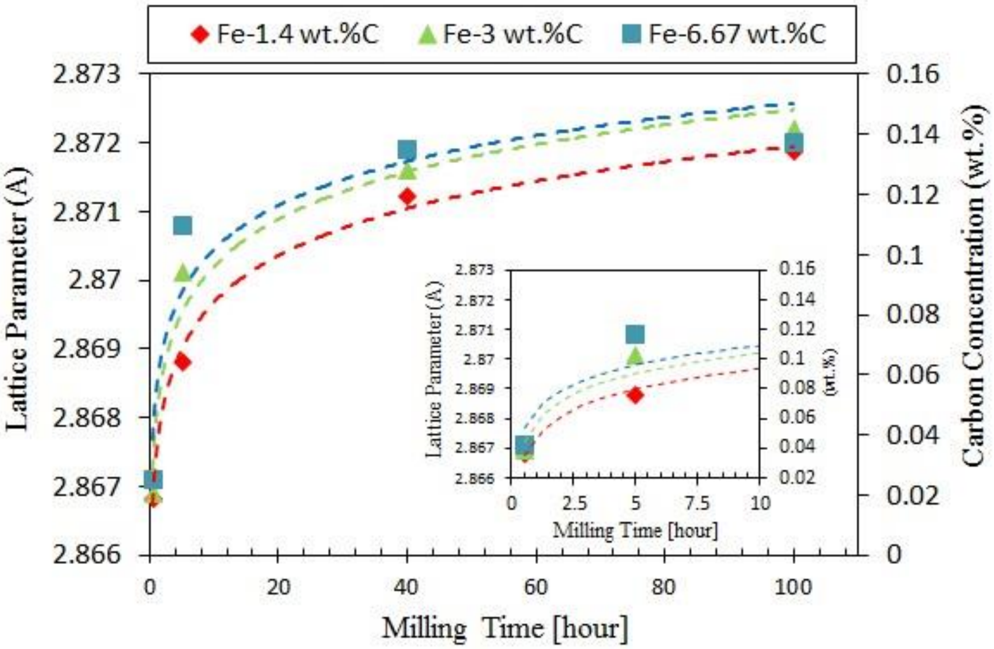

Fig. 4.2 Lattice parameter of α-Fe (calculated from the {110}, {200}, and {210}) and the amount of carbon dissolved in the crystalline α-Fe as a function of milling time for high-carbon Fe-C alloys.

The average crystallite size markedly decreased and reached its steady-state after 40h of milling. Increase in carbon content of the powder seemed to affect the reduction of the crystallite size of α-Fe with milling time, higher carbon alloys had smaller crystallite size. The brittle ceramic graphite particles assisted in the grain size refinement. The lattice stain of α-Fe also increased and approached a steady-state after 40h. The rate of strain increase was very rapid in the beginning of milling and then slowed down. The lattice strain increase was related to dislocation density increase with milling time [70]. After 40h of milling most of the alloying as evident by lattice parameter and grain size refinement had occurred.

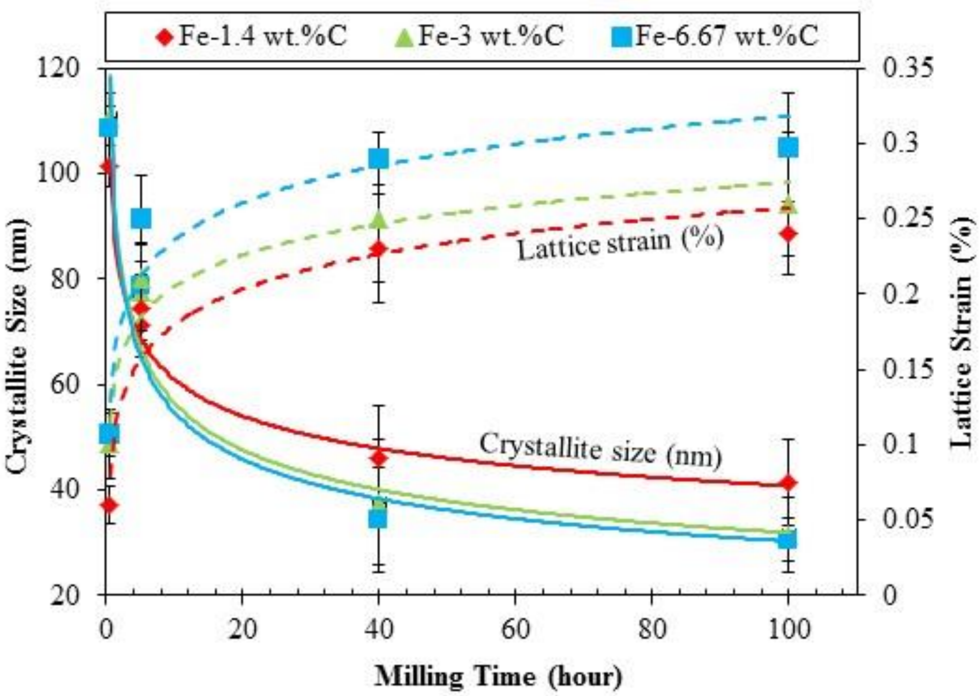

Fig. 4.3 Crystallite size (solid lines) and lattice strain (dashed lines) α-Fe in high-carbon Fe-C milled alloys powders as a function of milling times as determine from Williamson-Hall method.

Mossbauer spectra were used to analyze the alloy formation process. The room temperature Mossbauer spectra taken at different alloy composition and milling times are shown in Fig. 4.4. The Mossbauer spectra were first fitted using a hyperfine field distribution. Then, according to the best refinement, all the spectra were described by the mixture of α-Fe and Fe_3C. As for the 0.5 hour alloyed sample, the Mossbauer spectrum showed that only α-Fe phase was observed, while α-Fe and Fe_3C phases were detected after 5h of milling as shown in Fig. 4.4a. No amorphous phase was observed in the Mossbauer spectra. Figure 4.5 exhibits the variation of area fraction for α-Fe and Fe_3C phases that were estimated from the Mossbauer spectra of the mechanically milled of the alloys. It was obvious that (in the milled powders of Fe-1.4wt.%C alloy) the amount of Fe_3C increased to reach about 30% after 100h of milling (Fig. 4.5a). Figure 4.5b shows that the amount of Fe_3C increased with carbon concentration in the milled for 40h. At the same milling time, it was clear that the amount of Fe_3C phases increased from around

21% in Fe-1.4 wt.%C to about 62% in Fe-6.67 wt.%C milled powders. With the Mossbauer spectra analysis, it was now obvious that Fe_3C formation took place even though this was not evident in the XRD analysis.

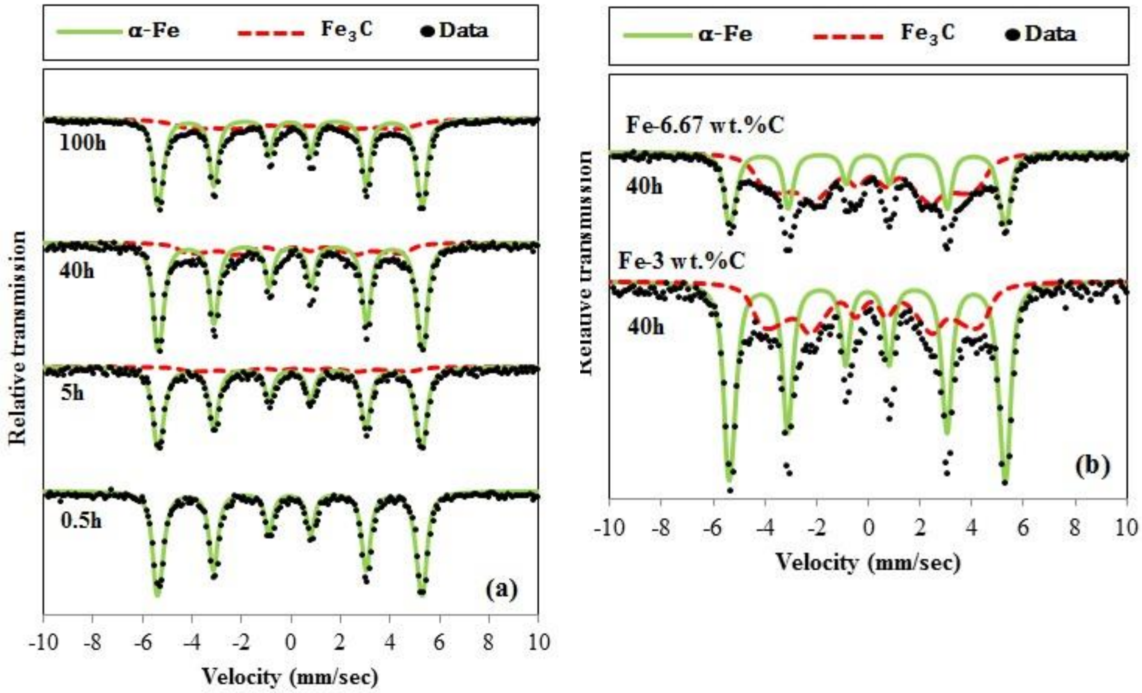

Fig. 4.4 Room temperature Mossbauer spectra of (a) Fe-1.4 wt.% C and (b) Fe-3 and 6.67 wt.% C powders mechanically alloyed for several times.

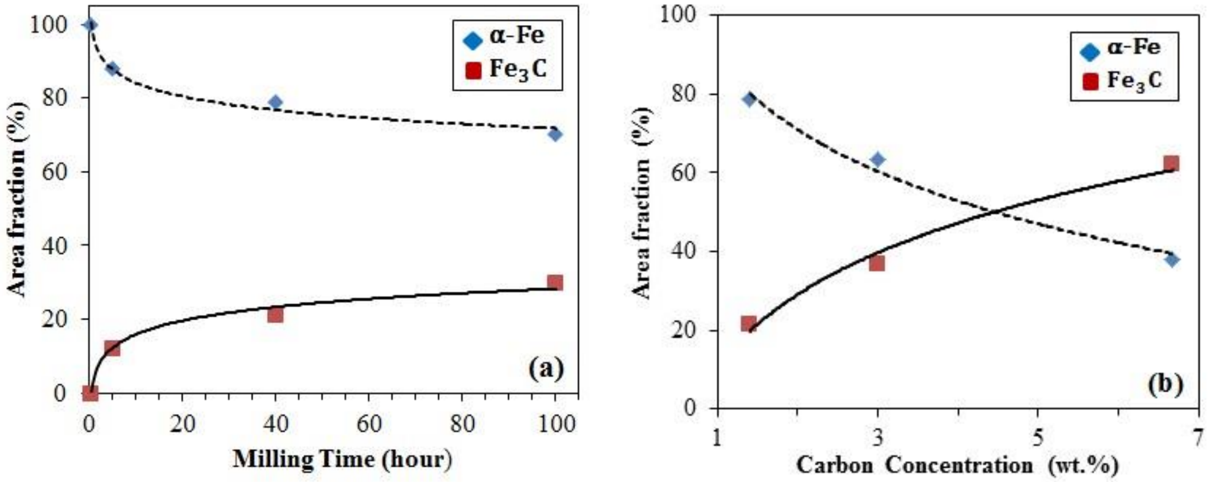

Fig. 4.5 Area fraction (area under the curve) estimated from Mossbauer spectra of (a) milled powders of Fe-1.4 wt.% C alloy with milling time; (b) milled powders for 40h of Fe-1.4, 3, and 6.67 wt.% C alloys.

Particle size analyzer and SEM were used to assess the effect of milling time on the particle size distribution and the morphology of the milled powders. Figure 4.6 illustrates the particle size distribution of the milled powders of the three high-carbon Fe-C alloys as a function of milling time. The particle size increased to maximum values between 160µm and 230µm after 0.5h and then dropped to steady state values of between 20µm and 30µm for the three alloys. Overall the higher the carbon concentration of the alloy, the smaller the particles would be. The representative SEM micrographs of milled powders of Fe-1.4 wt.%C alloy are shown in Fig. 4.7. After 0.5 h of milling, particles appeared as composite of graphite and Fe and were deformed and flattened, as shown in Fig. 4.7a. With continued milling and the accumulation of deformation strain, powder fracture events increased and eventually dominate welding events leading to powder particles becoming finer and equiaxed.

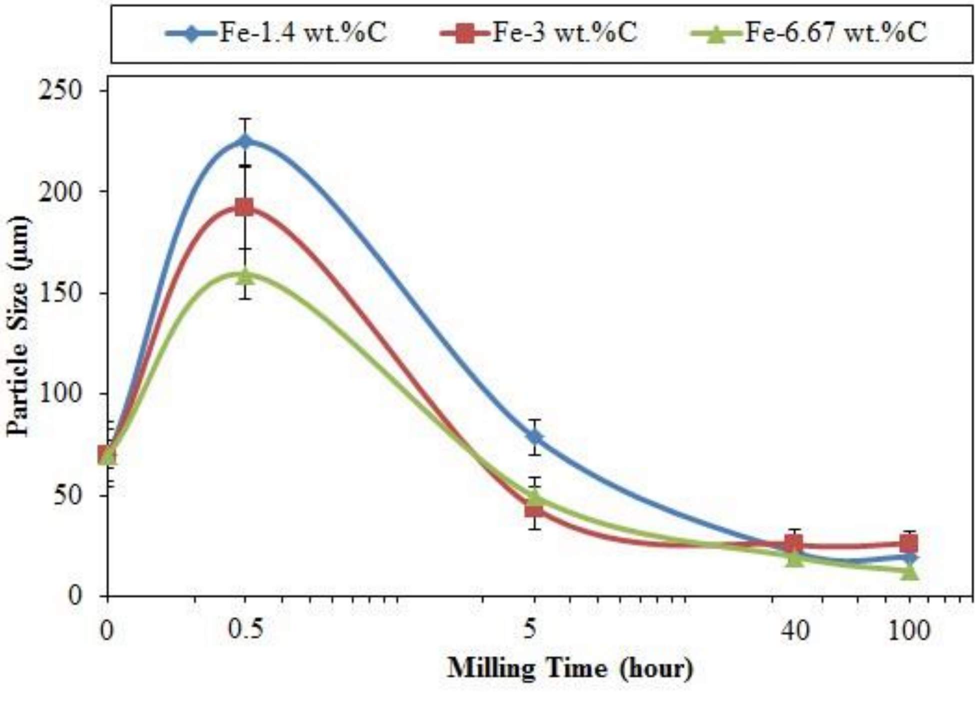

Fig. 4.6 Average particle size of milled powders of Fe-1.4, 3, and 6.67 wt.%C alloys against milling time.

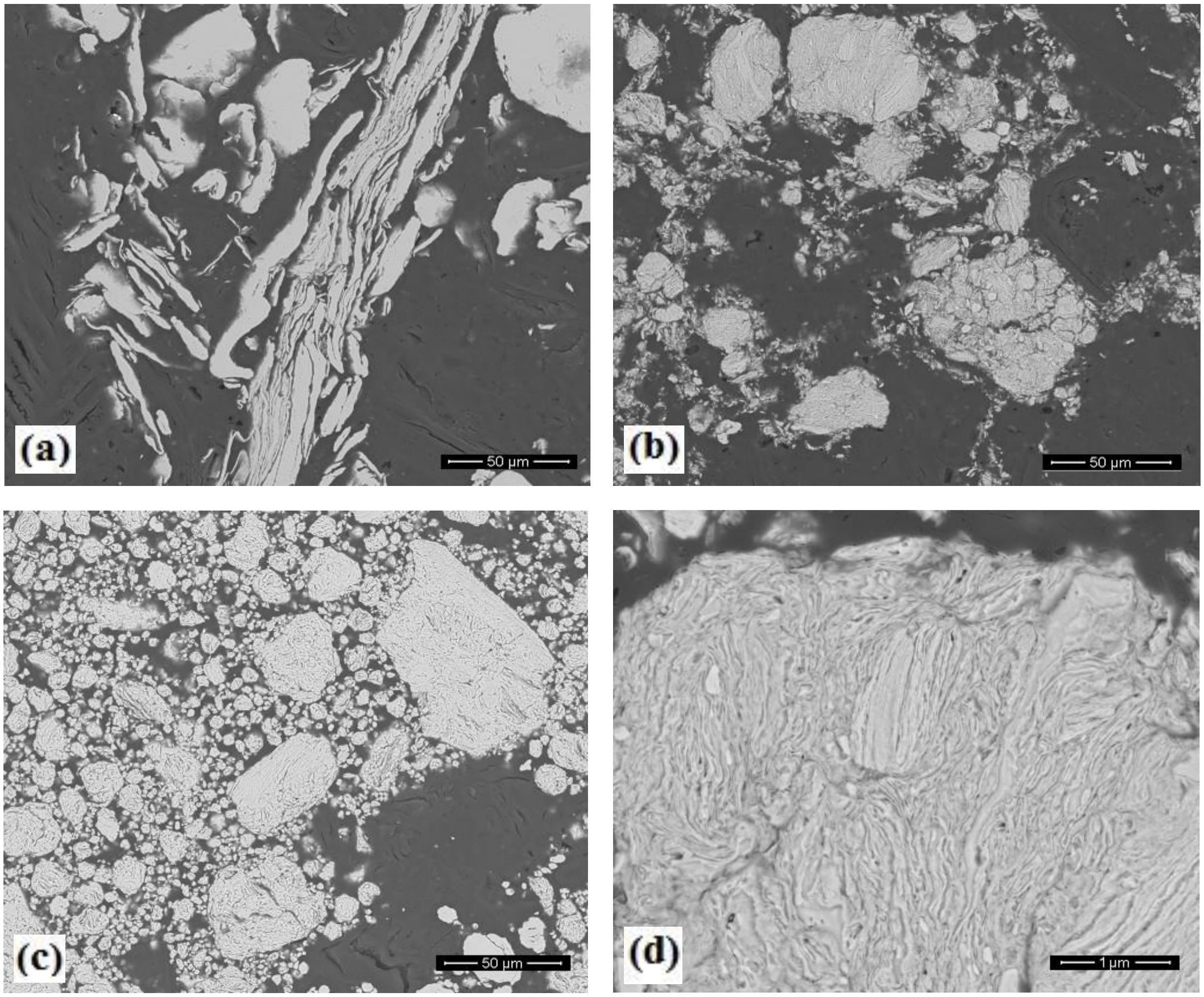

Fig. 4.7 SEM micrographs showing the evolution of microstructure in mechanically alloyed Fe-1.4 wt.%C alloy. The powders milled for (a) 0.5h, (b) 5h, (c) 40h, (d) 100h. The brighter regions are mixture of Fe-C and the darker areas are conductive mounting. Etchant: 4% nital.

Microstructural examinations were conducted for selected milled powders by TEM using JEOL 2100. A representative TEM bright filed micrograph and its corresponding selected area electron diffraction (SAED) pattern obtained for Fe-1.4 and 6.67 wt.%C powders milled for 100h are shown in Fig. 4.8. The bright field micrograph displayed nanocrystalline α-Fe and Fe_3C. It has been reported that nanocrystalline α-Fe and Fe_3C or an amorphous α-Fe phase was observed in mechanically milled Fe-C powders [8, 26, 71-73]. The formation of theses phases was found to be critically dependent on the milling conditions such as milling time and ball-to-powder weight ratio [8]. The selected area electron diffraction pattern for the 1.4 wt.%C alloy showed a large number of continuous diffraction spots, arranged along the Debye's circles (Fig. 4.8a). After analyzing these diffraction spots, it was found that they belong to α-Fe and Fe_3C (Fig 4.8a top left). This result was supported by the Mossbauer spectra (Fig. 4.4a). Figure 4.8b exhibits that the Fe_3C was also observed in Fe-6.67 wt.%C powders milled for 100h.

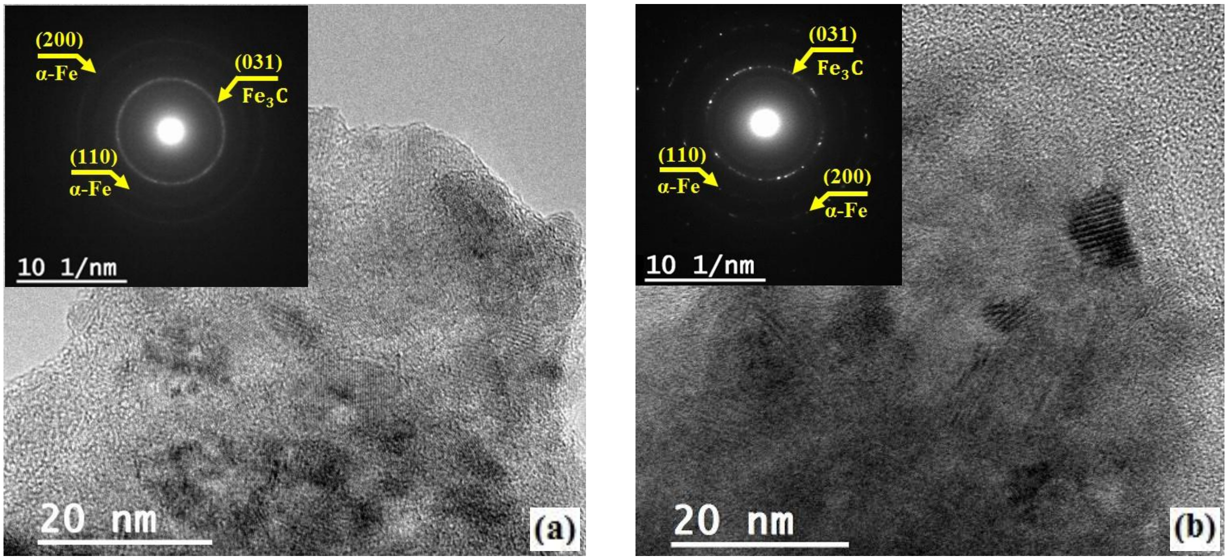

Fig. 4.8 TEM analysis of powders milled for 100h of (a) Fe-1.4 wt.%C; (b) Fe-6.67 wt.%C. The bright filed TEM micrograph showing nanocrystalline α-Fe and Fe_3C. SAED pattern (top left) shows the Debye's circles of diffracted spots of mixture of α-Fe and Fe_3C.

4.4.2 Micro-hardness test

Micro-hardness test was performed for the milled powders of the three high-carbon Fe-C alloys. Micro-hardness values were plotted against milling time to assess the effects of milling time and carbon concentration on the alloys' hardness (Fig. 4.9). Regardless of carbon concentration, hardness of the milled powders markedly increased with milling time. Hardness also increased with carbon concentration. For all alloys, hardness tended to approach a steady-state with milling time, in the same way that the amount of carbon dissolved in α-Fe, lattice strain, crystallite size, and amount of Fe_3C formed approach steady states. All of these made contribution to hardness. Evidence for strengthening due to strain hardening and grain size refinement of the α-Fe matrix was respectively demonstrated by strain energy accumulation and decrease in crystallite size as a function of milling time displayed in Fig. 4.3. Additionally, there was increase in the amount of carbon dissolved in the α-Fe and amount of Fe_3C formed with milling time. All of these events tended to approach a steady-state hence it was not surprising that hardness tended to approach steady state as well. It was also important to note that for a given milling time, the amount carbon dissolved in α-Fe increased, lattice strain increased, and crystallite size decreased with carbon concentration. These corresponded with the observed increase in hardness with carbon concentration. In addition to the Fe_3C, the remnant graphite particles were expected to contribute to strengthening. This explained why the increase of hardness with carbon concentration was so big.

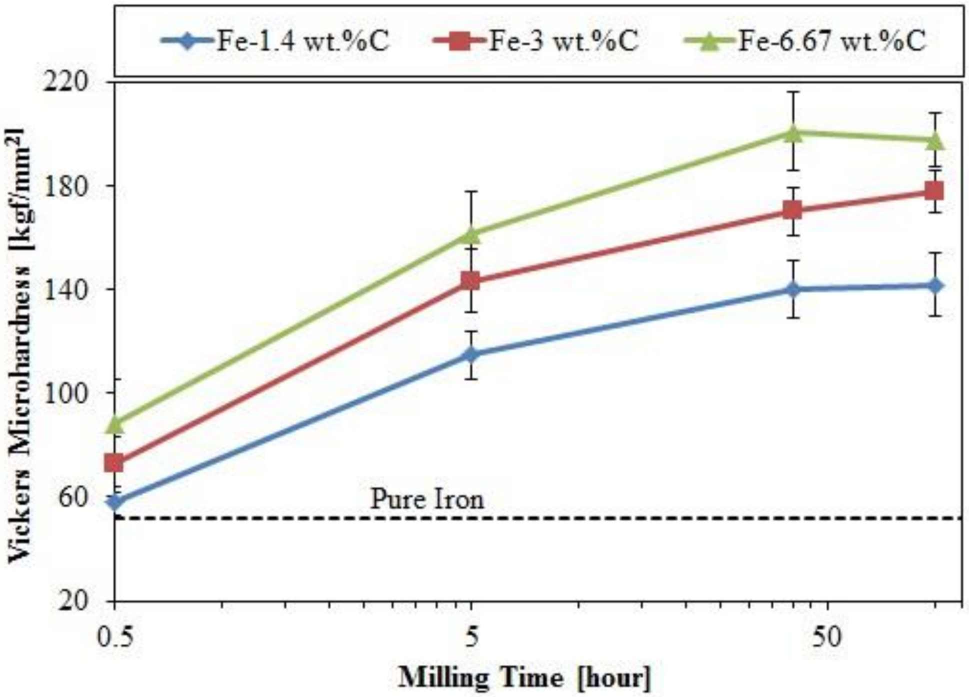

Fig. 4.9 Micro-hardness values of milled powders of high-carbon Fe-C alloys (the solid lines) and pure iron (the dashed line).

4.4.3 Thermal behavior

Differential Scanning Calorimetry (DSC) was used to monitor heat effects associated with phase transitions as a function of temperature for the milled powders. DSC curves for milled powders of Fe-1.4 and 6.67 wt.%C are shown in Figs. 4.10 and 4.11, respectively. An endothermic peak (Peak A in Figs. 4.10 and 4.11) around 770°C was observed in as-received powder (0h). The same peak is also observed in in all milled powders of Fe-3 and 6.67 wt.%C alloys. This peak is known to represent the transformation of α-Fe to γ-Fe [14, 16, 17]. In this study, the transformation temperature of the endothermic peak decreased with milling time. This could be due to attribute of the defects generated during milling, which enhanced the diffusion process and facilitated nucleation and growth of the γ-Fe phase [74].

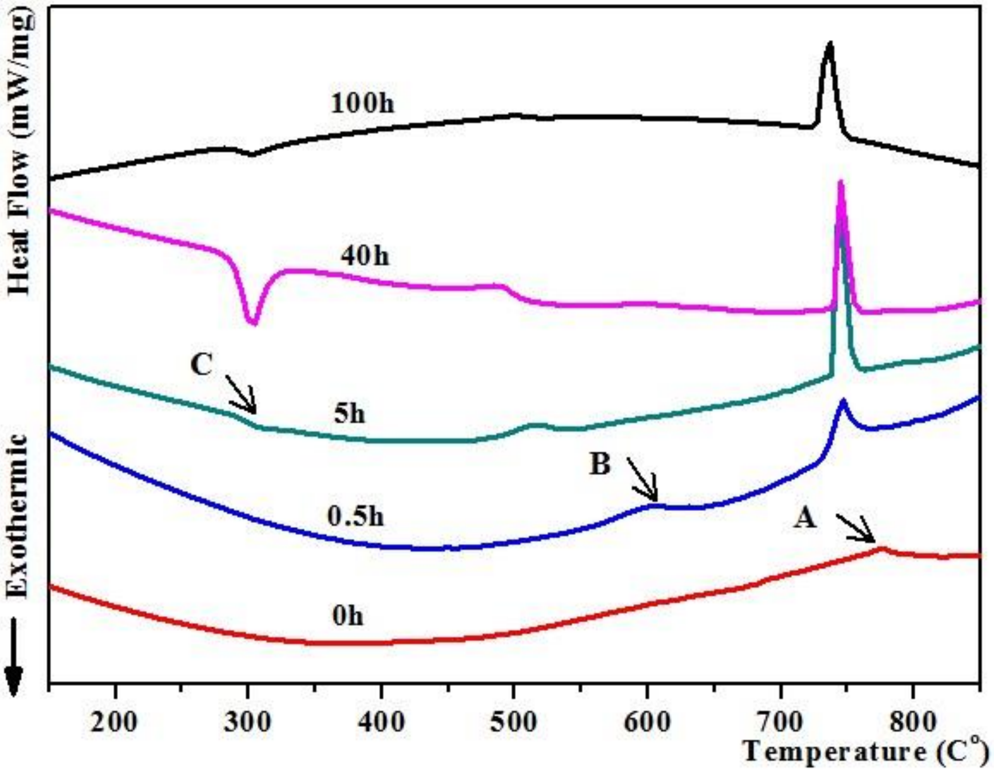

Fig. 4.10 DSC curves of Fe-1.4 wt.%C powders milled for different times.

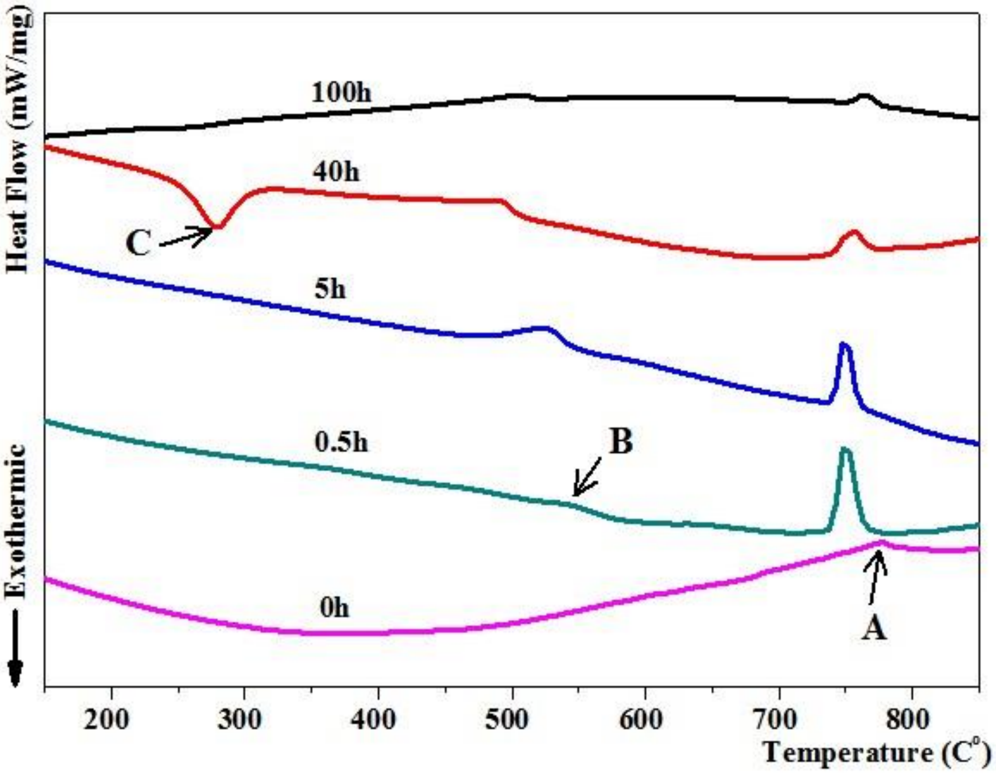

Fig. 4.11 DSC curves of Fe-6.67 wt.%C powders milled for different times

Figure 4.12 indicates that the energy absorbed (area under the DSC curve) during the endothermic reaction in milled powders was higher compared to the as-received powders. Figure 4.12 also shows that the energy absorbed for the milled powders increased rapidly and then decreased after 5h of milling for the 1.4 and 3 wt.%C alloys and after 0.5h for Fe-6.67 wt.%C alloy. This increase in the energy was due to work hardening and alloying which made the transformation difficult. As mentioned above, this endothermic reaction was due to the transformation of α-Fe into γ-Fe. In the Mossbauer spectra, the amount of Fe_3C increased with milling time and carbon concentration (Fig. 4.5). The amount of α-Fe increased with the formation of Fe_3C in milled powders, which led to decrease the energy absorbed during the endothermic reaction with milling time. It was clear that the energy absorbed in Fe-6.67 wt.%C alloy milled powders decreased after 0.5h that was due the formation of high amount of Fe_3C.

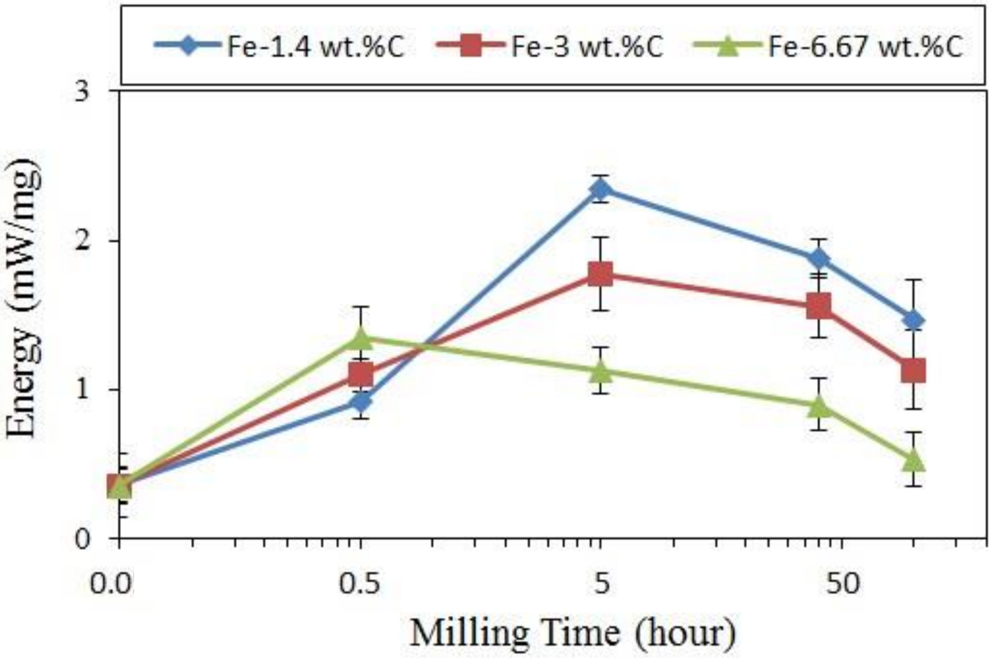

Fig. 4.12 Energy absorbed (area under the DSC curves) during the endothermic reaction (Peak A in Figs. 10 and 11) against milling time.

Afterwards, the decrease in the energy absorbed with milling time indicated that the reaction became easier, but it was still high compared to the as-received powders. A second endothermic peak (Peak B in Figs. 4.10 and 4.11) around 600°C was detected in powders milled for 0.5h and longer. The same peak was also observed in all milled powders of Fe-3 and 6.67 wt.%C alloys. This peak has been detected in Fe-C milled powders elsewhere [14, 16, 17], and no explanation has been found for it in the literature. The transformation temperatures of this reaction decreased with milling time. The energy absorbed (area under the DSC curve) during this reaction was plotted as a function of milling time, as shown in Fig. 4.13. To determine the reason for this peak, the 40h milled powder of Fe-1.4 wt.%C alloy was annealed at 450°C and 550°C which enclose Peak B and slowly cooled to room temperature. The annealing was carried out in the DSC under argon atmosphere. Subsequently, the powders were characterized by XRD and TEM.

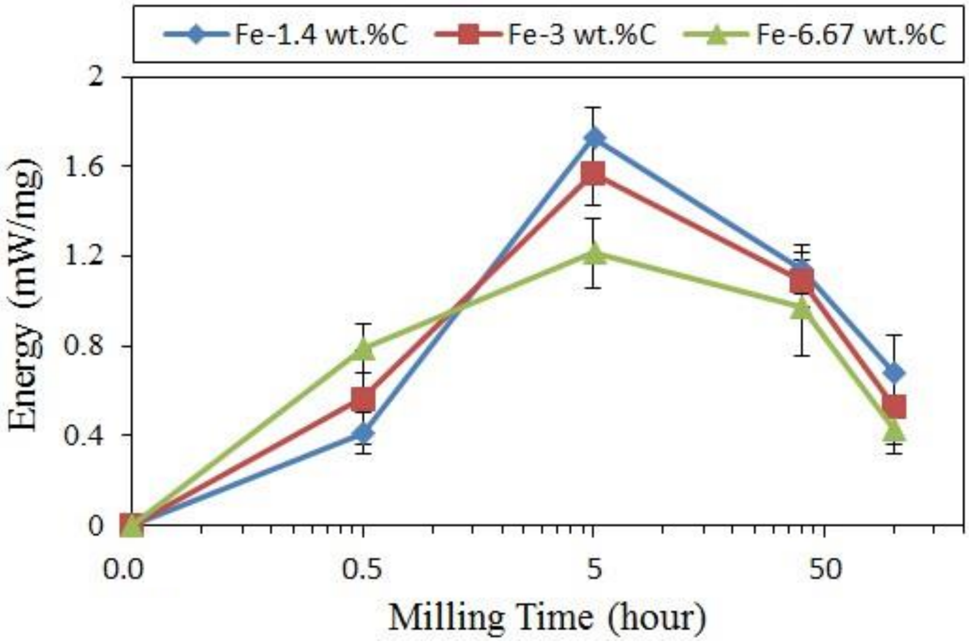

Fig. 4.13 Energy absorbed (area under the DSC curves) during endothermic reaction (Peak B in Figs. 10 and 11) against milling time.

Figure 4.14 shows the XRD patterns of 40h milled powder of Fe-1.4 wt.%C alloy before and after annealing at 450°C and 550°C. Only ferrite peaks was observed in powders milled for 40h (Fig. 4.14a). Ferrite and tiny Fe_3C peaks were detected after annealing at 450°C. Large amount of Fe_3C was observed after annealing at 550°C (Fig.4.14c). This indicates that the endothermic peak B in Figs. 4.10 and 4.11 was due to the formation of Fe_3C. It was clear that the energy observed through the Peak B in the milled powders for 5h and longer of Fe-6.67 wt.%C was lower that was because high amount of Fe_3C already formed during milling. TEM micrograph of the 40h milled powders showed that Fe_3C was observed after annealing at 550°C as shown in Fig. 4.15, which supported the XRD data (Fig. 4.14).

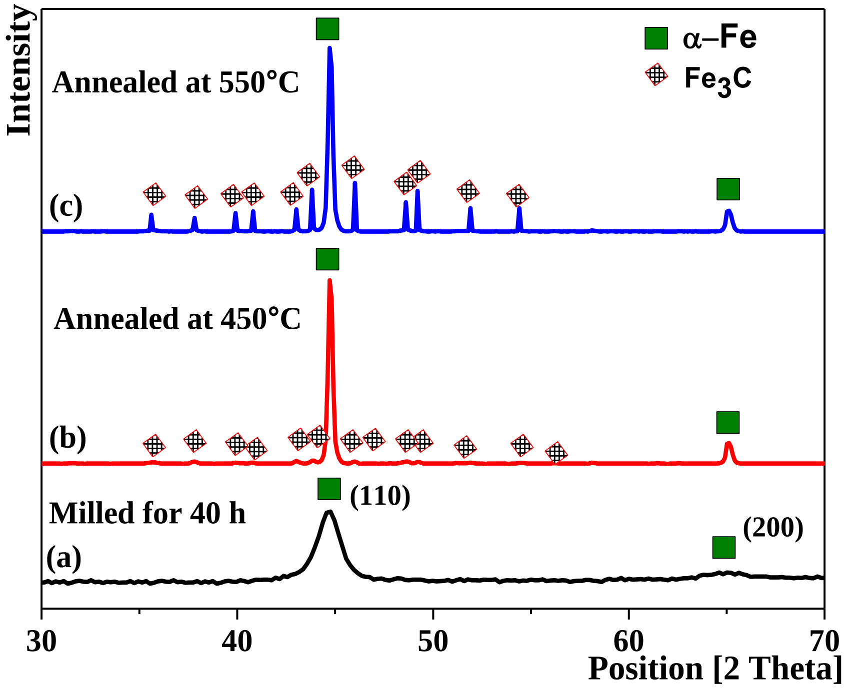

Fig. 4.14 XRD profiles of Fe-1.4 wt.%C powders (a) milled for 40h, (b) annealed at 450°C, and (c) 550°C.

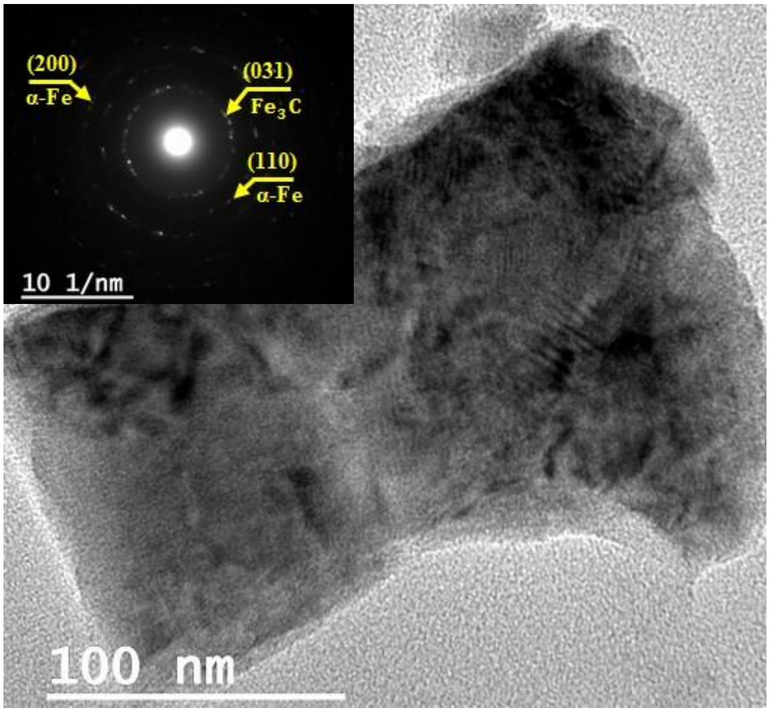

Fig. 4.15 TEM analysis of Fe-1.4 wt.%C powder milled for 40h and then annealed at 550°C, bright filed TEM micrograph showing nanocrystalline structure and SAED pattern (top left) showing the Debye’s circles of diffracted spots of mixture of α-Fe and Fe_3C.

Around 300°C, an exothermic peak (Peak C in Figs. 4.10 and 4.11) was detected in powders milled for 5h and longer in Fe-1.4 wt.% C alloy and after 40h in Fe-3 and 6.67 wt.%C alloys. This peak also shifted to lower temperatures with milling time. The energy released (area under the DSC curve) through this reaction was plotted as a function of milling time as shown in Fig. 4.16. In milled powders, the energy released decreased after 40h of milling. The energy released was higher for lower carbon concentration. However, a number of research groups believed that this peak was due to the crystallization of an amorphous phase of a mixture of α-Fe and Fe_3C [14, 15, 17]. In this work and based on the TEM micrographs and Mossbauer spectra, no amorphous phase was observed in the milled powders even after 100h of milling.

To find a better explanation for the origin of this peak, the 40h milled powder of Fe-1.4 wt.%C alloy was annealed at 350°C in the DSC. Subsequently, the structure of the 40h milled powders before and after annealing was evaluated using TEM. Figure 4.17 shows the TEM analyses of the 40h milled powder of Fe-1.4 wt.%C alloy before and after annealing. Nanocrystalline structures of α-Fe and Fe_3C were observed in the 40h milled powders before annealing (Fig. 4.17a); after annealing at 350°C, growth of the nanocrystalline structure was observed (Fig. 4.17b). Literature shows that this exothermic was due to crystallization of amorphous Fe_3C and α-Fe [14-17]. Figure 4.17 confirmed that the exothermic peak in the DSC around 300°C arose from a combination of recovery and/or recrystallization of both Fe_3C and α-Fe.

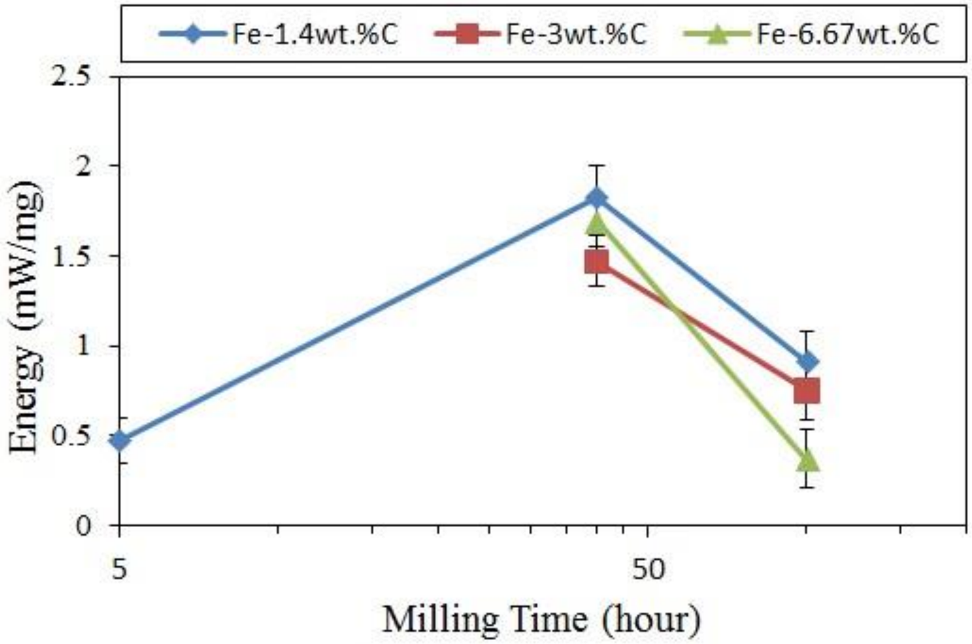

Fig. 4.16 Energy released (area under the DSC curves) through exothermic reaction (peak C in Figs. 10 and 11) against milling time.

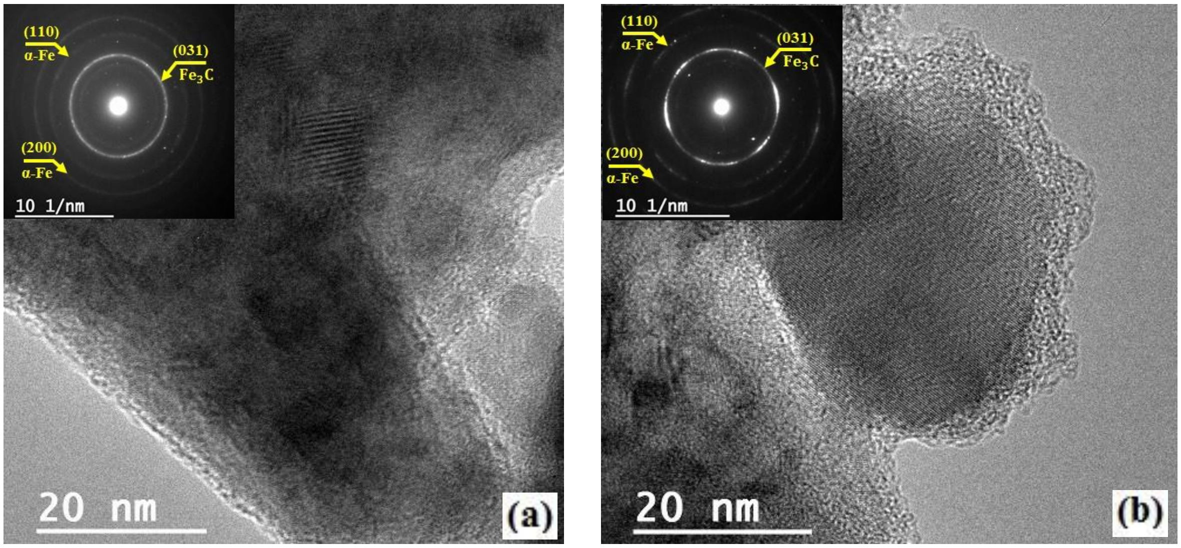

Fig. 4.17 TEM analyses of Fe-1.4 wt.%C powder (a) milled for 40h and (b) annealed at 350°C. Consisting of bright filed TEM micrographs showing nanocrystalline structure and SAED pattern (top left) showing the Debye's circles of diffracted spots of mixture of α-Fe and Fe_3C.

4.5 Summary

In the present work, the effects of milling time and carbon concentration on hardness and powder morphology of high-carbon Fe-C alloys were investigated. Phase transformation observed during milling as well as the heating of milled powders was studied. Reduced elemental iron and 1.4, 3, and 6.67 wt.% pre-milled graphite powders mixture are mechanically alloyed in a SPEX mill for up to 100h. The important observations are summarized as follows:

1. The amount of carbon dissolved in α-Fe increased with milling time. The maximum concentration of carbon dissolved in α-Fe was found to be around 0.15 wt.% in powders milled for 100h.

2. Particles size of milled powders decreased with milling time to reach 9µm after 100h of milling. Spheroidized particles with convoluted lamellae structures were observed after 40h of milling.

3. No significant effect of carbon concentration on the particles size distribution was noticed.

4. Micro-hardness of milled powders increased with milling time as well as carbon concentration.

5. An exothermic peak around 300°C was detected in powders milled for 40h and longer. This peak was found to be due to recrystallization and/or recovery of α-Fe and growth of Fe_3C.

6. An endothermic peak around 600°C was detected in all powders milled. This peak was due to the formation of Fe_3C.

4.6 Acknowledgement

The authors would like to thank the Materials Science and Engineering Department at Virginia Tech for providing financial support. We would also like to thank Professor William Reynolds for the helpful discussion. Special thank is giving to Dr. Christopher Winkler and Mr. Steve McCartney of NCFL at Virginia Tech in scanning and transmission electron microscopes. The help of Mr. Peter Solheid, of IRM at University of Minnesota, in Mossbauer spectroscopy is appreciated.

5 Effects of Milling Time and Carbon Concentration on the Microstructural Evolution of Mechanically Alloyed High-Carbon Fe-C Alloys

5.1 Abstract

The effects of milling time and carbon concentration on the microstructural evolution of high-carbon Fe-C alloys were investigated. High-energy ball milling and powder metallurgy methods were used to produce sintered samples of high-carbon Fe-C alloys. Mixtures of elemental iron and 1.4, 3, and 6.67 wt.% pre-milled graphite powders were mechanically alloyed for up to 100h. Milled powders were pressed and then sintered at temperatures ranging between 900°C and 1200°C for 1h and 5h followed by furnace cooling. Sintered samples were examined using X-ray diffraction, scanning and transmission electron microscopes. Based on the XRD data, α-Fe phase was dominate in all sintered samples, while Fe_3C phase was detected only in sintered samples prepared from powders milled for 0.5h. In sintered samples, the decrease in Fe_3C occurred at the same time as an increase in graphite-rich areas. Nanoparticles of Fe_3C were observed in graphite-rich regions and α-Fe matrix in samples prepared from powders milled for 40h and 100h.

5.2 Introduction

Fe-C system has been extensively studied due to its importance to the steel industry and its wide range of applications. Studies involving very high carbon steels (>1.5 wt.% C) have been limited due to the difficulty of processing cast slabs with high-carbon concentration [75]. Mechanical alloying (MA) being a solid state process makes it possible to process much higher carbon concentration of Fe-C alloys and producing fine microstructures [8]. In order to achieve the desired microstructure and properties, MA processing parameters need to be optimized. The key MA processing parameters are mill type, milling time, charge ratio, milling media, and milling temperature [28]. These parameters are interrelated; for example, selecting the optimum milling time depends on the milling media, milling temperature, and charge ratio. In this work, milling time was set as the only variable among these processing parameters. Milling time is very important to ensure the high effectiveness of the MA process. Milling time should be optimized because some undesired phases may form and the level of contamination increases when the materials are milled for times longer than required [76]. A number of research groups have studied the effects of milling time and other MA processing parameters on the structural evolution and properties of Fe-C alloys [4-7, 9-14, 16, 26, 52, 53, 58, 77].

Hussain Zuhailawati et al. [7] investigated the effects of milling time and carbon concentration on the microstructure and the hardness of Fe-C alloys. Iron and graphite powders were milled in a planetary mill with stainless steel milling media for up to 8h. Milled powders were pressed and then sintered at 1150°C for 0.5h. In their results, they found that the amount of Fe_3C increased with milling in sintered samples. Similar results are reported elsewhere [5, 6, 16, 53]. Zuhailawati suggested that during milling carbon diffused into iron which facilitated the formation of Fe_3C during sintering as a result of reduced diffusion distance. Nowosielski et al. [6] studied the structure and properties of Fe-6.67 wt.%C alloy processed using mechanical alloying and spark plasma sintering. In their work, mixture of iron and graphite powders was mechanically alloyed in a SPEX mill with tungsten carbide milling media for 25h and 150h. Milled powders were then sintered at 900°C for 3 minutes. In the sintered samples, fine grains of α-Fe and pearlite colonies were observed.

The work being reported here, Fe-1.40, 3.0, and 6.67 wt.%C alloys were mechanically alloyed, sintered, and then characterized. The primary focus of this work was to investigate the effects of milling time and the carbon concentration on the microstructural evolution of high-carbon Fe-C alloys. In the preliminary result of this work, it was found that the amount of Fe_3C decreased with milling time, contrary to what was found in the literature. The goal of this work was also to better understand the suppression of Fe_3C evolution in sintered samples with milling time.

5.3 Materials and Methods

The starting powders were a mixture of reduced elemental iron (99.8% purity and 140μm particle size) and graphite (99.999% purity and $<$ 2μm particle size) in 12.8g batches. The graphite powders were milled for 35h. The alloy chemical compositions were Fe-1.4, 3, and 6.67 wt.% of pre-milled graphite. The mechanical alloying process was performed in a standard SPEX 8000 laboratory mill with tungsten carbide milling media. The powder mixtures were milled for up to 100h. The milling was done under an argon atmosphere to minimize oxidation during milling, and the ball-to-powder weight ratio was 2:1. The milled powders were cold-compacted in a uniaxial steel mold at 550 MPa stress. Cold-compacted samples were then sintered in a tube furnace under hydrogen and argon gases flow at temperatures ranging between 900°C and 1200°C for 1h and 5h followed by furnace cooling. Sintered samples were characterized using the following characterization techniques: (i) X-ray diffraction (XRD) in a PANalytical X'Pert Pro powder diffractometer using filtered CuKα radiation at 45kV and 40mA, (ii) Scanning electron microscopy (SEM, FEI Quanta 600 FEG) coupled with energy dispersive X-ray spectroscopy (EDS), (iii) optical microscopy, (iv) Transmission electron microscopy (TEM JEOL 2100), (v) Bruker Q4 Tasman advanced CCD-based optical emission spectrometer. Selected sintered samples were prepared for SEM and optical microscopy using standard metallographic techniques. Samples were then etched in 4% nital which brought up α-Fe grain boundaries as well as Fe_3C. Slices of selected sintered samples were ground to a thickness of approximately 100μm. From this thin slice a disc 3mm in diameter was cut using a Gatan ultrasonic cutter. This smaller disc was further thinned to a thickness of about 30μm and then ion milled with a Fischione Model 1010 until a hole roughly 100μm in diameter had formed. The sample was then examined by a JEOL 2100 TEM at 120kV. The JEOL 2100 TEM was used to detect the presence cementite particles through bright and dark field micrographs and selected area diffraction patterns.

5.4 Results and discussion

5.4.1 Phase Analysis

To understand the suppression of Fe_3C evolution in sintered samples with milling time, carbon concentration in α-Fe in sintered samples was estimated. Also, the chemical composition of sintered samples was measured. In addition, transmission electron microscopy was used to observed presence phases in sintered samples. Only the XRD patterns of the sintered samples at 1200°C for 5h of Fe-1.4 wt.%C alloy are shown here, because the XRD patterns of other sintered samples were similar. Figure 5.1a shows the represantive XRD patterns of sintered samples of Fe-1.4 wt.%C powders milled for various times. The samples were sintered at 1200°C for 5h followed by furnace cooling. Recrystallization occurred simultaneously during sintering. XRD peaks of sintered samples became narrow and their intensities increased (Fig. 5.1a) compared to the XRD peaks of milled powders (Fig. 5.1b). In sintered samples, Fe_3C peaks were observed in 0.5h milled powders, while no Fe_3C peaks were detected in powders milled for 5h and longer. XRD profiles of samples sintered at 900°C, 1000°C, and 1100°C were similar to the XRD profiles of samples sintered at 1200°C. In addition, the XRD profiles of sintered samples of Fe-3 and 6.67 wt.%C powders milled for different times were similar to the XRD profiles of Fe-1.4 wt.%C alloy.

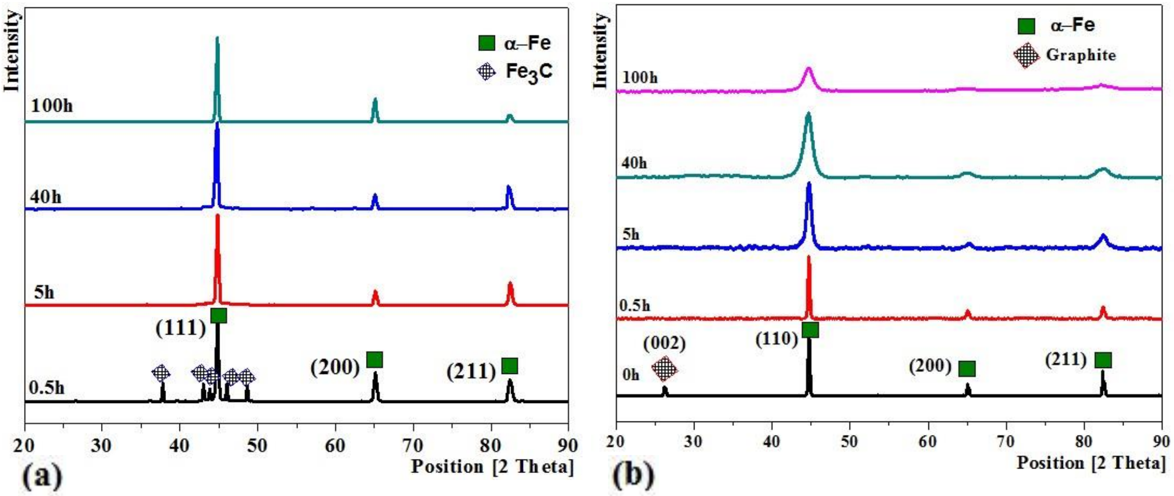

Fig. 5.1 XRD patterns of Fe-1.4 wt.%C alloy (a) samples sintered at 1200C for 5h, (b) milled powders.

The carbon concentration of α-Fe in milled powders and sintered samples were determined as a function of the lattice parameter of α-Fe using Equation 5.1 [62].

$$a_{\alpha-Fe} = 2.8664 + 0.0387761\,X \tag{5.1}$$

where $a_{\alpha-Fe}$ is the lattice parameter (Å) of dilated α-Fe lattice and X is the carbon concentration (wt.%) of iron solid solution. The lattice parameter $a_{(\mathrm{Fe+C})}$ of α-Fe was calculated as a function of d-spacing (d_{hkl}) and planes (hkl) generating the peak [61]. Carbon concentration of α-Fe of both milled powders and sintered samples were plotted as a function of milling time as shown in Fig. 5.2. Only carbon concentration in α-Fe of Fe-1.4 wt.%C powder milled and sintered samples were shown here. Previously discussed in Section 4.4.1, concentration of carbon dissolved in α-Fe of milled powders increased with milling time. After sintering, the carbon concentration in α-Fe drastically dropped. For instance, carbon concentration in α-Fe decreased from about 0.14 wt.% in powder milled for 100h to about 0.03 wt.% in the samples sintered at 1200°C for 5h. Carbon atoms diffused out of α-Fe to form Fe_3C and graphite (in the case of longer milled samples) in α-Fe matrix, which caused a decrease in the carbon concentration. The same behavior was observed in all sintered samples.

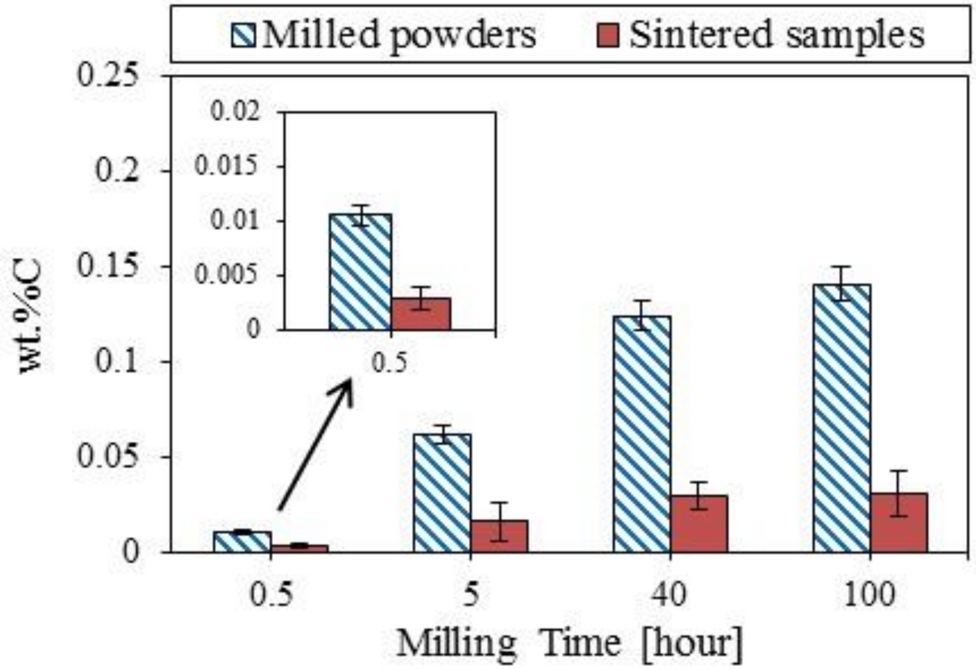

Fig. 5.2 Carbon concentration (wt.%) of α-Fe of milled powders and sintered samples of Fe-1.4 wt.%C. Sintering was performed at 1200°C for 5h.

5.4.2 Chemical composition analysis

Chemical compositions of the sintered samples were estimated using Bruker Q4 Tasman advanced CCD-based optical emission spectrometer. This technique was used to monitor the loss of carbon during process. Figure 5.3 shows the chemical compositions of selected sintered samples of Fe-1.4, 3, and 6.67 wt.%C powders milled for 0.5h and 40h. It was obvious that the carbon concentration in the sintered samples was slightly decreased after processing. The average decrease in carbon concentrations were about 16.5%, 10%, and 5.5% in sintered samples of Fe-1.4, 3, and 6.67 wt.%C alloys, respectively. This decrease in carbon concentration could be due to the milling process and/or sublimation of carbon during the sintering process. Also, the milling time did not seem to have any effect on the carbon concentration. As will be seen in Section 5.4.3 in samples prepared from powders milled for 0.5h, carbon tended to form Fe_3C , and carbon was primarily in the form of graphite in samples prepared from powders milled for 40h and longer.

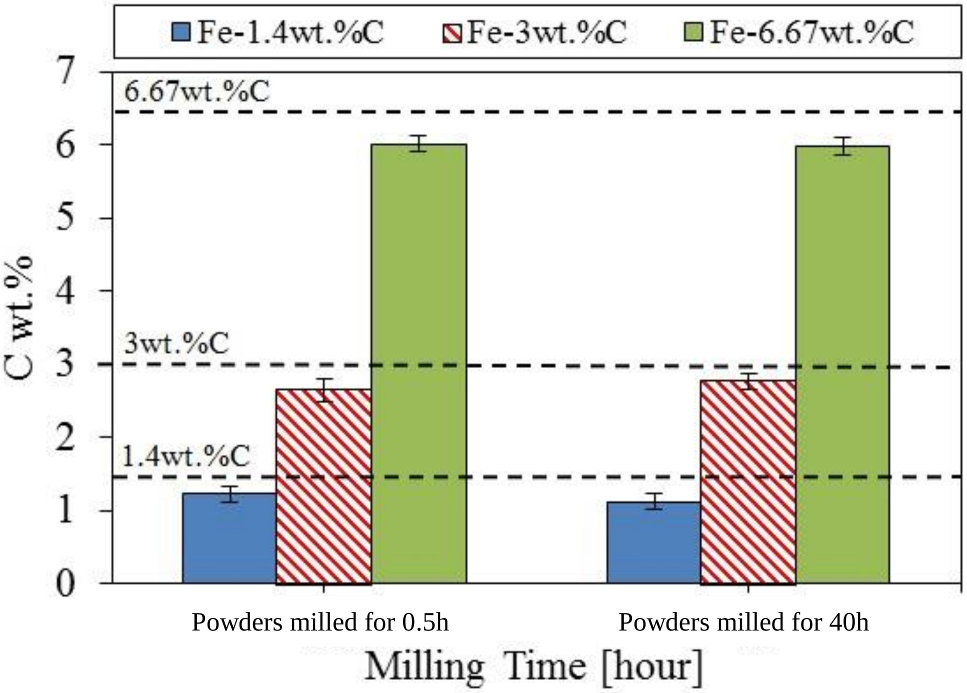

Fig. 5.3 The chemical composition of sintered samples of Fe-1.4, 3, and 6.67wt.%C prepared from powders milled for 0.5h and 40h. Samples sintered at 1200°C for 5h for of Fe-1.4 wt.% alloy and at 1100°C for 5h for Fe-3 and 6.67 wt.%C alloys. Horizontal dashed lines represent carbon concentration in the alloys.

5.4.3 Microstructural evolution

SEM and optical micrographs were used to assess phases present in sintered samples. Here, only the SEM micrographs of samples sintered at 1200°C and 1100°C for 5h were displayed. Figure 5.4 shows the SEM micrographs of sintered samples of Fe-1.4 wt.%C powders milled for various times. In sintered samples at 1200°C for 5h, almost 100% pearlitic structure was observed in powders milled for 0.5h (Fig. 5.4a), while the amount of the pearlitic structure slightly decreased in 5h milled powder (Fig. 5.4b). Pearlite phase formed from austenite during cooling. The first step of pearlite formation was the nucleation of α-Fe or Fe_3C on γ-Fe grain boundaries. After nucleation of α-Fe and Fe_3C, a colony of lamellar of α-Fe and Fe_3C grew [78]. The α-Fe phase was dominant and no Fe_3C was observed in samples prepared from powders milled for 40h and 100h (Figs. 5.4c and 5.4d). In these sintered samples, carbon was in the form of graphite, contrary to what was found in the literature. Literature showed that the amount of Fe_3C in sintered Fe-C alloys increased with milling time [4, 7, 11-13, 15, 52]. Segregation of carbon to dislocation, grain boundaries, and pre-existing Fe_3C particles in steel may explain the decrease of pearlite with milling. For instance, F. G. Caballero et al. [79] reported that carbon was trapped at dislocation in the vicinity of the ferrite-austenite interface, which promoted to prevent the decarburization of super-saturated ferrite and the carbide precipitation sequence during low-temperature bainite formation. S. Ohsaki et al. [80] stated that carbon was strongly segregated at the grain boundaries of the nanocrystalline ferrite produced by mechanically milling pearlitic steel. They found that the carbon concentration at grain boundaries was much higher than that within the grains by a factor of six. J. Z. Zhao et al. [81] concluded that the segregation of carbon to pre-existing cementite particles increased with the decrease of particle radius. These carbon segregation cases were promoted the nucleation of graphite, which grew to graphite-rich regions during cooling. Upon prolonged milling, these carbon segregation cases increased, which led the carbon to form graphite-rich areas instead of Fe_3C. These sinks for absorbing carbon were not enough to absorb all the carbon in the cementite. It was clear also that the decrease in pearlite occurred at the same time as an increase in graphite-rich areas. In addition, longer milling time facilitated the nucleation of graphite during sintering. The preferential growth of graphite during sintering prevented Fe_3C from forming, thereafter, pearlite disappeared.

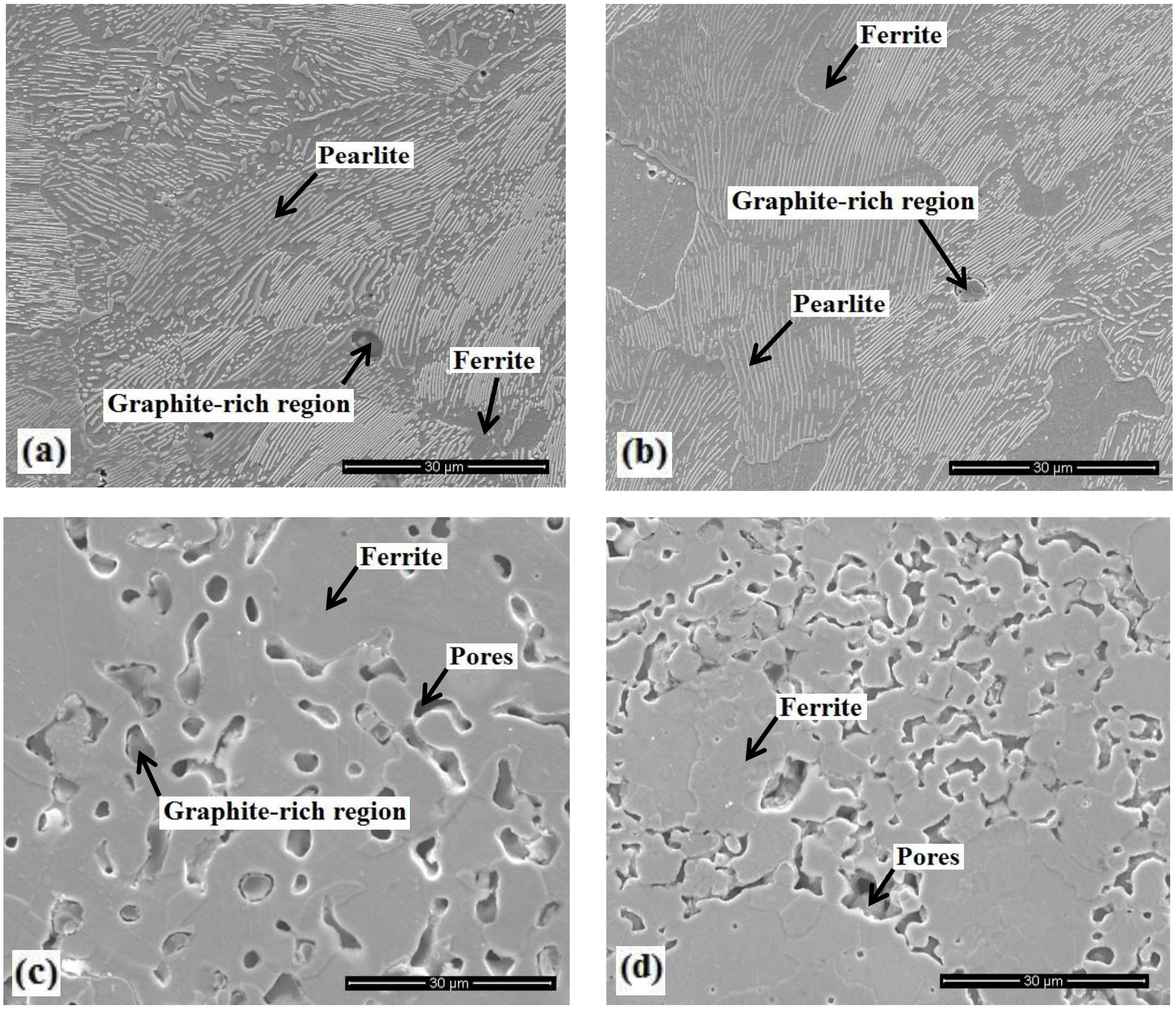

Fig. 5.4 SEM micrographs of sintered samples of Fe-1.4 wt.%C prepared from powders milled for: (a) 0.5h; (b) 5h; (c) 40h; (d) 100h. All samples sintered at 1200°C for 5h followed by furnace cooling. Etchant: 4% nital.

Samples sintered at 900°C, 1000°C, and 1100°C showed the same phase transformation behavior as samples sintered at 1200°C. It was also noticed that the volume of porosity increased with milling time (Figs. 5.4a - 5.4d). Most of the porous volume was occupied by graphite that fell out during sample preparation for imaging. Figure 5.5 illustrates the TEM analysis of sample sintered at 1200°C for 5h of Fe-1.4 wt.%C powder milled for 40h. The bright field of the sintered samples and its corresponding selected area electron diffraction pattern (SAED) are shown in Figs. 5.5a and 5.5b. After analyzing the diffraction spots, it was found that they belong to ferrite and Fe_3C. The TEM analyses confirmed that the Fe_3C formed but were not observed in the SEM micrographs because of their fine size.

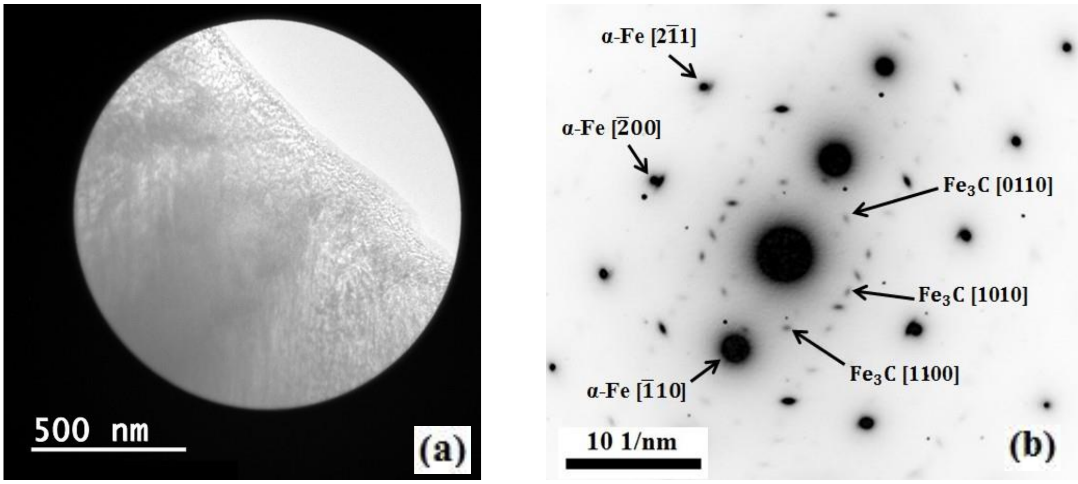

Fig. 5.5 TEM analysis of sample sintered at 1200°C for 5h of Fe-1.4 wt.%C powder milled for 40h:(a) bright field micrograph; (b) corresponding SAED pattern.

Figure 5.6 shows selected SEM micrographs of sintered samples of Fe-3 wt.%C powders milled for different times. In the 0.5h milled sample sintered at 1100°C for 5h, the microstructure had the semblance of hypereutectoid steel (Fig. 6a), whereas the 5h milled sample had the features of hypoeutectoid steel. The amounts of Fe_3C and pearlite regions decreased in 5h and longer milled samples with the decrease being drastic in the 100h milled samples (Fig. 5.6b). As shown in Fig. 5.3, the carbon concentration did not change much with milling time; the carbon manifested itself as very fine carbide particles and graphite. The volume of graphite increased with milling time. Areas that looked like pores were actually spaces initially occupied by graphite which fell out during sample preparation for imaging.

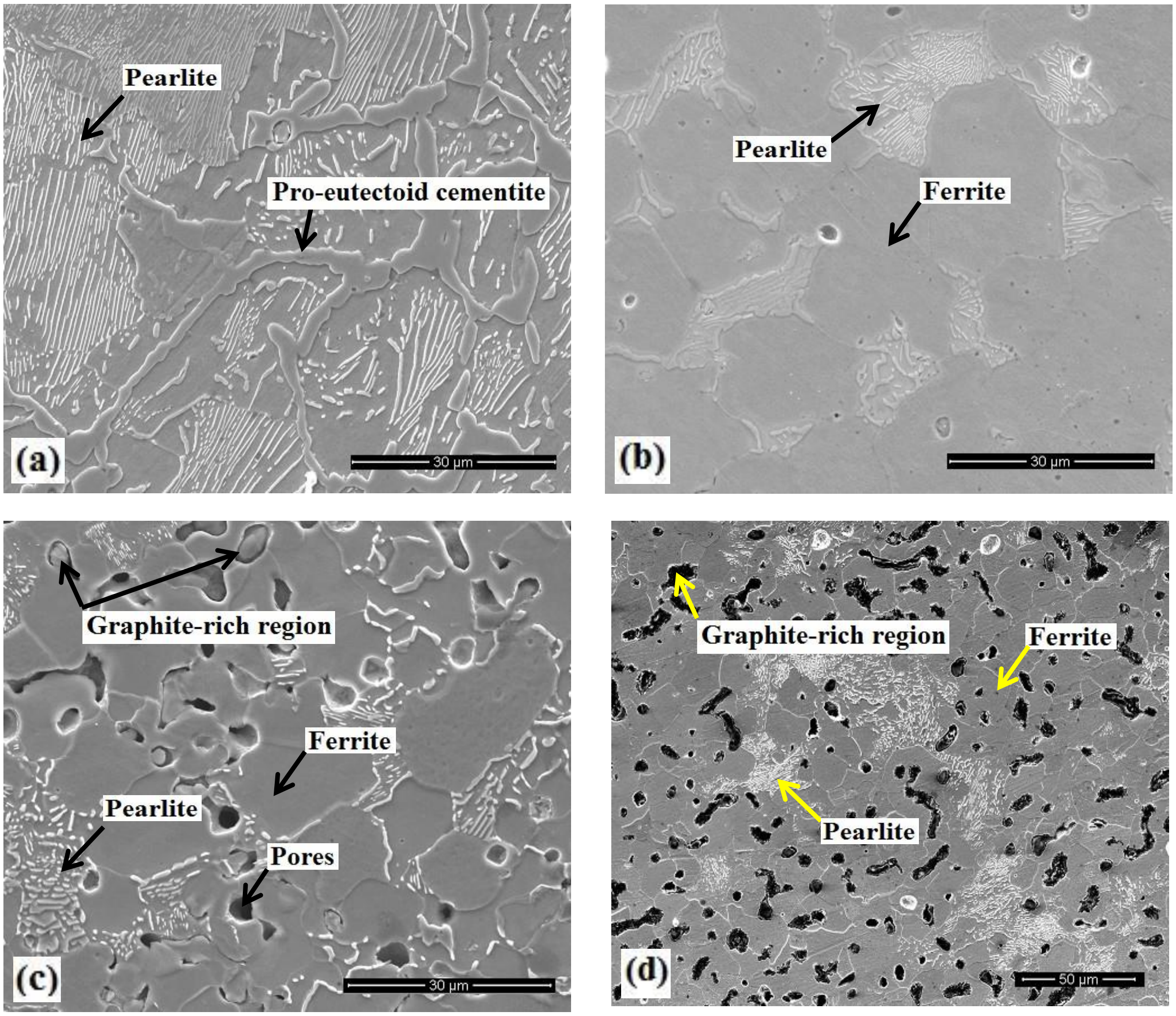

Fig. 5.6 SEM micrographs of sintered samples of Fe-3 wt.%C prepared from powders milled for: (a) 0.5h; (b) 5h; (c) 40h; (d) 100h. All samples sintered at 1100°C for 5h followed by furnace cooling. Etchant: 4% nital.

Selected SEM micrographs of sintered samples of Fe-6.67 wt.%C powders milled for different times are shown in Fig. 5.7. The samples were sintered at 1100°C for 5h followed by furnace cooling. Almost 100% pearlitic structure was observed in the sintered sample of 0.5h milled powder (Fig. 5.7a). The amount of Fe_3C decreased with further milling as shown in Figs. 5.7b and 5.7c. Equiaxed Fe_3C particles were observed in certain areas of the sintered sample of 100h milled powder, while a large amount of graphite-rich regions was revealed (Fig. 5.7d). In all sintered samples, the graphite-rich regions were in the form of coarse flake graphite type that was due to the very low cooling rate [82].

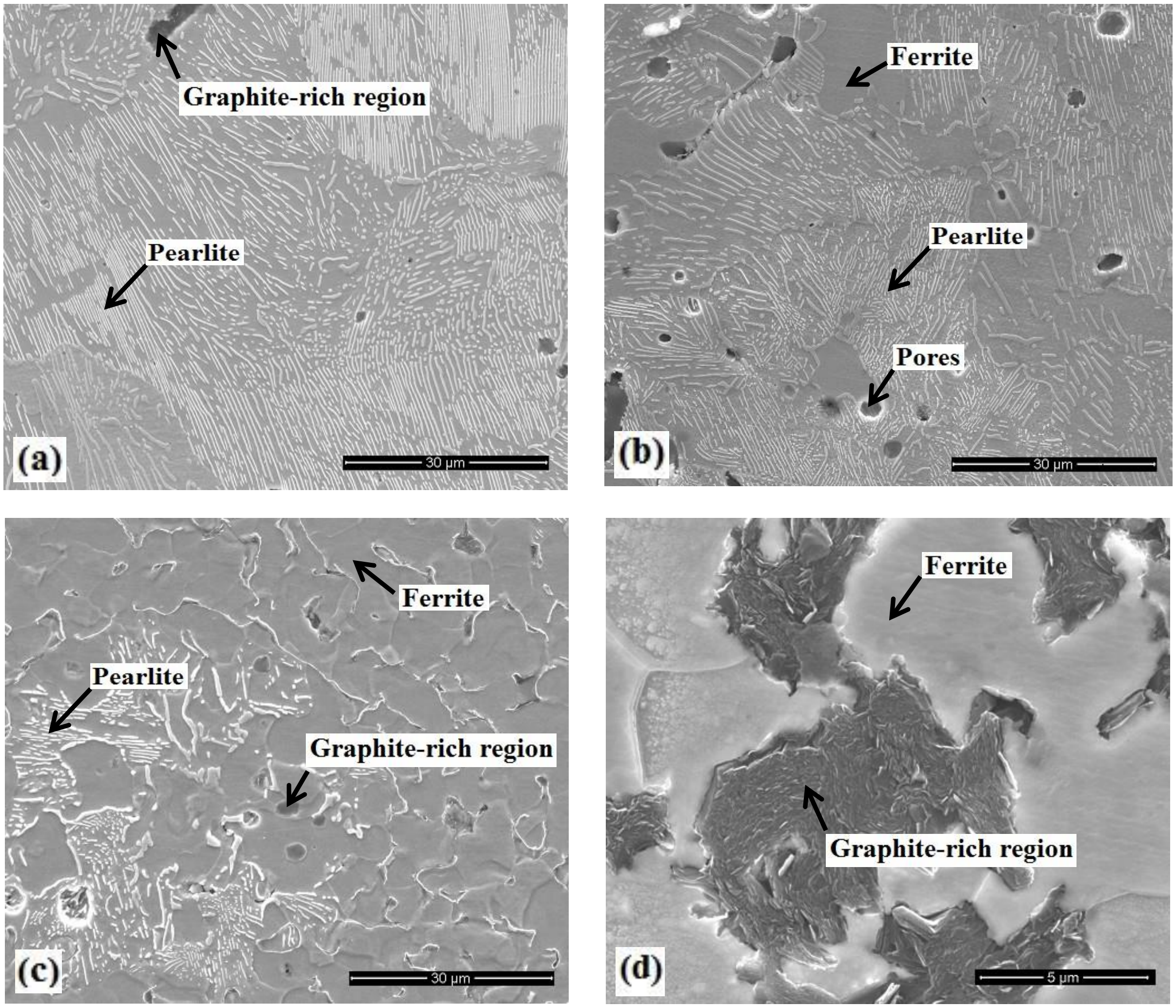

Fig. 5.7 SEM micrographs of sintered samples of Fe-6.67 wt.%C prepared from powders milled for: (a) 0.5h; (b) 5h; (c) 40h; (d) 100h (focusing on the graphite-rich region). All samples sintered at 1100°C for 5h followed by furnace cooling. Etchant: 4% nital.

The TEM analyses of sintered sample of Fe-6.67 wt.%C powder milled for 40h are shown in Figs. 5.8 and 5.9. Bright field micrographs exhibited particles of hundred-nanometer in size within the α-Fe matrix (Fig. 5.8a) and graphite-rich regions (Fig.5.8b). It was found that these particles were Fe_3C. Selected area electron diffraction of the matrix showed that there were small and large diffraction spots. The same diffraction patterns were observed in sintered sample of Fe-1.4 wt.%C powder milled for 40h (Fig. 5.5b). After examining these diffraction patterns, it was found that these diffraction spots belong to α-Fe and Fe_3C phases. Figure 5.9 shows TEM micrographs of the graphite-rich region. High magnification micrograph of the graphite-rich region showed ordered graphite layers (Fig. 5.9b).

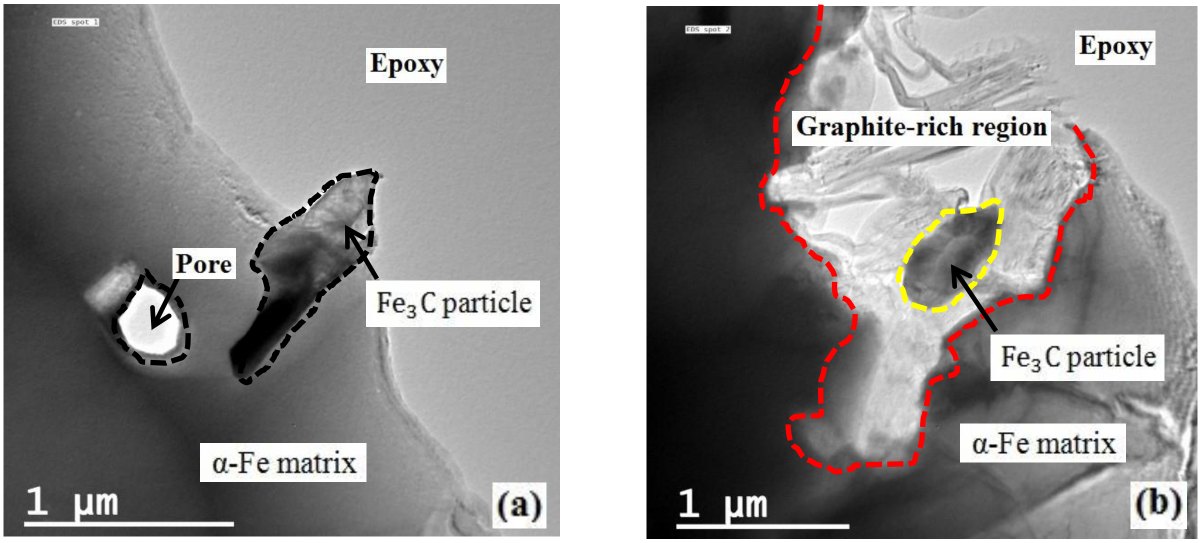

Fig. 5.8 Bright field micrographs of bulk Fe-6.67 wt.%C alloy milled for 40h and sintered at 1100°C for 5h shows Fe_3C particle embedded in (a) α-Fe matrix; (b) graphite-rich region.

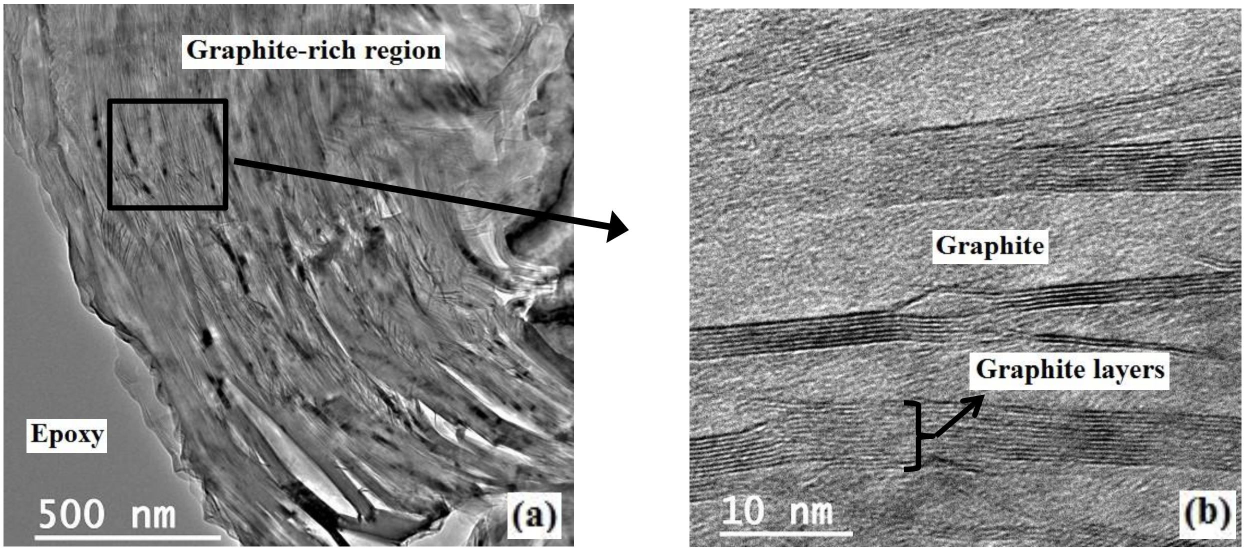

Fig. 5.9 TEM analysis of bulk Fe-6.67 wt.%C alloy milled for 40h and sintered at 1100°C for 5h; (a) bright field image of graphite-rich region; (b) high magnification micrograph of the graphite-rich region showing graphite layers.

5.5 Summary

The effects of milling time and carbon concentration on the microstructural evolution of high-carbon Fe-C alloys were investigated. Mixtures of iron and pre-milled graphite powders were milled, compacted, and then sintered between 900°C and 1200°C for 1h and 5h followed by furnace cooling. Sintered samples were characterized using XRD, SEM, and TEM. The important observations are summarized as follows:

1. Almost 100% pearlitic structure was observed in sintered samples prepared from powders milled for 0.5h, and thereafter, the pearlitic structure decreased with milling time.

2. The decrease in pearlite occurred at the same time as an increase in graphite-rich areas. The decrease of Fe_3C with milling could be featured to the segregation of carbon to crystal defects and pre-existing Fe_3C particles. In addition, longer milling time facilitated the nucleation of graphite during sintering.

3. TEM analyses of samples prepared from powders milled for 40h revealed that particles of Fe_3C were embedded both in the graphite-rich areas and the ferrite matrix.

5.6 Acknowledgement

The authors express their gratitude to the Materials Science and Engineering Department at Virginia Tech for their financial support. The beneficial discussion with Professor William T. Reynolds is gratefully acknowledged. In addition, the assistance of Dr. Christopher Winkler and Mr. S. McCartney in transmission electron microscopy, and Professor Alan P. Druschitz in chemical composition analysis are gratefully appreciated.

6 Effects of Milling Time and Carbon Concentration on the Densification and Hardness of Mechanically Alloyed High-Carbon Fe-C Alloys

6.1 Abstract

This work was aimed to investigate the effects of mechanical alloying milling time and carbon concentration on the densification and the hardness of sintered high-carbon Fe-C alloys. Mixtures of elemental iron and 1.4, 3, and 6.67 wt% pre-milled graphite powders were mechanically alloyed in a SPEX mill with tungsten carbide milling media for up to 100h. Milled powders were cold-compacted and then sintered at temperatures ranging between 900°C and 1200°C for 1h and 5h. The green density of compacted powders decreased with milling time and carbon concentration that negatively affected the density of sintered samples. Micro-hardness of the sintered samples decreased with milling time as Fe_3C decreased. Sintered samples prepared from 0.5h milled powders of Fe-6.67 wt.%C alloy had the highest hardness of 430 Kgf/mm^2.

6.2 Introduction

The growing demand for newer materials characterized by improved properties was the reason for developing unconventional processing techniques such as mechanical alloying (MA) [8, 28, 72], chemical vapor deposition (CVD) [83-85], and rapid solidification processing (RSP) [86-88]. MA is a solid state powder processing technique, which is performed in a high-energy ball mill under an inert atmosphere [89]. MA was first developed at the Paul D. Merica Research Laboratory of the International Nickel Company (INCO) by J. Benjamin and his co-workers in 1960s [8]. MA represents a new process for non-equilibrium amorphous and nanocrystalline structures, extended solubility limit in alloys and intermetallic phases [8].

It has been utilized to process metal alloys, ceramics, and polymers. Among the metal alloys, the Fe-C system has been investigated using MA more than most because of the wide range of steel applications. Research into this system continues unabated [7]. MA has made it possible to process high-carbon Fe-C alloys with very fine microstructure and excellent properties [17, 53]. Mechanical properties of metal alloys are affected by microscale structure and densification process such as compaction pressure and sintering temperatures. The microscale structure depends on the alloy composition and the processing technique. In Fe-C alloys, for instance, when carbon concentration exceeds its limit, the excess carbon forms graphite-rich regions instead of forming iron carbides. The effect of MA processing parameters and alloy composition on the densification and hardness of the alloys have been studied by a number of groups [7, 53, 57].

Hussain Zuhailawati et al. [7] investigated the effect of milling time and carbon concentration on the microstructure and hardness of Fe-C alloys. They found that with increasing milling time pores in the alloy microstructure increased. Also, they reported that hardness increased with milling time and decreased when the carbon content exceeded 2 wt.%. W. Ángel et al. [57] concluded that a higher compaction pressure and lower carbon content gave a denser alloy. They also reported that Fe-C alloys with higher carbon content were harder.

The aim of this work was to investigate the effects of MA milling time and carbon concentration on the densification and the hardness of sintered high-carbon Fe-C alloys.

6.3 Materials and Methods

Reduced elemental iron (99.8% purity and 140μm particle size) and pre-milled graphite (99.999% purity and < 2μm particle size) were mechanically alloyed for up to 100h. The graphite powder was milled for 35h. The high-carbon Fe-C alloys compositions were Fe-1.4, 3, and 6.67 wt.%C. The mechanical alloying was performed in a laboratory SPEX mill with tungsten carbide milling media. Powders handling and sealing of the vial were performed under an argon atmosphere in a glove box to minimize oxidation during milling. The balls weight to powders weight ratio was 2:1. Milled powders were cold-compacted in a uniaxial steel mold at 550 MPa stress and held for 5 minutes. Cold-compacted samples were sintered in a tube furnace at temperatures ranging between 900°C and 1200°C for 1h and 5h followed by furnace cooling. Sintered samples were characterized using scanning electron microscopy (SEM) coupled with energy dispersive X-ray spectroscopy (EDS) to assess phases present and porosities. Micro-hardness of sintered samples were measured using a Phase II Micro Vickers Hardness Tester at load 0.98N and dwell time 15 seconds. At least five measurements were taken for each sample and plots of hardness against milling time were generated. The density measurements were performed using Archimedes' principle [64, 65].

6.4 Results and discussion

6.4.1 Effects of milling time and carbon concentration on density of sintered high-carbon Fe-C alloys

The relative green densities of compacted milled powders and the densities of sintered samples of high-carbon Fe-C alloys were measured using the Archimedes' principle. It was clear that the green density of the compacted milled powders decreased with milling time as shown in Fig. 6.1. This decrease in density with milling time could be due to work hardening and alloying that were introduced into the powders during milling [8]. The high work hardneing rate led to increase the hardness of the milled powders, exhibiting much greater resistance to plastic deformation during compaction. The micro-hardness of the milled powders of Fe-1.4, 3, and 6.67 wt.%C alloys are shown in Fig. 6.2. Increase the hardness of the milled powders with milling time and carbon concentration resulted in poor compaction and consequently decreased the green density [90]. It was clear that there was a negative effect of the hardness of the milled powders on powder compaction behavior. Figure 6.1 also showed that densities of green compacts increased after sintering, which was expected. During sintering, reduction in pore volume occurred because the powder particles moved closer together and the amount of grain-to-grain contact area increased which both led to increase in density [91]. The density of sintered samples of Fe-1.4 wt.%C alloy decreased with milling time as shown in Fig. 6.1. In samples sintered at 900°C for 5h, density decreased from about 93.5% for 0.5h milled powders to about 75.1% for 40h milled powders. The densities of samples sintered at 1200°C were higher than samples sintered at 900°C. The density of samples sintered at 1200°C decreased with milling time as well. It was obvious that the densities of sintered samples increased with sintering temperature and decreased with milling time.

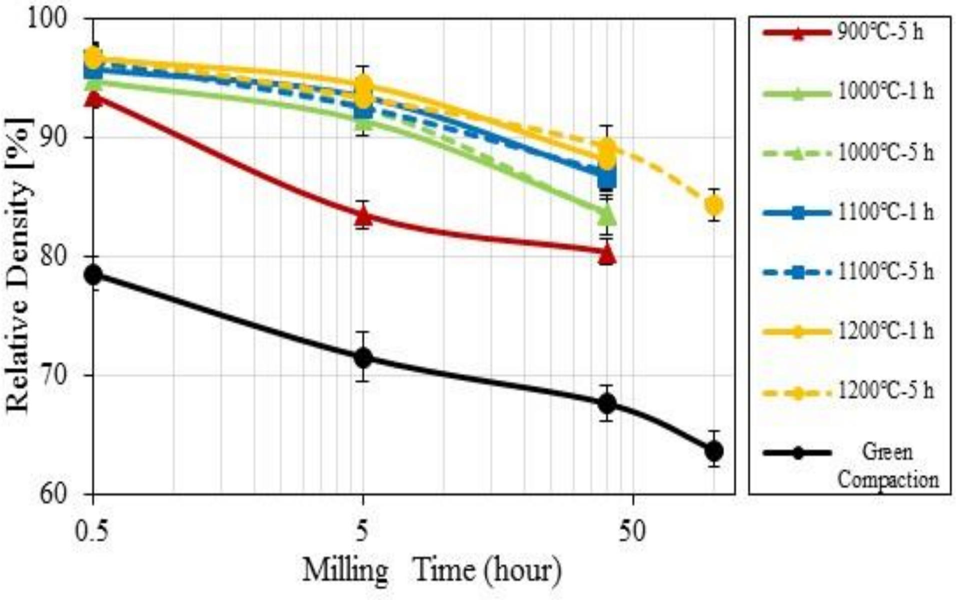

Fig. 6.1 Relative densities of green compactions and sintered samples of Fe-1.4 wt.%C alloy against milling time.

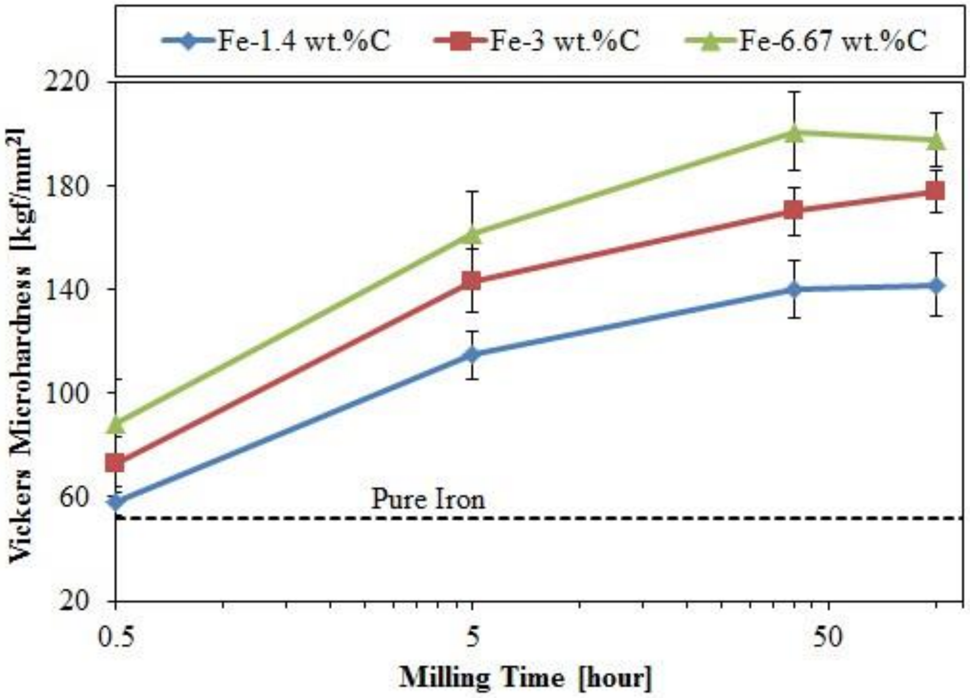

Fig. 6.2 Micro-hardness values of milled powders of high-carbon Fe-C alloys (the solid lines) and pure iron (the dashed line).

The enhancement in density with sintering temperature was due to the increase in sintering rate, which was caused by the increase in the diffusion rate. The evolution of microstructure with milling time and sintering temperatures is shown in Figs. 6.3 and 6.5. Selected SEM micrographs of sintered samples of Fe-1.4 wt.%C alloy prepared from powders milled for 0.5h and 40h are shown in Fig. 6.3. SEM micrographs showed the effect of milling time and the sintering temperature on the densification and the microstructure. Sintered samples prepared from 0.5h milled powders appeared to be denser than that the one prepared from 40h milled powders as shown in Figs 6.1 and 6.3.

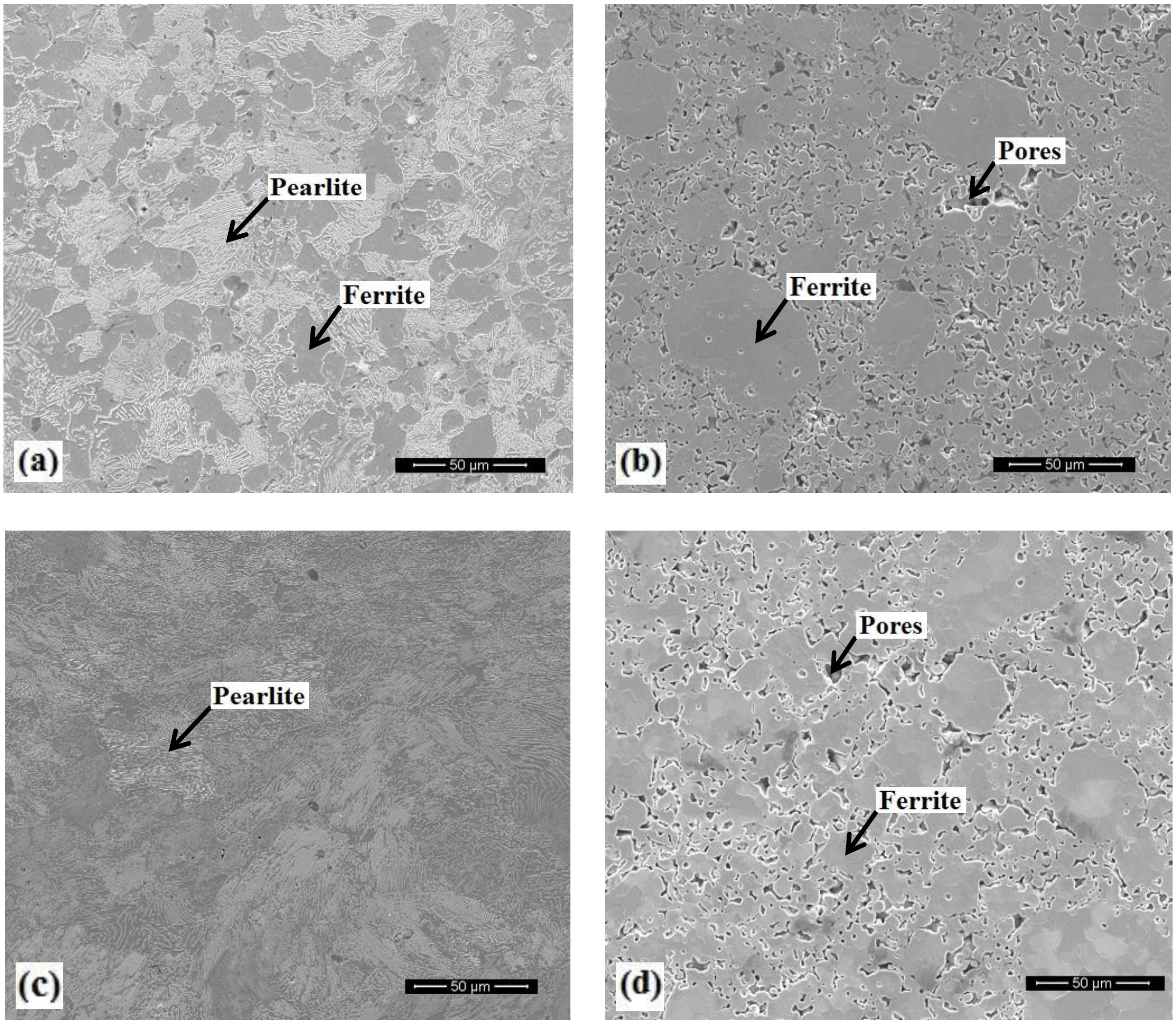

Fig. 6.3 SEM micrographs of sintered samples of Fe-1.4 wt.%C prepared from powders milled for: (a) 0.5h and (b) 40h, and both sintered at 900°C for 5h; (c) 0.5h and (d) 40h, and both sintered at 1200°C for 5h. Etchant: 4% Nital.

Expectedly, the density dropped as milling time increased for green compacts, as shown in Figs 6.1 and 6.3. Figure 6.4 illustrates the relative densities of green compactions and sintered samples of Fe-6.67 wt.%C alloy. In general, the relative density of green compaction decreased with milling time. The green density of Fe-6.67 wt.%C milled powders was lower than the green density of Fe-1.4 wt.%C milled powders. This decrease in the green density could be due to the high carbon concentration which led to poor adhesion between iron powder particles. The density of sintered samples of Fe-6.67 wt.%C alloy were lower than the density of sintered samples of both Fe-1.4 and 3 wt.%C alloys. This decrease in densty was likely related to the decrease in the green density. It was clear that densities of both green compaction and sintered samples decreased with milling time.

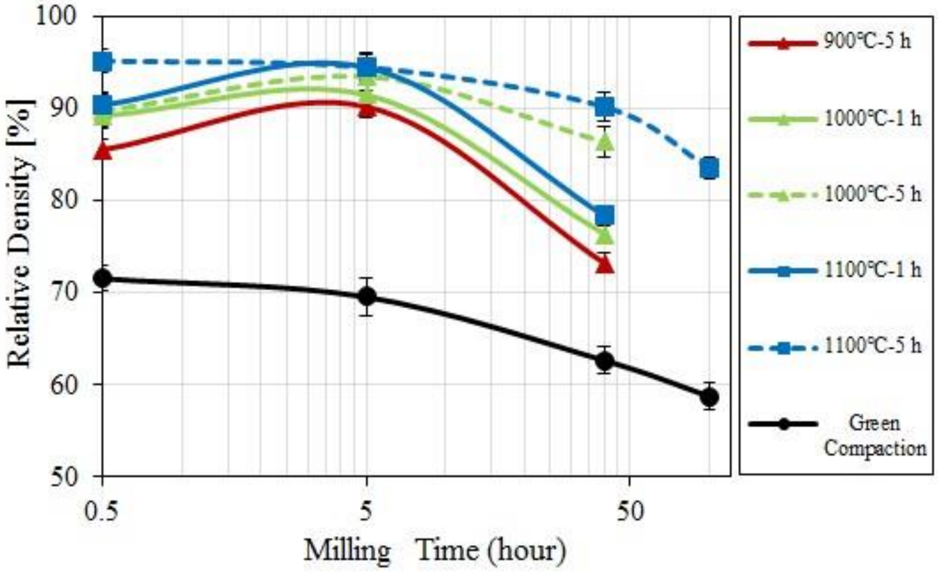

Fig. 6.4 Relative densities of green compactions and sintered samples of Fe-6.67 wt.%C alloy against milling time.

SEM micrographs of sintered samples of Fe-6.67 wt.%C powders milled for 0.5h and 40h and sintered at different temperatures are shown in Fig. 6.5. In the sintered samples, high Vol.% of pores were observed in 100h milled powders compared to 0.5h milled powders. Most of the pore volume was occupied by graphite, which fell out during sample preparation for imaging. Also, high amount of graphite-rich regions was observed in sintered samples, especially the 40h milled powders (Fig. 6.5b and d) that was confirmed using EDS. In samples prepared from powders milled for 40h and 100h, TEM analysis confirmed that the Fe_3C formed but were not observed in the SEM micrographs because of their fine size. It was noticed that the decrease in Fe_3C occurred at the same time as an increase in graphite-rich areas. Also, longer milling time facilitated the nucleation of graphite during sintering. More details on the microstructural evolution were discussed in Section 5.3.3. The relative densities of green and sintered samples of Fe-3 wt.%C alloy (not shown here) were in between Fe-1.4 wt.%C and Fe-6.67 wt.%C alloys.

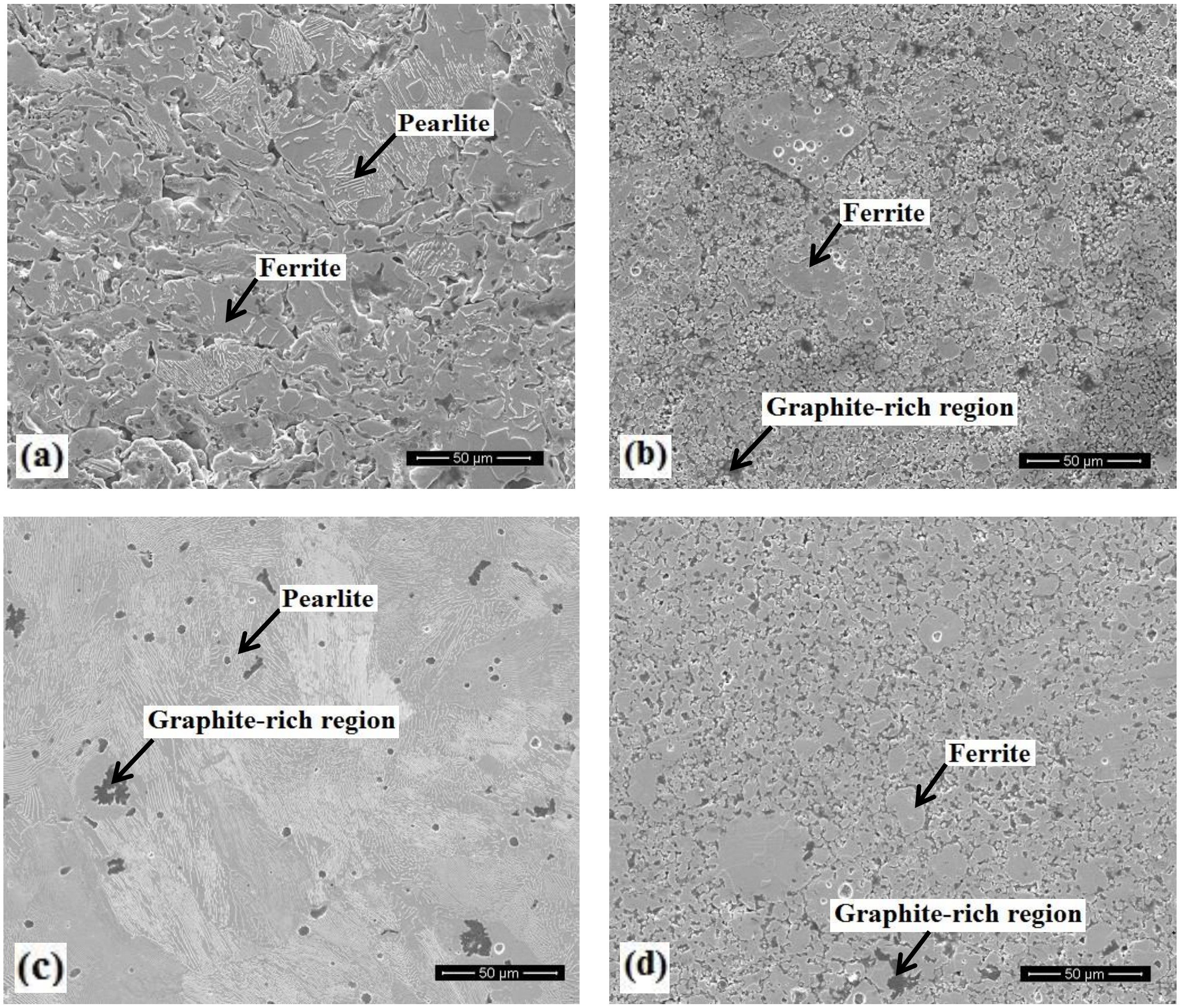

Fig. 6.5 SEM micrographs of sintered samples of Fe-6.67 wt.%C prepared from powders milled for: (a) 0.5h and (b) 40h, and both sintered at 900°C for 5h; (c) 0.5 h and (d) 40h, and both sintered at 1100°C for 5h. Etchant: 4% Nital.

6.4.2 Effects of milling time and carbon concentration on hardness of sintered high-carbon Fe-C alloys

Vickers micro-hardness of sintered samples of high-carbon Fe-C alloys was measured to evaluate the effects of milling time and carbon concentration on the mechanical properties. Micro-hardness of the sintered samples was then plotted against milling time as shown in Fig.

6.6. The maximum hardness was obtained in the 0.5h milled powders; afterwards the hardness decreased with milling time as the amount of Fe_3C decreased. In the literature, the hardness of sintered samples of Fe-C alloys increased with milling time as the amount of the Fe_3C increased.

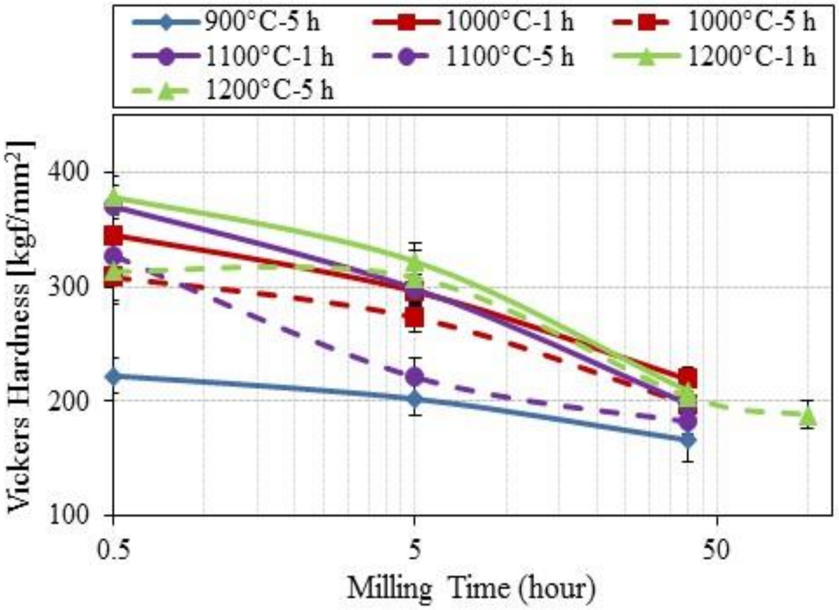

Fig. 6.6 Micro-hardness of sintered samples of Fe-1.4 wt.%C alloy against milling time.

In sintered samples, almost 100% pearlitic structure was observed in samples prepared from 0.5h milled powders, thereafter decreased with milling time (Figs. 6.3 and 6.5). The reduction of pearlite structure amount with milling time was possibly related to the decrease in hardness with milling. Samples sintered at 1200°C were harder compared to the samples sintered at lower sintering temperatures. The increase in hardness was due to two reasons. First, the amount of pearlite structure was very high in samples sintered at 1200°C compared to lower temperatures (Figs. 6.3 and 6.5). Second, samples sintered at 1200°C were denser than the samples sintered at lower temperatures, as shown in Fig. 6.1. The increase in hardness was possibly due to the influence of both the density and high Vol.% of Fe_3C. Figure 6.7 shows the relationship between micro-hardness and milling time for sintered samples of Fe-3 wt.%C alloy at different sintering temperatures.

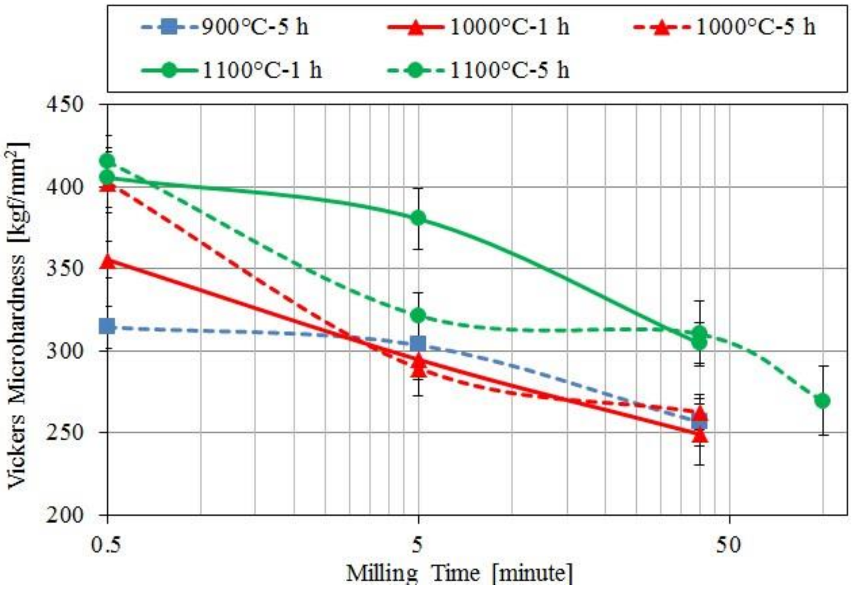

Fig. 6.7 Micro-hardness of sintered samples of Fe-3 wt.%C alloy against milling time.

The hardness of sintered samples of Fe-3 wt.%C alloy was higher than the hardness of Fe-1.4 wt.% C. Also, the hardness values decreased with milling time. Hardness values of sintered samples of Fe-6.67 wt.%C alloy versus milling time are shown in Fig. 6.8. It was obvious that the micro-hardness of sintered samples of Fe-6.67 wt.%C alloy was higher than that of both Fe-1.4 and 3 wt.%C alloys. That increase in hardness could be due to the high-carbon concentration which led to forming the high amount of pearlitic structure as shown in Fig. 6.5. It was also noticed that the hardness values decreased with milling similar to what were observed in both Fe-1.4 and 3 wt.%C alloys.

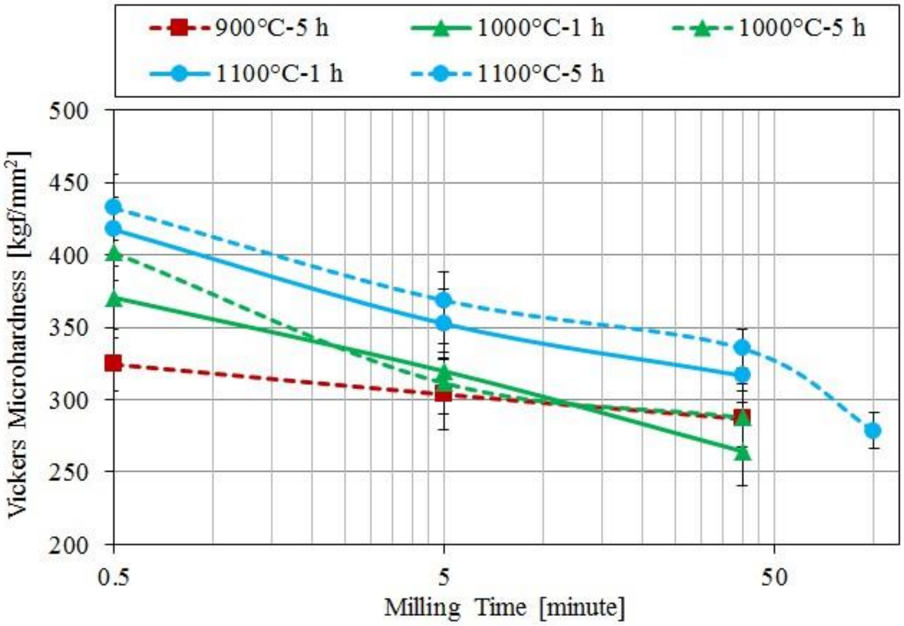

Fig. 6.8 Micro-hardness of sintered samples of Fe- 6.67 wt.%C alloy against milling time.

6.5 Summary

The effects of milling time and carbon concentration on the densification and the hardness of high-carbon Fe-C alloys were investigated. Elemental iron and pre-milled graphite were mechanically alloyed, compacted, and then sintered between 900°C and 1200°C for 1h and 5h followed by furnace cooling. Sintered samples were characterized using XRD, SEM, EDS, and TEM. Micro-hardness was measured for all sintered samples. The important observations are summarized as follows:

1. The relative green density of compacted milled powders decreased with milling time. This was due to the high amount of work hardening and alloying which led to increase the hardness of the milled powders, exhibiting much greater resistance to plastic deformation during compaction.

2. The relative density of sintered samples decreased with milling time that was possibly due to the decrease of the green density with milling time. Also, the excess carbon

adhered to the surface of iron powders this reduced the contact area, leading to lower density.

3. Sintered samples of Fe-6.67 wt.%C alloy were found to be the hardest alloys. Hardness values decreased with milling in all sintered samples. Hardness was found to be dependent on the density and the amount of Fe_3C in the sintered samples.

6.6 Acknowledgements

The authors are grateful to the support of the Materials Science and Engineering Department at Virginia Tech for providing financial support and access to laboratory and equipment. In addition, the assistance of Dr. Christopher Winkler and Mr. S. McCartney in scanning and transmission electron microscopes is appreciated.

7 Dissertation Summary

Reduced elemental iron and 1.4, 3, and 6.67 wt.% pre-milled graphite powders mixture were mechanically alloyed in a SPEX mill with tungsten carbide milling media for up to 100h. Milled powders were then cold-compacted and pressure-less sintered at temperatures ranging between 900°C to 1200°C for 1h and 5h following by furnace cooling. The goal of this work was to investigate the effects of milling time and carbon concentration on the microstructural evaluation, densification, and hardness of high-carbon Fe-C alloys. The important observations are summarized as follows:

1. The concentration of dissolved carbon in α-Fe increased with milling time. The maximum amount of dissolved carbon in α-Fe in Fe-6.67 wt.%C alloy reached about 0.15 wt.% in powders milled for 100h.

2. Particle size of milled powders decreased with milling time to reach 9µm after 100h of milling, while no significant effect of carbon concentration on the particles size distribution was noticed.

3. Micro-hardness of milled powders increased with milling time as well as carbon concentration.

4. An endothermic peak in DSC around 600°C was detected in all milled powders and its transformation temperature decreased with milling time. This peak was due to the formation of Fe_3C, based on the TEM and XRD analyses.

5. An exothermic peak in DSC around 300°C was observed in powders milled for 5h and longer. This peak was found to be due to recovery and/or recrystallization of α-Fe and growth of Fe_3C, based on the TEM analysis.

6. Almost 100% pearlitic structure was observed in samples prepared from 0.5h milled powders, and thereafter decreases with milling time.

7. The decrease in pearlite occurred at the same time as an increase in graphite-rich areas. The decrease of Fe_3C with milling could be featured to the segregation of carbon to crystal defects and pre-existing Fe_3C particles. In addition, longer milling time facilitated the nucleation of graphite during sintering.

8. TEM analyses of samples prepared from powders milled for 40h showed that particles of Fe_3C were embedded in the graphite-rich areas and the ferrite matrix.

9. The relative green density of the compacted milled powders decreased with milling time and carbon concentration. This was due to the deformation and alloying which led to increase the hardness of the milled powders, exhibiting much greater resistance to plastic deformation during compaction.

10. The relative density of sintered samples decreased with milling time that was possibly due to the decrease in the green density. Also, the excess carbon adhered to the surface of iron powders this reduced the contact area, leading to lower density.

11. Sintered samples of Fe-6.67 wt.%C alloy were found to be the hardest alloys. Hardness values decreased with milling in all sintered samples. Hardness was found to be dependent on the density and the amount of Fe_3C in the sintered samples

8 Summary of Accomplishment

Basically, the goal of this work was to investigate the effects of mechanical alloying milling time and carbon concentration on microstructural evolution and hardness of high-carbon Fe-C alloys. However, preliminary results showed that the amount of Fe_3C decreased with milling time, contrary to what was found in the literature. Also, in the DSC curves, an endothermic peak around 600°C was detected in all Fe-C milled powders. The same peak was observed in Fe-C milled powders by other research groups, but no explanation was giving. Additionally, an exothermic peak around 300°C was detected in powders milled for 40h and longer. Many researchers believe that this peak was due to the crystallization of amorphous Fe_3C and Fe/C phases [15, 16, 29, 59].

In the preliminary results, the Vol.% of pearlite phase decreased with milling time, in the sintered samples. Experiments were designed to find better explanation for the suppression of Fe_3C evolution with MA milling time. A mixture of Fe-C powders was mechanically alloyed for up to 40h. Milled powders were pressed, sintered, and then characterized. It was found that the Vol.% of pearlite decreased with milling time and graphite-rich areas were observed in the sintered samples. For confirmation, sintered samples were prepared from powders milled for 100h. It was found that ferrite phase was dominate in these sintered samples as well. TEM analyses of the sintered samples prepared from 40h milled powders showed that fine Fe_3C particles were observed in the α-Fe matrix and graphite-rich areas. This observation suggested that the Fe_3C was formed but it was not representative to the carbon content in the alloy. The chemical composition of the sintered samples was measured to find out if there was a match in the carbon composition. It was found that the amount of carbon slightly decrease after processing, but this mismatch in the carbon composition was not significant enough to affect the phase transformation. Literature showed that carbon segregated to dislocations, grain boundaries, and pre-existing Fe_3C particles during strain aging of steel [81]. These carbon segregation cases were highly occurred in sintered samples prepared from long milled powders. The decrease in pearlite occurred at the same time as an increase in graphite-rich areas. In addition, longer milling time facilitated the nucleation of graphite during sintering. This could be a possible explanation for the decrease of pearlite with milling time.

As for the endothermic and exothermic peaks, experiments were designed, and characterization techniques were used to find better explanation for what caused them. The 40h milled powder was annealed before and after the peak observation in the DSC. The annealed powders were then characterized using XRD and TEM. In the XRD data, Fe_3C peaks were detected this was supported by the TEM analyses. Thus, this peak was due to the formation of Fe_3C. Also, the 40h milled powder was selected to find what caused the exothermic peak. The 40h milled powders were annealed after the observation reaction in the DSC. TEM analyses showed that the exothermic peak was due to the recrystallization and/or recovery of α-Fe and growth of Fe_3C.

9 References

1. Gilman, P. and J. Benjamin, *Mechanical alloying.* Annual Review of Materials Science, 1983. **13**(1): p. 279-300.
2. Dastanpoor, E. and M. Enayati, *Effect of milling intensity on mechanical alloying of Cu-Zr-Al system.* Indian Journal of Engineering & Materials Sciences, 2015. **22**: p. 521-526.
3. Brick, R.M., *Structure and properties of engineering materials*, 1977.
4. Nowosielski, R. and W. Pilarczyk, *The Fe-C alloy obtained by mechanical alloying and sintering.* Journal of Achievements in Materials and Manufacturing Engineering, 2006. **18**(1-2): p. 167-170.
5. Zhang, H., et al., *Fabrication of bulk nanocrystalline Fe–C alloy by spark plasma sintering of mechanically milled powder.* Scripta materialia, 2005. **53**(7): p. 863-868.
6. Nowosielski, R. and W. Pilarczyk, *Structure and properties of Fe–6.67% C alloy obtained by mechanical alloying.* Journal of Materials Processing Technology, 2005. **162**: p. 373-378.
7. Zuhailawati, H., T.C. Geok, and P. Basu, *Microstructure and hardness characterization of mechanically alloyed Fe–C elemental powder mixture.* Materials & Design, 2010. **31**(4): p. 2211-2215.
8. Suryanarayana, C., *Mechanical alloying and milling.* Progress in materials science, 2001. **46**(1): p. 1-184.
9. Chen, Y., et al., *Nanocrystalline Fe–C alloys produced by ball milling of iron and graphite.* Acta Materialia, 2013. **61**(9): p. 3172-3185.
10. Srinivasarao, B., K. Oh-ishi, and K. Hono. *Microstructure and mechanical properties of Fe-C alloy produced by mechanical alloying and spark plasma sintering*. in *Journal of Physics: Conference Series*. 2009. IOP Publishing.
11. Ghosh, B. and S. Pradhan, *Microstructure characterization of nanocrystalline Fe 3 C synthesized by high-energy ball milling.* Journal of Alloys and Compounds, 2009. **477**(1): p. 127-132.
12. Yoo, Y.-G., et al., *Structural evolution of Fe80C20 alloy with alloying times.* Journal of applied physics, 2005. **97**(10): p. 10F909.
13. Yelsukov, E., et al., *Initial stage of mechanical alloying in the Fe–C system.* Materials Science and Engineering: A, 2004. **369**(1): p. 16-22.
14. Campbell, S., et al., *Ball milling of Fe 75-C 25: formation of Fe 3 C and Fe 7 C 3.* Materials Science and Engineering: A, 1997. **226**: p. 75-79.
15. Tanaka, T., et al., *Mechanical alloying of the high carbon Fe・C system.* Journal of the Less Common Metals, 1991. **171**(2): p. 237-247.
16. Rochman, N.T., et al., *Effect of milling temperature and additive elements on an Fe–C system alloy prepared by mechanical alloying.* Journal of Materials Processing Technology, 1999. **89**: p. 367-372.

17. Rochman, N.T., et al., *Effect of milling speed on an Fe–C–Mn system alloy prepared by mechanical alloying.* Journal of materials processing technology, 2003. **138**(1): p. 41-46.
18. Anantharaman, T. and C. Suryanarayana, *Review: A decade of quenching from the melt.* Journal of Materials Science, 1971. **6**(8): p. 1111-1135.
19. Suryanarayana, C., *Non-equilibrium processing of materials*. Vol. 2. 1999: Elsevier.
20. Basariya, M.R., V. Srivastava, and N. Mukhopadhyay, *Effect of Milling Time on Structural Evolution and Mechanical Properties of Garnet Reinforced EN AW6082 Composites.* Metallurgical and Materials Transactions A, 2015. **46**(3): p. 1360-1373.
21. Murty, B. and S. Ranganathan, *Novel materials synthesis by mechanical alloying/milling.* International materials reviews, 1998. **43**(3): p. 101-141.
22. Lu, L., M. Lai, and S. Zhang, *Diffusion in mechanical alloying.* Journal of materials processing technology, 1997. **67**(1): p. 100-104.
23. Lu, L. and M. Lai, *Formation of new materials in the solid state by mechanical alloying.* Materials & Design, 1995. **16**(1): p. 33-39.
24. El-Eskandarany, M.S., *Mechanical alloying: For fabrication of advanced engineering materials*. 2001: William Andrew.
25. Chauruka, S., et al., *Effect of mill type on the size reduction and phase transformation of gamma alumina.* Chemical Engineering Science, 2015. **134**: p. 774-783.
26. Wang, G., et al., *Ball-milling of Fe-C (20–75% Fe).* NanoStructured Materials, 1995. **6**(1): p. 389-392.
27. Froes, F., C. Suryanarayana, and D. Eliezer, *Synthesis, properties and applications of titanium aluminides.* Journal of materials science, 1992. **27**(19): p. 5113-5140.
28. Soni, P., *Mechanical alloying: fundamentals and applications*. 2000: Cambridge Int Science Publishing.
29. Wang, G., et al., *Synthesis and structural evolution of tungsten carbide prepared by ball milling.* Journal of Materials Science, 1997. **32**(6): p. 1461-1467.
30. Neamţu, B., et al., *Amorphisation of Fe-based alloy via wet mechanical alloying assisted by PCA decomposition.* Materials Chemistry and Physics, 2016. **183**: p. 83-92.
31. Lee, C.H., T. Fukunaga, and U. Mizutani, *Temperature dependence of mechanical alloying and grinding in Ni・Zr, Cu・Ta and Fe・B alloy systems.* Materials Science and Engineering: A, 1991. **134**: p. 1334-1337.
32. Fu, Z. and W. Johnson, *Nanophase Zr・Al solid solutions by mechanical alloying at elevated temperatures.* Nanostructured Materials, 1993. **3**(1): p. 175-180.
33. Klassen, T., U. Herr, and R. Averback, *Ball milling of systems with positive heat of mixing: Effect of temperature in Ag-Cu.* Acta materialia, 1997. **45**(7): p. 2921-2930.
34. Koch, C., *Research on metastable structures using high energy ball milling at North Carolina State University (overview).* Materials Transactions, JIM, 1995. **36**(2): p. 85-95.
35. Schaffer, G. and J. Forrester, *The influence of collision energy and strain accumulation on the kinetics of mechanical alloying.* Journal of materials science, 1997. **32**(12): p. 3157-3162.

36. Magini, M., A. Iasonna, and F. Padella, *Ball milling: an experimental support to the energy transfer evaluated by the collision model.* Scripta Materialia, 1996. **34**(1): p. 13-19.
37. Magini, M. and A. Iasonna, *Energy transfer in mechanical alloying (overview).* Materials Transactions, JIM, 1995. **36**(2): p. 123-133.
38. Magini, M., *Correlation between energy transfer and end products in the mechanical alloying process.* TRANSLATIONS-VE RIECANSKY, 1996.
39. Liu, L. and M. Magini, *Correlation between energy transfers and solid state reactions induced by mechanical alloying on the Mo 33 Si 66 system.* Journal of materials research, 1997. **12**(09): p. 2281-2287.
40. Singh, S., et al., *Effect of milling energy on mechanical activation of (Mo+ Si 3 N 4) powders during the synthesis of Si 3 N 4–MoSi 2 in situ composites.* Journal of the European Ceramic Society, 2009. **29**(10): p. 2069-2077.
41. Burgio, N., et al., *Mechanical alloying of the Fe− Zr system. Correlation between input energy and end products.* Il nuovo cimento D, 1991. **13**(4): p. 459-476.
42. Murty, B., M.M. Rao, and S. Ranganathan, *Milling maps and amorphization during mechanical alloying.* Acta Metallurgica et Materialia, 1995. **43**(6): p. 2443-2450.
43. Basset, D., P. Matteazzi, and F. Miani, *Measuring the impact velocities of balls in high energy mills.* Materials Science and Engineering: A, 1994. **174**(1): p. 71-74.
44. Basset, D., P. Matteazzi, and F. Miani, *Designing a high energy ball-mill for synthesis of nanophase materials in large quantities.* Materials Science and Engineering: A, 1993. **168**(2): p. 149-152.
45. German, R.M., *Powder metallurgy science.* Metal Powder Industries Federation, 105 College Rd. E, Princeton, N. J. 08540, U. S. A, 1984. 279, 1984.
46. Upadhyaya, G., *Powder metallurgy technology*. 1997: Cambridge Int Science Publishing.
47. Wilkinson, D.S. and M. Ashby, *Pressure sintering by power law creep.* Acta Metallurgica, 1975. **23**(11): p. 1277-1285.
48. Nagarathnam, K., et al., *Development of 1000-Ton Combustion-Driven Compaction Press for Materials Development and Processing.* ADVANCES IN POWDER METALLURGY AND PARTICULATE MATERIALS, 2007. **1**: p. 03.
49. Zhan, Y., et al., *Cu–Cr–Zr alloy matrix composite prepared by powder metallurgy method.* Powder metallurgy, 2006. **49**(3): p. 253-257.
50. German, R.M., *Sintering theory and practice.* Solar-Terrestrial Physics (Solnechno-zemnaya fizika), 1996: p. 568.
51. Fang, Z.Z., *Sintering of advanced materials*. 2010: Elsevier.
52. Nowosielski, R. and W. Pilarczyk, *Mechanical alloying of Fe-C alloys.* International Journal of Microstructure and Materials Properties, 2007. **2**(2): p. 202-213.
53. Arik, H. and M. Turker, *Production and characterization of in situ Fe–Fe 3 C composite produced by mechanical alloying.* Materials & design, 2007. **28**(1): p. 140-146.

54. Lu, K. and J. Lu, *Nanostructured surface layer on metallic materials induced by surface mechanical attrition treatment.* Materials Science and Engineering: A, 2004. **375**: p. 38-45.
55. Liu, Z., H. Fecht, and M. Umemoto, *Microstructural evolution and nanocrystal formation during deformation of Fe–C alloys.* Materials Science and Engineering: A, 2004. **375**: p. 839-843.
56. Davidson JE. In: Mills K, D.J., Refsnes SK, Sanders BR,, *Compressibility of metal powders* ASM Handbook. Vol. 7. 1993.
57. Wong-Ángel, W.D., et al., *Effect of carbon on the density, microstructure and hardness of alloys formed by mechanical alloying.* Materials & Design, 2014. **60**: p. 605-611.
58. Victoria-Hernández, J., D. Hernández-Silva, and M. Vite-Torres, *Microstructural characterization and sliding wear behavior of ultra high carbon steels processed by mechanical alloying.* Wear, 2009. **267**(1): p. 340-344.
59. Rochman, N.T. and H. Sueyoshi, *Fe-C System Alloys Prepared by Mechanical Alloying and Powder Metallurgy.* 粉体および粉末冶金, 2003. **50**(11): p. 976-980.
60. Callister, W.D. and D.G. Rethwisch, *Materials science and engineering: an introduction*. Vol. 7. 2007: Wiley New York.
61. Cullity, B.D. and J.W. Weymouth, *Elements of X-ray Diffraction.* American Journal of Physics, 1957. **25**(6): p. 394-395.
62. Fasiska, E. and H. Wagenblast, *Dilation of alpha iron by carbon.* AIME MET SOC TRANS, 1967. **239**(11).
63. Williamson, G. and W. Hall, *X-ray line broadening from filed aluminium and wolfram.* Acta metallurgica, 1953. **1**(1): p. 22-31.
64. Loverude, M.E., C.H. Kautz, and P.R. Heron, *Helping students develop an understanding of Archimedes' principle. I. Research on student understanding.* American Journal of Physics, 2003. **71**(11): p. 1178-1187.
65. Smith, W.F. and J. Hashemi, *Foundations of materials science and engineering*. 2006: Mcgraw-Hill Publishing.
66. Benjamin, J.S., *Dispersion strengthened superalloys by mechanical alloying.* Metallurgical transactions, 1970. **1**(10): p. 2943-2951.
67. Turker, M., C. Karatas, and S. Saritas. *Comparation of flow behaviors of mechanically alloyed and turbola processed powder PIM feedstock by capillar rheometer*. in *Powder Metallurgy Word Congress*. 2000.
68. Zhao, J., et al., *Structural evolution in the graphitization process of activated carbon by high-pressure sintering.* Carbon, 2009. **47**(3): p. 744-751.
69. Meier, M.L., *Measuring crystallite size using X-ray diffraction, the Williamson-Hall method.* University of California, Davis, 2005.
70. Gómez, B., E. Gordo, and J. Torralba, *Influence of milling time on the processing of Fe–TiCN composites.* Materials Science and Engineering: A, 2006. **430**(1): p. 59-63.

71. Le Caër, G., P. Delcroix, and J. Foct. *Contribution of Mössbauer spectrometry to the study of mechanically alloyed materials and of nanomaterials*. in *Materials science forum*. 1998. Trans Tech Publ.
72. Suryanarayana, C., *Recent advances in the synthesis of alloy phases by mechanical alloying/milling.* Metals and Materials International, 1996. **2**(4): p. 195-209.
73. Koch, C., *The synthesis and structure of nanocrystalline materials produced by mechanical attrition: a review.* Nanostructured materials, 1993. **2**(2): p. 109-129.
74. Suryanarayana, C., T. Klassen, and E. Ivanov, *Synthesis of nanocomposites and amorphous alloys by mechanical alloying.* Journal of materials science, 2011. **46**(19): p. 6301-6315.
75. Zhukov, A. and R. Snezhnoi, *The iron-carbon system. New developments—II. A new approach to the metastable iron-carbon system.* Acta Metallurgica, 1973. **21**(3): p. 199-201.
76. Yadav, T.P., R.M. Yadav, and D.P. Singh, *Mechanical milling: a top down approach for the synthesis of nanomaterials and nanocomposites.* Nanoscience and Nanotechnology, 2012. **2**(3): p. 22-48.
77. Lenin, G., *Development of iron-iron carbide composite by planetary milling and conventional sintering*, 2014, National Institute of Technology Rourkela.
78. Porter, D.A., K.E. Easterling, and M. Sherif, *Phase Transformations in Metals and Alloys, (Revised Reprint)*. 2009: CRC press.
79. Caballero, F.G., et al., *Atomic scale observations of bainite transformation in a high carbon high silicon steel.* Acta Materialia, 2007. **55**(1): p. 381-390.
80. Ohsaki, S., et al., *Characterization of nanocrystalline ferrite produced by mechanical milling of pearlitic steel.* Scripta materialia, 2005. **52**(4): p. 271-276.
81. Zhao, J., A. De, and B. De Cooman, *Formation of the Cottrell atmosphere during strain aging of bake-hardenable steels.* Metallurgical and Materials Transactions A, 2001. **32**(2): p. 417-423.
82. Angus, H.T., *Cast iron: physical and engineering properties*. 2013: Elsevier.
83. Reina, A., et al., *Large area, few-layer graphene films on arbitrary substrates by chemical vapor deposition.* Nano letters, 2008. **9**(1): p. 30-35.
84. Veríssimo, C., et al., *Different carbon nanostructured materials obtained in catalytic chemical vapor deposition.* Journal of the Brazilian Chemical Society, 2006. **17**(6): p. 1124-1132.
85. Hampden-Smith, M.J. and T.T. Kodas, *Chemical vapor deposition of metals: Part 1. An overview of CVD processes.* Chemical Vapor Deposition, 1995. **1**(1): p. 8-23.
86. Sastry, S., et al., *Rapid solidification processing of titanium alloys.* JOM, 1983. **35**(9): p. 21-28.
87. Das, S. and L. Davis, *High performance aerospace alloys via rapid solidification processing.* Materials Science and Engineering, 1988. **98**: p. 1-12.

88. Lavernia, E.J., J. Ayers, and T.S. Srivatsan, *Rapid solidification processing with specific application to aluminium alloys.* International materials reviews, 1992. **37**(1): p. 1-44.
89. Benjamin, J. and T. Volin, *The mechanism of mechanical alloying.* Metallurgical Transactions, 1974. **5**(8): p. 1929-1934.
90. Livne, Z., et al., *Consolidation of nanoscale iron powders.* Nanostructured materials, 1998. **10**(4): p. 503-522.
91. Narasimhan, K.S. and F.J. Semel, *Sintering of Powder Premixes-A Brief Overview.* ADVANCES IN POWDER METALLURGY AND PARTICULATE MATERIALS, 2007. **1**: p. 05.